

Aus der Klinik und Poliklinik für Frauenheilkunde und Geburtshilfe
der Universität zu Köln
Direktor: Universitätsprofessor Dr. med. P. Mallmann

Entwicklung eines Prototypen zur Prognose von Frühgeburten
Ein Biomedizintechnischer Ansatz

Inaugural-Dissertation zur Erlangung der Würde eines
Doktor rerum medicinalium
der Hohen Medizinischen Fakultät
der Universität zu Köln

vorgelegt von
Hakan Oflaz
aus Merzifon / Türkei

Promoviert am

12.09.2012

Dekan : Universitätsprofessor Dr. med. Dr. h. c. Th. Krieg
1. Berichterstatter : Universitätsprofessor Dr. med. P. Mallmann
2. Berichterstatter : Universitätsprofessor Dr. rer. nat. M. Scaal

Erklärung

Ich erkläre hiermit, dass ich die vorliegende Dissertationsschrift ohne unzulässige Hilfe Dritter und ohne Benutzung anderer als der angegebenen Hilfsmittel angefertigt habe; die aus fremden Quellen direkt oder indirekt übernommenen Gedanken sind als solche kenntlich gemacht.

Bei der Auswahl und Auswertung des Materials sowie bei der Herstellung des Manuskriptes habe ich keine erhalten.

Weitere Personen außer denen von auf Seite II genannten waren an der geistigen Herstellung der vorliegenden Arbeit nicht beteiligt. Insbesondere habe ich nicht die Hilfe einer Promotionsberaterin/eines Promotionsberaters in Anspruch genommen. Dritte haben von mir weder unmittelbar noch mittelbar geldwerte Leistungen für Arbeiten erhalten, die im Zusammenhang mit dem Inhalt der vorgelegten Dissertationsschrift stehen.

Die Dissertationsschrift wurde von mir bisher weder im Inland noch im Ausland in gleicher oder ähnlicher Form einer anderen Prüfungsbehörde vorgelegt.

Hakan Oflaz

Köln, den 26.06.2012

Die in dieser Arbeit angegebenen Experimente sind nach entsprechender Anleitung durch die Laboratorien von Prof. Dr. Rer. Nat. Habil. G. Artmann, Prof. Dr. Dr. (TR) A. (Temiz) Artmann und Dr. med M. Valter von mir selbst ausgeführt worden.

Die dieser Arbeit zugrunde liegenden Experimente sind von mir mit Unterstützung von P. Linder, E. Wiemer, S. Kuckelkorn, N. C. Dinc durchgeführt worden.

Acknowledgement

At this point, I would like to thank everybody who helped and supported me to finish this doctorate thesis.

First of all I want to thank Prof. Dr. Dr. (TR) Aysegül (Temiz) Artmann and Prof. Dr. rer. nat. habil. Gerhard Artmann for giving me the opportunity to work and complete my thesis in their laboratories. I appreciate your support and your insight during our scientific and private talks.

I would also like to thank Prof. Dr. med P. Mallmann for being my supervisor, and Dr. med. M. Valter for all of his help. Dr. M.Valter provided the required fetal membranes for the experiments and helped to answer outstanding questions in a warm manner. Thank you for your personal and friendly cooperation.

I would like to thank the whole laboratory team for providing an awesome environment. You always made it a pleasure for me to work and spend my time here. It was a great experience to be part of this international team. A sincere thank you to Peterli for his amazing ideas, Eric Wiemer, S. Kuckelkorn, and Cagdas who worked together with me on this project and became good friends of mine, and Serap as well for her supports in the field of Histology. Thank you Eylem and Taylan for encouraging me to make my Ph.D. abroad. I will not forget you, Taylan.

Also I would like to thank Dr. GereonHüttmann at the University of Luebeck Institute of Biomedical Optics, for his scientific suggestions and support in all OCT matters.

Finally I must thank my family and friends for their help and support, and for forgiving my neglect over the last few months. Thank you to my parents and to my sister, whom have always supported me in every way and gave me the chance to develop freely. I never took it for granted, and I am pleased to have you as parents. A special thanks to my wife Gamze for all of her support. Thank you for your understanding, thank you for always having an open ear for me, and thank you for always being with me.

This thesis of doctor of philosophy is dedicated to;

my father, mother, sister and wife with love.

In memory of my all family members.

Table of Contents

List of Abbreviations 1

1 Introduction 3

2 Background: 5

 A. Biological Knowledge 5

 A.1. Pregnancy 5

 A.2. Fetal Membrane (FM)..... 8

 A.2.1. MMPs, TIMPs and Hyaluronic Acid..... 10

 A.2.2. Glycosaminoglycans (GAGs)..... 13

 A.2.3. Collagen..... 14

 A.2.4. Collagen in Fetal Membranes 15

 A.3 Type of Births 17

 A.3.1 Prelabour Rupture of the Fetal Membrane (PROM) 18

 A.4 Medical Versus Parental Care 21

 B. Prediction Methods 23

 B.1 Existing Methods in the Prediction of Preterm Birth 23

 B.1.1. Risk Scoring Systems 23

 B.1.2. Home Uterus Activity Monitoring..... 24

 B.1.2. Cervical Assessment 24

 B.1.3. Fetal Fibronectin Test 25

 B.1.4. Cytokines 26

 B.1.5. Matrix Metalloproteinases 26

 B.1.6. Additional Markers 26

 B.2. Existing Technology That Can Be Used in the Prediction of Preterm Birth.. 27

 B.2.2. Spectrophotometer 27

 B.2.3. Autofluorescence 28

 B.2.3.1. Special Autofluorescence Characteristics of Collagen 30

 B.2.4. Optical Coherence Tomography 31

 C. Purpose, Questions, Tasks and Suggestions of This Study 34

3 Methods 36

 3.1 Device for the Investigation of the Mechanical Properties of the Amniotic Sac Tissue (DIMPAST) 36

 3.1.1 Measurement Principle 36

3.1.2 Components and Technical Design for In-Vitro Measurements	37
Laser-triangulation-sensor	37
Air Pumping Unit	38
Pressure sensor	38
Tissue Chamber	39
Data Interface	40
3.1.3 Construction of the Experimental Device (DIMPAST)	41
3.1.4 Software.....	42
OCT Control Window	42
Data Acquisition Window	42
3.2 Sample Collection	44
3.3 Sample Preparation.....	45
3.4 Measurements.....	46
3.4.1 Thickness Comparison Between Histological Technique and OCT	46
A. Data Groups:.....	46
B. Measurement Technique:.....	47
B.1 Thickness Measurements with a Histological Method:	47
B.1.1 Light Microscopic Examination	48
B.2 Thickness Measurements with OCT:.....	50
3.4.2 Evaluation of Mechanical Properties of FM with the DIMPAST	51
A. Data Groups:.....	51
B. Measurement Technique:	51
B.1 Thickness measurement:	54
B.2 Bursting pressure measurement:	56
B.3 Stress-Strain Ratio:	57
3.4.3 Extra Measurements for In-Vitro Probe Designing	59
A. Deflection Measurements	59
B. Spectral Absorbance Measurements.....	61
C. Autofluorescence Measurements.....	61
3.5 Statistical analysis:	62
4 Results	63
4.1. Comparing the OCT Technique with the Histological Technique	63
4.2. Mechanical Properties of the Fetal Membrane.....	68

4.2.1. Thickness Results:	68
4.2.2 Bursting Pressure Results:	69
4.2.3. Stress-strain ratio Results:	70
4.3. Extra Results for In-Vitro Probe Designing	71
4.3.1. Deflection Results	71
4.3.2. Spectral Absorbance Results	74
4.3.3. Autofluorescence Results	76
5 Discussion.....	77
6 First Version of the OCT Probe.....	83
6.1. Preliminary Data With The New OCT Probe.....	91
7 Conclusion	95
7.1 Outlooks	95
8 Summary.....	98
9 Zusammenfassung	101
10 Reference List.....	104
11 Figure Legends:	115
12 Lebenslauf	124

List of Abbreviations

AE	A mniotic cuboidal E pithelium
AF	A mniotic F luid
AFV	A mniotic F luid V olume
AST	A mniotic S ac T issues
BM	amniotic B asal M embrane
C	C ompact layer
DIMPAST	D evice for the I nvestigation of the M echanical P roperties of the A mniotic S ac T issue
ECM	E xtracellular M atrix
F	F ibroblast layer
fFN	f etal F ibronectin
FFT	F ast F ourier T ransformation
FM	F etal M embrane
FWHM	F ull W idth at H alf M aximum
GAG	G lycosamnoglycan
HA	H yaluronic A cid
HUAM	H ome U terus A ctivity M onitoring
IAP	I ntraamniotic P ressure
IL	I nterleukin
MMP	M atrix M etalloproteases
NB	N ormal B irth
OCT	O ptical C oherence T omography
PAS	P eriodic A cid S chiff S tain
PBM	P seudoasal B asal M embrane
PRB	P reterm B irth
PROM	P relabour R upture of the F etal M embrane
PROMB	P relabour R upture of the F etal M embrane B irth
PPROM	P relabour P remature R upture of the F etal M embrane
PPROMB	P relabour P remature R upture of the F etal M embrane B irth

Ps	Static Pressure
R	Reticular layer
S	Spongy layer
SD	Standart Deviation
SROCT	Spectralis Optical Coherence Tomography
T	Trophoblast layer
TIMP	Tissue Inhibitors of Matrix Metalloproteases
UV	Ultra Violet
WOG	Weeks Of Gastation

1 Introduction

Preterm births are one of the most frequent causes of mortality during or after birth (Gratacos, Sanin-Blair, Lewi, Toran, Verbist, Cabero, and Deprest , 2006). 15% of all preterm births can be attributed to ascending vaginal infections, preterm uterus contractions, cervical malfunction, fetal anomalies, bleeding, abruption placenta, and other irregularities. However, 85% of all cases seem to occur without any visible or known reason, since the ethiology of prelabour rupture is still poorly understood. Fortunately, the majority of births are considered “fullterm” with labour occurring at between 37 to 42 completed weeks of gestation (Alger and Pupkin, 1986). A birth is considered “preterm” if the gestational age is less than 37 completed weeks of gestation. In both fullterm and preterm births, the fetal membrane can rupture prematurely. There is considerable lack of uniformity in the terminology to describe rupture of the fetal membranes (Taylor and Garite , 1984). When rupture of the fetal membranes occurs before the onset of labour, it is best referred to as prelabour rupture of the fetal membrane (PROM)(Roland Devlieger , 2003), but also can be used as premature rupture of the fetal membrane. Existing literature specifies that PROM occurs in 10% of all fullterm pregnancies (Mead , 1980), and approaches 40% of all preterm births (Keirse , 1989).

The purpose of this study was to examine the mechanical properties of the fetal membrane (FM) in order to interpret the causality of prelabour ruptures and preterm births. Furthermore, the results of this study were used to design a risk assessment profile and diagnostic tool, capable of prognosticating prelabour ruptures and preterm delivery. A device capable of making in-vitro measurements was designed in three steps, and has become the basis for further potential projects. Traditional measuring methods have biomechanical limitations and must be conducted in non-physiological and non-homogeneous conditions. For instance, Uni-axial testing causes lateral contraction of the tissue and does not remotely mimic natural conditions. Penetrating and puncture tests performed with a probe also do not match actual physiological conditions since the pressure distribution on the whole fetal membrane is inhomogeneous. These tests were initially developed to help determine what causes premature rupture of the FM and preterm delivery. Regardless of the effectiveness of such tests, a better understanding of the causation could aid doctors in assessing the risk

of a woman having a prelabour rupture of membranes and/or preterm delivery. Therefore, the focus of this study is to define the mechanical properties of the FM using in-vitro evaluation techniques to better understand the complex relationship between the biomechanical structure and the prelabour rupture of the fetal membranes. An additional focus of this thesis is to design an in-vivo diagnostic probe which could be used to predict prelabour rupture of the membranes and preterm delivery.

2 Background:

The work presented here resembles a highly interdisciplinary topic. It will be read by medical doctors, engineers and natural scientists. Thus, we tried to make sure in our introduction that it satisfies their reading and understanding.

A. Biological Knowledge

A biological background is necessary to understand the whole topic, especially for engineers and natural scientists.

A.1. Pregnancy

Pregnancy is the act of bearing offspring brought forth by the mother (Dictionary.com , 2010). Human birth is defined as the time at which the fetus comes out of the mother's uterus into the world, i.e. starting with the onset of labour as regular contractions that lead to the dilation of the uterus cervix as the first section of the birth canal (Dictionary.com , 2010).

The duration of a normal pregnancy usually is between 37 and 42 completed weeks after the last menstrual period (for historical reasons), i.e., between 35 and 40 completed weeks after conception (Carrascosa, Yeste, Copil, Almar, Salcedo, and Gussinye , 2004; Holanda and Melo , 2006).

During the early days of pregnancy, typically accompanying physical signs may not be apparent. After fertilization as the fusion of the maternal egg and the paternal sperm inside the tube, the embryo migrates into the uterus during the following week in order to implant there into the uterus wall and develop into a fully formed infant, all within the mothers' uterus (Laura Riley , 2006). This is a crucial time in the baby's development during which the mother's body adapts including by production of additional hormones and blood cells (Laura Riley , 2006). The baby's development is divided into three stages: the 1st trimester, 2nd trimester, and 3rd trimester. The baby will already look like a baby at the end of the first trimester until which it is called "embryo", complete with eyelids, a nose, a mouth, arms and legs, etc. (Laura Riley , 2006). The baby will be able to move, too. The growth and maturation during the following second trimester ,from which on it is called "fetus", will result in a potential

viability on an intensive care unit, if prematurely born, and in the late third trimester already in purely parental care. Images of different developmental stages of a baby are presented below.

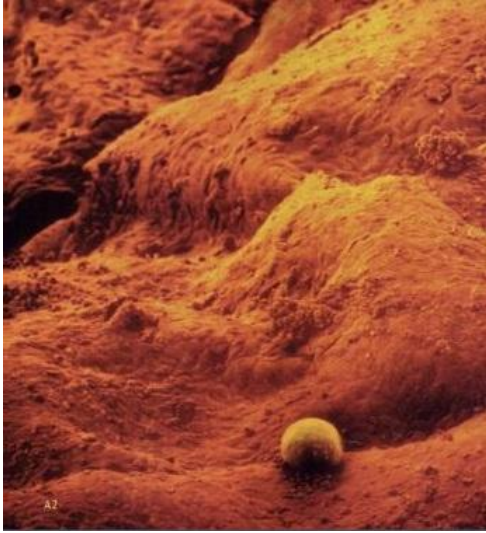


Figure 1: Stage of life: 8 days. Shown here is an 8-day-old embryo (that's the round object near the bottom) implanted in a uterus (Laura Riley , 2006).



Figure 2: Figure on the left hand side: Stage of life - 46 days. This embryo, which is less than 2,54cm long, gets all the nutritional supply it needs from the blood that flows to and from it through vessels in the umbilical cord (Laura Riley , 2006). Figure on the right hand side: Stage of life - 13 weeks. This baby has just been through an ultrasound exam and is having a rest in this photograph. The round object above the baby's head is the yolk sac (Laura Riley , 2006).



Figure 3: Figure on the left hand side: Stage of life - 17 weeks. It is easy to count 10 toes and 10 fingers on this fetus, and facial features are also becoming more defined. The amniotic fluid that surrounds the fetus gradually increases throughout pregnancy to allow the baby to move about (Laura Riley , 2006). Figure on the right hand side -Stage of life: 24 weeks. By now the baby is almost 30,48cm (12 inches) long and weighs a little over 450 grams (1 pound). There's still a lot of growing to do, however, in the next 16 weeks! A fullterm "average" baby usually weighs between 2700 – 3600 grams (6 – 8 pounds) at birth (Laura Riley , 2006).

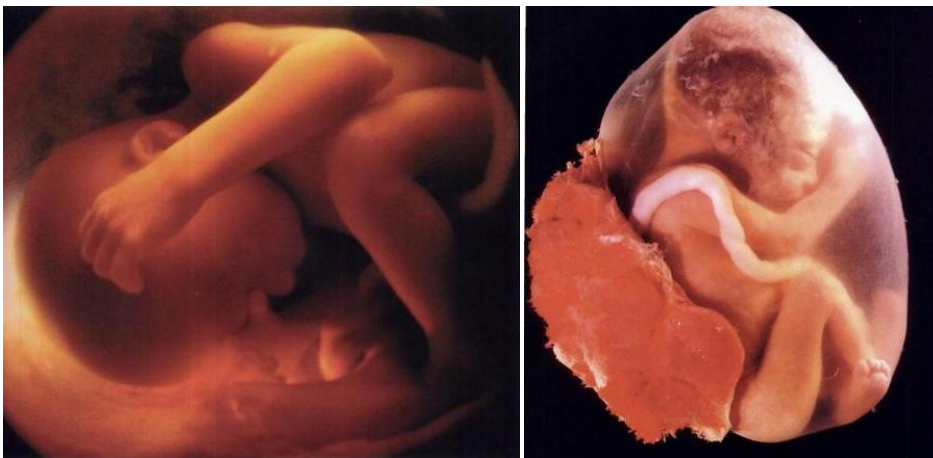


Figure 4: Figure on the left hand side: Stage of life - 27 weeks. The cheeks aren't quite as chubby as they will be at birth (this baby will still gain about 1800 grams (four pounds) before it enters the world), but the face is completely developed. The eyes even open and shut (Laura Riley , 2006). Figure on the right hand side: Stage of life - 36 weeks. It won't be long now until this baby is born. During the next few weeks, the baby's lung will finish developing; they are the last organ that needs to mature. By now the baby has learned to suck in preparation for feeding and may have even started sucking his or her thumb (Laura Riley , 2006).

Women have an extra-embryonic tissue during the pregnancy period. That tissue contains the fetus and is known collectively as the placenta with the fetal membrane. The fetal membrane ensures the health of the fetus and mother during pregnancy by protecting them from external incidents and the outside environment(Laura Riley , 2006). Therefore, a structural integrity of the fetal membrane is important. Any irregularities in the membrane structure, such as collagen degradation of the fetal tissue, could severely affect the health of the fetus and the mother.

A.2. Fetal Membrane (FM)

All vertebrates share accessory embryonic sac tissues containing the fetus, known collectively as the fetal membranes (Roland Devlieger , 2003). Simultaneously, there is a proliferation of villi at the decidua basalis, where the embryonal part of the placenta arises (chorionfrondosum) (Roland Devlieger , 2003). As the embryo and gestational sac increase in size, the deciduacapsularis fuses with the deciduasparietalis and obliterates the cavity(Reynolds and Redmer , 1995). The FM evolves from the inner cell mass of trophoblasts(Roland Devlieger , 2003). The first detailed ultrastructural description of fetal membranes using transmission electronic microscopy was performed in Leuven(van Herendael, Oberti, and Brosens , 1978).

The fetal membrane is a bi-layer thin membrane, but is remarkably tough(Jabareen, Mallik, Bilic, Zisch, and Mazza , 2009). It holds a developing embryo and serves as a barrier (Jabareen, Mallik, Bilic, Zisch, and Mazza , 2009). The FM contains amniotic liquid, which serves several important functions including: providing a medium in which the fetus can readily move, cushioning the fetus against possible injury, helping maintain an even temperature, and providing useful information concerning the health and maturity of the fetus(Fischbach and Dunning , 2008).

The FM contains an embryonic pole, also called conceptus, which develops into the embryo. After duration of approximately 10 days, the amniotic sac is formed and the blastocyst cavity closes, at which time the conceptus becomes known as the embryo. The amniotic sac starts to fill with amniotic fluid and expands with the growth of the embryo. About 12 weeks after conception, the endometrial cavity is filled out by the amniotic sac. From this point forward, the amniotic sac fills the uterus cavity.

The inner layer of the FM is called the amnion, and the outer layer of the FM is called the chorion. The amnion and the chorion are subdivided into many distinct layers (Figure 5) so the human FM consists of many sublayers. A stratum intermedium, also called the intermediate layer, is located between the amnion and the chorion. The amnion and the chorion are composed of an epithelial-like layer and a connective tissue. A histological cross section with toluidine-blue staining is shown in Figure 5, where the different layers are visualized using 200 times magnification.

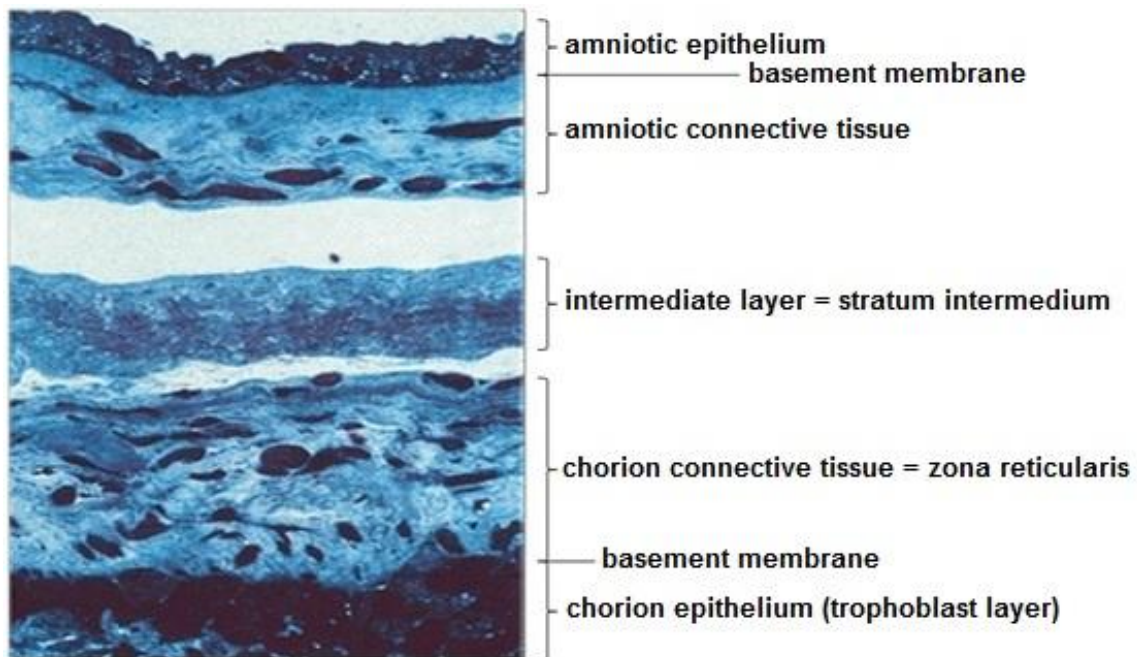


Figure 5: *Histologic cross-sectional view of the Fetal Membrane (FM) under microscope (Halberstadt , 1984). Magnification: 200 times.*

The thickness of all layers together may vary between 100 to 800 μm . The inner layer of the fetal membrane which is in contact with the amniotic fluid is the amniotic epithelium. It is separated from the second layer, the amniotic connective tissue, by the basement membrane. The amniotic connective tissue consists of the zona compacta, the fibroblast layer, and the zona spongiosa.

If the amnion and chorion are separated, a cavity opens in between these layers, which is filled by a third layer, known as the intermediate layer. The chorion connective tissue, also named as zona reticularis, is the fourth layer and consists mainly of collagen. The last of the five layers is the chorionic epithelium, which is made of trophoblasts. This

layer, combined with a pseudo-basal cell layer, indicates the boundary of the deciduas (Halberstadt , 1984).

While the chorion has been observed to be thicker than the amnion, the strength of membrane depends primarily on the amnion (Parry and Strauss, III , 1998). The purpose of the amnion is to contain the amniotic fluid inside of the fetal membranes and also to secrete it during the early weeks of pregnancy. At later stages, the amniotic fluid depends on fetal urination. The function of the fluid is to protect the baby against external influences like mechanical interferences and together with the membranes against infections, but also to enable free movements inside the amniotic sac and allow for the growth of the baby (Modena and Fieni , 2004). Normally the amniotic fluid volume (AFV) is about 800 ml after 40 weeks of pregnancy and it is almost composed of 98% to 99% of water (Modena and Fieni , 2004). Other constituent parts are proteins, hormones, electrolytes, peptides, lipids and carbohydrates (Cho, Shan, Winsor, and Diamandis , 2007). The **amniotic fluid (AF)** is a dynamic fluid, which means that its constituent parts vary during the different weeks of pregnancy. For example, the osmolarity of the AF decreases as the pregnancy progresses. This effect is based on the fetal urine which is hypotonic and mixes with the AF inside the fetal membranes. As a result, it is possible to get some information about the growth progress of the fetus and the metabolic status of the fetoplacental unit by measuring the composition of the AF (Modena and Fieni , 2004). The structure of the fetal membrane is also important in regards to its functions. If its structure starts to change then its function is as also affected.

A.2.1. MMPs, TIMPs and Hyaluronic Acid

The degradation and breakdown of the fetal membranes is essential for the advancement of labour and birth. The degradation of the extracellular matrix can be enzymatical or non-enzymatical. Enzymatical degradation is accomplished with serine proteases or matrix metalloproteases (MMPs) (Gonzalez, Dong, Romero, and Girardi , 2011; Fortunato, LaFleur, and Menon , 2003; Gonzalez, Franzke, Yang, Romero, and Girardi , 2011). Most of the participating proteases belong to the group of MMPs, which are necessary to enable embryonic development, morphogenesis, reproduction and tissue resorption and remodeling (Bruce Alberts, Alexander Johnson, Julian Lewis, Martin Raff, Keith Roberts, and Peter Walter , 2007; Nagase H , 1996). Nowadays a

minimum of 28 mammalian types of MMPs are known, which are listed with their MMP-numbers and their trivial name in the following table (Table 1).

<u>MMP-number</u>	<u>Collagenases</u>
MMP-1	Collagenase 1
MMP-2	Gelatinase A
MMP-3	Stromelysin 1
MMP-7	Matrilysin
MMP-8	Collagenase 2
MMP-9	Gelatinase B
MMP-10	Stromelysin 2
MMP-11	Stromelysin 3
MMP-12	Macrophage elastase
MMP-13	Collagenase 3
MMP-14	MT-1-MMP
MMP-15	MT-2-MMP
MMP-16	MT-3-MMP
MMP-17	MT-4-MMP
MMP-18	Collagenase 4
MMP-19	No trivial name
MMP-20	Enamelysin
MMP-21	XMMP (Xenopus)
MMP-22	CMMP (chicken)
MMP-23	no trivial name
MMP-24	MT-5-MMP
MMP-25	MT-6-MMP
MMP-26	Madrilysin 2, Endometase
MMP-27	human homologue of CMMP (MMP-22)
MMP-28	Epilysin

Table 1: Schedule of mammalian MMPs (Woessner, Jr. 1991).

The antagonists of MMPs are the tissue inhibitors of matrix metalloproteinases (TIMPs), which are tissue-specific counter-regulatory proteins. Four types of TIMPs are currently known. They are named as TIMP-1 to TIMP-4 and all of them are present in amniotic sac tissue (Fortunato, Menon, and Lombardi , 1998). Due to their ability to inhibit MMPs, TIMPs are indispensable in maintaining the balance between extracellular matrix components in physiological processes until the end of pregnancy (Fortunato, Menon, and Lombardi , 1998; Gomez, Alonso, Yoshiji, and Thorgeirsson , 1997).

TIMPs could also play a pivotal role in preventing preterm birth, since they are needed to counteract MMPs, which are synthesized during intrauterus inflammation (Gonzalez, Dong, Romero, and Girardi , 2011;Fortunato, LaFleur, and Menon , 2003;Gonzalez, Franzke, Yang, Romero, and Girardi , 2011). Some cases of preterm birth caused by the preterm premature rupture of membranes (PPROM) are related to ascending intrauterus inflammation. However, the main reasons have not yet been discovered.

The latest studies revealed that the synthesis of MMP-9 in fetal membranes depends especially on the existence of intrauterine inflammation, whereas an increased amount of MMP-2 is commonly measured at the end of a normal pregnancy (Gonzalez, Dong, Romero, and Girardi , 2011;Fortunato, LaFleur, and Menon , 2003;Gonzalez, Franzke, Yang, Romero, and Girardi , 2011). Hence, it is especially MMP-9, which is mentioned in relation to PPRM cases. The substrates of this gelatinase (MMP-9) are the collagens of type I, III, IV and V, which are the main components of the extracellular matrix of fetal membranes. The physiological inhibitors of MMP-9 are TIMP-1 and TIMP-2. It was also observed that MMP-9 degrades collagen fibers of type III more severely than fibers of type I (Hampson, Liu, Billett, and Kirk , 1997). This change in composition of collagen fibers in the extracellular matrix could affect the mechanical properties of the fetal membranes. A fast degradation of collagen type III leads to a loss of elasticity of the tissue, especially when taking into consideration that type III collagen fibers are found to be more concentrated on the outer layer of fetal membranes than in the amniotic layer. In the event of excessive stress, the weakened chorion would not matter for the biomechanical integrity of the amniotic sac because the chorion would naturally rupture earlier. Such instances could cause premature ruptures of the fetal membrane before onset of labour. Therefore, the mechanical and biochemical properties of the fetal membrane are important and should first be studied in-vitro. Based on the results of that study, prediction methods and tools for preterm birth can be created.

Another fundamental element of the extracellular matrix is Hyaluronic acid (HA), because it is an important component of proteoglycan organization (Gonzalez, Dong, Romero, and Girardi , 2011;Fortunato, LaFleur, and Menon , 2003;Gonzalez, Franzke, Yang, Romero, and Girardi , 2011). It is the main anatomic-functional element of connective tissue and can be found in most of the tissues and organs of the human body,

including the fetal membranes (Skinner and Liggins , 1981). One of its distinguishing characteristics is its unique ability to bind multiple water molecules. One gram of HA is capable of binding up to six liters of water (Skinner and Liggins , 1981). As the pregnancy passes its 37th week, the concentration of HA increases noticeably, which is contrary to the decreasing content of collagen (Meinert, Malmstrom, Tufvesson, Westergren-Thorsson, Petersen, Laurent, Uldbjerg, and Eriksen , 2007).

Hospitals in northern Europe recognized the importance of this relationship and conducted a study which analyzed the effect of labour on the biomechanical structure of fetal membranes (Di Lullo, Sweeney, Korkko, la-Kokko, and San Antonio , 2002). This study compared normal vaginal births with periodic regular labour to cesarean births without any labour. The measurements included the content of collagen, HA, and the proteoglycans decorin and biglycan. The study also took into account the location of the sampling point. The two areas of critical importance were the cervical area, where labour has a strong influence, and the middle zone close to the placenta. It was determined that normal vaginal births with regular labour caused a biomechanical change in the cervical amnion, with a decreased amount of collagen and decorin, and an increased amount of biglycan and HA present. Furthermore, it was discovered histologically that HA in a gelatin-like form was accumulated between the two main layers of the fetal membranes, which causes the separation of these layers. This process accelerates the rupture of fetal membranes (Di Lullo, Sweeney, Korkko, la-Kokko, and San Antonio , 2002).

A.2.2. Glycosaminoglycans (GAGs)

In addition to collagens, Glycosaminoglycans (GAGs) are of equal importance to the composition of the extracellular matrix. They are long unbranched polysaccharides, consisting of a repeating disaccharide unit. GAGs are negatively charged and are therefore surrounded by cations, especially Na⁺ anions which are osmotically active (Joerges, Schulz, Wegner, Schumacher, and Prehm , 2012). This affects the absorption of water into the extracellular matrix, which influences swelling of the membrane. This swelling enables the tissue to resist compressive forces, while the collagen works in parallel to resist stretching forces. In the connective tissue as well as in fetal membranes, GAGs represent only 10% of the total weight of fibrous proteins, but due to their hydrated gel properties they occupy most of the space in the extracellular matrix.

This allows them to function as a regulator for the traffic of molecules and cells according to their charge and size (Bruce Alberts, Alexander Johnson, Julian Lewis, Martin Raff, Keith Roberts, and Peter Walter , 2007).

There are two different kinds of GAGs, sulfated and non-sulfated. The sulfated GAGs like chondroitin sulfate, dermatan sulfate, keratan sulfate, heparan sulfate and heparin are covalently attached to a core protein. Hyaluronic acid (HA) belongs to the group of non-sulfated GAGs (Peter von Theobald, Carl W.Zimmerman, and G.Willy Davila , 2011).

In the case of the human fetal membranes, the only existing unsulfated GAG is HA. The main sulfated GAGs are dermatan sulfate and chondroitin sulfate, whereas dermatan sulfate only occurs in very small amounts. It has been observed that as the term approaches full maturity, the concentration of HA increases, while the concentrations of the sulfated GAGs decrease (Skinner and Liggins , 1981).

A.2.3. Collagen

Collagen belongs to the group of fibrous structural proteins whose functions are quite different from those of the group of globular proteins such as enzymes (Werkmeister and Ramshaw , 2012). It is the main protein in the connective tissue of animals, and the most abundant protein in mammals, making up about 25% to 35% of the whole-body protein content (H.Lodish, A.Berk, S.L.Zipursky, P.Matsudaira, D.Baltimore, and J.E.Darnell , 2001). Bundles of collagen, so-called collagen fibers, are the major component of the extracellular matrix that supports most human tissues, and they are generally responsible for counteracting overexpansion of tissue (S.Ayad, R.P.Boot-Hanford, M.J.Humphries, K.E.Kadler, and C.A.Shuttleworth , 1994). The collagen fibers could have a diameter of 10-300 nm and a length of hundreds of micrometers. A typical collagen molecule consists of three left-handed α -chains, which are made of about 1.000 amino-acids, with every third amino-acid being Glycine. This is important because Glycine has the smallest side-chain of all contained amino-acids and is able to fit into the middle of the very closely packed right-handed triple helix, which is built of three α -chains. Hydrogen bonds are responsible for the cohesion of the triple helix. The special characteristics possessed by these collagen fibers are a result of their own three-dimensional structure (H.Lodish, A.Berk, S.L.Zipursky, P.Matsudaira, D.Baltimore, and

J.E.Darnell , 2001;S.Ayad, R.P.Boot-Hanford, M.J.Humphries, K.E.Kadler, and C.A.Shuttleworth , 1994).

The biosynthesis of collagens takes place intracellular and extracellular. Intracellular synthesis proceeds inside and outside of the Golgi apparatus in fibroblasts and epithelial cells. The complete collagen fibers are formed extracellular (H.Lodish, A.Berk, S.L.Zipursky, P.Matsudaira, D.Baltimore, and J.E.Darnell , 2001). A single collagen fiber is a composition of several components. Tropo-collagen, which is a collagen molecule, is formed by three helices; several collagen molecules build up the micro fibrils, and several micro fibrils form fibers. The final result is a fiber bundle, which is formed of collagen fibers. Figure 6 illustrates the composition of a whole collagen bundle.

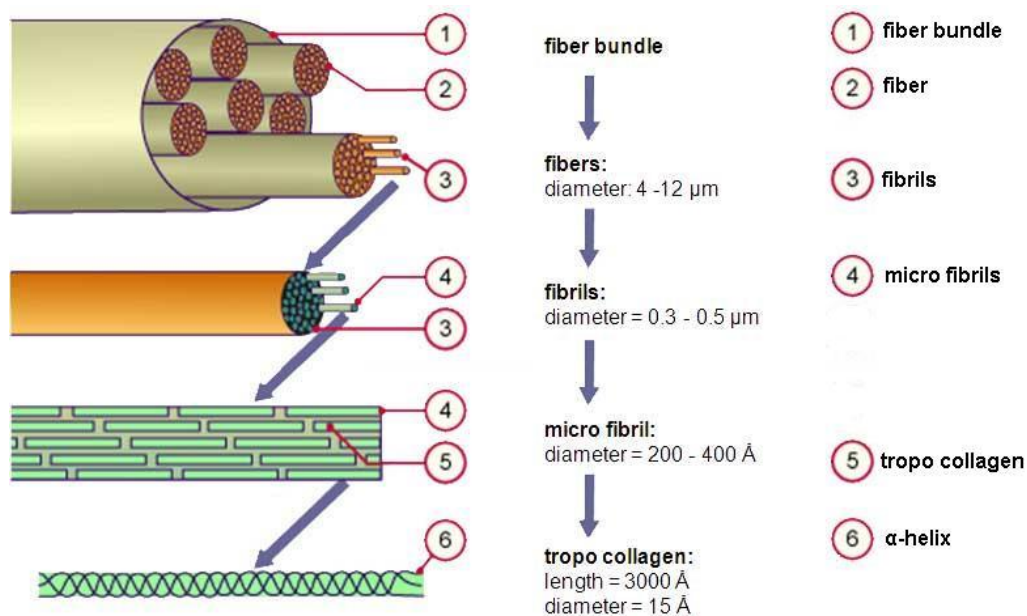


Figure 6: *Composition of a collagen fiber bundle* (S.Ayad, R.P.Boot-Hanford, M.J.Humphries, K.E.Kadler, and C.A.Shuttleworth , 1994).

A.2.4. Collagen in Fetal Membranes

There are 28 different known types of collagen in total, ranging from type I to type XXVIII (M.E.Nimni , 2005). The human fetal membrane is a collagen-containing tissue, whose mechanical characteristics resemble that of other soft tissues rich in type I collagen. However, the extracellular matrix also contains more collagen types, with

different characteristics like type III, IV, V and VI. Type I provides structural integrity to collagenous tissues because of its characteristics (Joyce, Moore, and Sacks , 2009). Type I is inherently crimped and can be found in the amniotic compact layer (Joyce, Moore, and Sacks , 2009). In its stress-free state, it has an undulated form. The following figures demonstrate different states of undulation at a specified level of stretch (λ), and how collagen fibers are behaving.

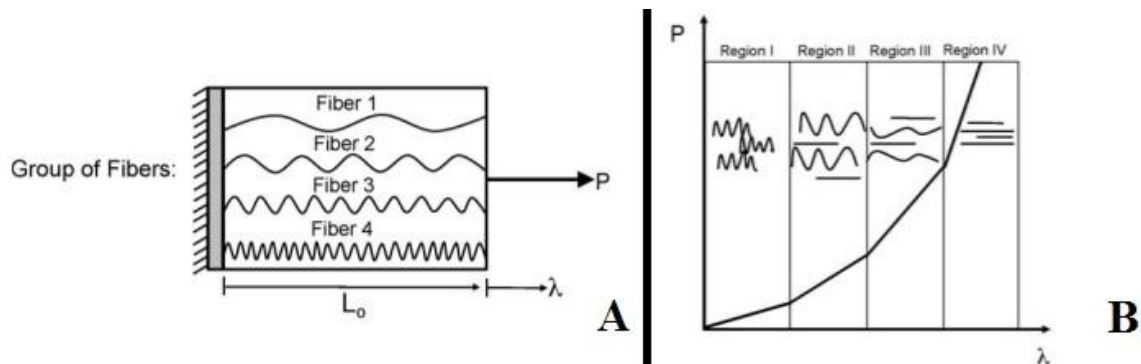


Figure 7: *Group of collagen fibers. Stretch (λ): A measure of deformation defined as $\lambda = L/L_0$, where L is the current length of the fiber and L_0 is the original length. Gradual recruitment of collagen fibers results in a non-linear stress strain relationship (Regions I, II, III). Once all collagen fibers straighten, the stress–stretch curve transitions into a linear region (Region IV) (Joyce, Moore, and Sacks , 2009).*

The examples of collagen fibers cited each have separate degrees of undulation and are thus at a different levels of stretch (λ). Fiber 1 has the least amount of collagen crimp, and so it straightens first. With increasing λ , Fiber 2 straightens, followed by Fibers 3 and then 4. At the bulk tissue level, this phenomenon translates to a non-linear P – λ response. In Region I of the P – λ response, most of the collagen fibers are crimped. However, with increasing λ , more and more fibers straighten and begin to support load (Regions II and III). Once all collagen fibers have straightened, the P – λ curve enters into a linear region (Region IV) (Joyce, Moore, and Sacks , 2009).

When this knowledge is transferred to the fetal membranes, it demonstrates that with increased stretching of the amnion and the chorion, the crimped collagen fibers begin to straighten. It was shown for example by Arikat’s study that the chorion always ruptures before the amnion layer (Skinner, Campos, and Liggins , 1981). This could be caused by the fact that in comparison to the amnion, the main types of collagen present in the

chorion consists of collagen type III, which is composed of thin reticular fibers. Interestingly, collagen type III differs greatly from type I, with respect to elasticity. Type III collagen is more elastic than type I, but the tear strength of type I is greater (H.Lodish, A.Berk, S.L.Zipursky, P.Matsudaira, D.Baltimore, and J.E.Darnell , 2001).

Other studies have also shown that in general, the concentration of collagen in the amnion of women having either fullterm or preterm births is lower with PROM than without PROM (Kanayama, Terao, Kawashima, Horiuchi, and Fujimoto , 1985). This observation indicate that FMs of births without PROM is more strength than FMs of births with PROM.

A.3 Type of Births

While both fullterm and preterm births and their variations have been previously discussed, they have not been clearly defined. Newborns are defined as a “preterm” if the gestational age is younger than 37 weeks, and “fullterm” stands for births taking place between 37-42 weeks of gestation (Ascencio, Collinet, Cosson, and Mordon , 2007;Carrascosa, Yeste, Copil, Almar, Salcedo, and Gussinye , 2004;Holanda and Melo , 2006). Prelabour rupture of membrane (PROM) can occur in both at fullterm and preterm births.

When birth occurs at fullterm without any PROM is called normal birth (NB). Similarly, if the birth occurs at preterm without any PROM is called preterm birth (PRB) (Holanda and Melo , 2006). However, if PROM occurs at fullterm, it is called prelabour rupture of membrane birth (PROMB), and if the PROM occurs at preterm then it is called preterm prelabour rupture of membrane birth (PPROMB)(Medina and Hill , 2006). In most cases PROMB occurs rather than PPROMB (Medina and Hill , 2006).

Birth Types	Abbreviation	Week of Gestation (WOG)
<i>Normal birth</i> ; birth occurs at fullterm without any prelabour rupture	NB	37 WOG < NB < 42 WOG
<i>Prelabour rupture of membrane birth</i> ; birth occurs at fullterm with prelabour rupture	PROMB	37 WOG < PROMB < 42 WOG
<i>Preterm birth</i> ; birth occurs at preterm without any prelabour rupture	PB	PROMB < 37 WOG
<i>Preterm prelabourruptre of membrane birth</i> ; birth occurs at preterm with prelabour rupture	PPROMB	PROMB < 37 WOG

Table 2: Terminology of birth types.

A.3.1 Prelabour Rupture of the Fetal Membrane (PROM)

PRB is a leading cause of perinatal and neonatal mortality (Gratacos, Sanin-Blair, Lewi, Toran, Verbist, Cabero, and Deprest , 2006). The shorter the duration of gestation, the greater is the risk of mortality and morbidity (Gratacos, Sanin-Blair, Lewi, Toran, Verbist, Cabero, and Deprest , 2006). The etiology of PRB remains inadequately understood however, many biochemical investigations have been undertaken in an attempt to determine the cause, or causes. In most pregnancies, labour begins at full term with an intact fetal membrane (Alger and Pupkin , 1986). However, PROM occurs in 10% of pregnancies at full term (Mead , 1980) and exceed 40% of pregnancies at preterm (Keirse , 1989). There are major and minor factors in a significant portion of preterm labour and PROM.

Fetal mortality is a serious issue. “Fetal mortality refers to the intrauterus death of a fetus at any gestational age (MacDorman and Kirmeyer , 2009). The National Survey of Family Growth estimates about 1 million fetal losses per year in the United States (Ventura, Abma, Mosher, and Henshaw , 2008) in 2008 with the vast majority of these occurring before 20 weeks of gestation (MacDorman and Kirmeyer , 2009).”

The National Vital Statistics System typically only displays data about fetal mortality for fetal deaths which have reached 20 weeks of gestation or more (MacDorman and Kirmeyer , 2009). Nonetheless, there are nearly as many fetal deaths as infant deaths in the US, even when only fetal deaths of 20 weeks or more are considered (MacDorman and Kirmeyer , 2009). A focus on fetal mortality may provide further opportunities for prevention.

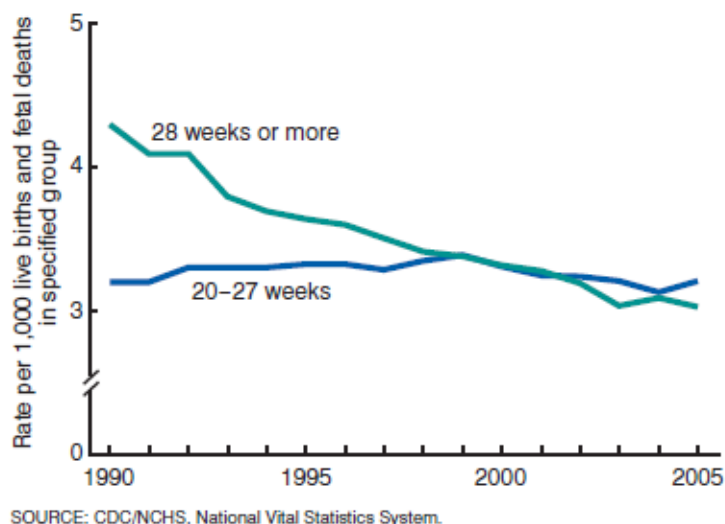


Figure 8: *Fetal mortality versus period of gestation graph: United States, 1990 – 2005. Data is presented according to maternal age, marital status, race, Hispanic origin, and state of residence; and by fetal gestational age at delivery, birth weight, plurality, and sex (MacDorman and Kirmeyer , 2009)*

Identifying at risk pregnancies is important, because advanced diagnostic and treatment methods and systems could be applied to provide optimal care for the mother and baby. As family planning becomes increasingly accepted, the importance of a satisfactory outcome of each pregnancy is emphasized. A variety of maternal or fetal diseases influence the outcome of pregnancies (Lubchenco, Searls, and Brazie , 1972). Mortality risk is based on both birth weight and gestational age (Lubchenco, Searls, and Brazie ,

1972). If maternal or fetal diseases exists, the relative risk of preterm delivery can be balanced against the risk of the basic disease when the pregnancy continues (Lubchenco, Searls, and Brazie , 1972). Moreover, after a baby is delivered, the risk, based on the birth weight and gestational age, can be used to anticipate the need for special care (Lubchenco, Searls, and Brazie , 1972). Generally, pregnancy complications and health problems in mother or in the fetus cause preterm deliveries (Iams , 2003).

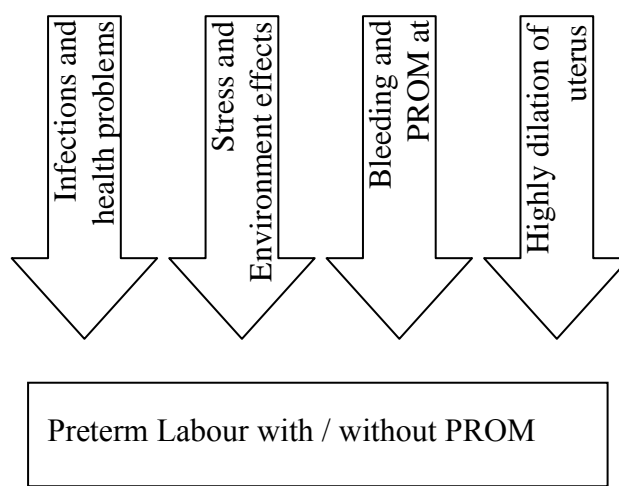


Figure 9: *Conditions and mechanisms that can lead to a preterm birth.*

There are several risk factors associated with PRB (Coleman AC , 1998) with prelabour rupture (PPROMB) which depend heavily upon the expecting mother. These risk factors include: dehydration, serious infections with fever during the pregnancy, recurring bladder and/or kidney infections, excessive amount of amniotic fluid, using recreational drugs, such as cocaine or amphetamines, domestic violence, extreme emotional or physical stress, smoking more than 10 cigarettes per day, carrying more than one baby, more than two second trimester miscarriages or elective abortions, abdominal surgery during pregnancy and/or cervical cerclage and also premature labour or delivery during a previous pregnancy (Coleman AC , 1998). The occurrence of these risk factors is not guaranteed to induce preterm labour however, the probability of preterm labour increases with PROM (Coleman AC , 1998).

A.4 Medical Versus Parental Care

Infants whom are born prior to 37 WOG and show physical signs of preterm effects may develop other problems. The earliest gestational age at which the infant may survive is referred to as the limit of viability (Aijaz Farooqi , 2008). When PROM occurs prior to the limit of viability, a prediction of gestation age should be calculated using the earliest available ultrasound and menstrual history (John T.Queenan, John C.Hobbins, and Catherine T.Spong , 2005). These patients should be advised with a realistic appraisal of potential fetal and neonatal outcomes (John T.Queenan, John C.Hobbins, and Catherine T.Spong , 2005). Regarding maternal morbidity, the management of PROM is associated with a high risk of choriamnionitis, endometritis, abruptio-placenta, and retained placenta with postpartum hemorrhage requiring curettage (John T.Queenan, John C.Hobbins, and Catherine T.Spong , 2005). The following applications can be applied to a mother to better manage this period of time:

- **Labour Induction:** High intravenous dose of oxytocin, and/or intravaginal prostaglandin E₁ and E₂, according to individual clinical circumstances (John T.Queenan, John C.Hobbins, and Catherine T.Spong , 2005).
- **Dilatation and evacuation:** Intracervicallaminaria placement prior to labour induction or dilation and evacuation may be helpful (John T.Queenan, John C.Hobbins, and Catherine T.Spong , 2005).
- **Conservative management:** Infection should be observed. Several ultrasounds are recommended to evaluate for fetal pulmonary growth. Antibiotic therapy can be applied to women with PROM before 23 WOG (John T.Queenan, John C.Hobbins, and Catherine T.Spong , 2005).

Many problems also exist for infants. General problems for infants younger than 34 WOG include jaundice, hypocalcemia, respiratory distress syndrome, prematurity-retinopathy, bronchopulmonary dysplasia, intracranial hemorrhaging andnecrotizing enterocolitis (E.Harris Ruddochk and T.Miller Neatby , 2005). Even if the infant survives, there is a risk of brain damage and developmental delay. As a result, the aggressiveness of care rendered to the infant in such circumstances has become an ethical controversy (Aijaz Farooqi , 2008).

The required care for premature infants differs greatly depending on the WOG, weight, and overall maturity. Other specific infant and family related issues might require additional attention (Dara Brodsky and Mary Ann Ouellette , 2007).

Infant Issues:

- Infant must have a stable respiratory status and be able to maintain acceptable oxygen saturations (Dara Brodsky and Mary Ann Ouellette , 2007).
- Infant should demonstrate appropriate weight gain on enteral feedings (Dara Brodsky and Mary Ann Ouellette , 2007).
- Medication regimens should not have any recent changes that would cause adverse effects (Dara Brodsky and Mary Ann Ouellette , 2007).
- Respiratory syncytial virus and influenza prophylaxis should be administered during appropriate high-risk months (Dara Brodsky and Mary Ann Ouellette , 2007).

Parents often have difficulty transitioning in parenthood. This affects their child's care, since they are unable to fulfill their expected roles. Studies have shown that the transition to parenthood for parents of preterm infants follows a different and longer course than that of parents with full-term infants, because there are some factors which have to be done by the parents.

Family Factors:

- An extensive teaching protocol should be followed (Dara Brodsky and Mary Ann Ouellette , 2007).
- The family must be able to count respiratory rate as well as identify retractions, nasal flaring, and grunting (Dara Brodsky and Mary Ann Ouellette , 2007).
- The family must have the ability to transport the child for follow-up appointments (Dara Brodsky and Mary Ann Ouellette , 2007).

This illustrates how delaying a premature birth can be from an economic and social aspect, an effective way to avoid or at least minimize infant and parental problems. However, determining the probability of a premature birth is still an unsolved mystery. All too often, deliveries have to be induced artificially or by Cesarean means, despite

weeks of total rest for the mother. The only way to prevent from effects of this problem by is designing a new diagnostic tool which can predict the risk factor of PROM.

B. Prediction Methods

B.1 Existing Methods in the Prediction of Preterm Birth

Despite advances in perinatal care, the incidence of preterm birth continues to rise, primarily because of the increased multiple pregnancies resulting from assisted reproduction (Lim, Butt, and Crane , 2011). The costs associated with preterm birth are substantial in economic, social and emotional terms. Clinical diagnosis of true preterm labour can be difficult because symptoms and signs of preterm labour can also occur during normal pregnancies (Pircon, Strassner, Kirz, and Towers , 1989; Jackson, Ludmir, and Bader , 1992). The best clinical indicators of preterm delivery occurring 24 h to 7 days prior to labour are: initial cervical dilatation ≥ 3 cm, cervical effacement $\geq 80\%$, vaginal bleeding, and ruptured membranes. While specific, these signs usually appear too late to allow effective intervention (Botsis, Makrakis, Papagianni, Kouskouni, Grigoriou, Dendrinou, and Creatsas , 2006). On the other hand, there is still no useful clinical method available to predict PPRM. Obviously more precise, cost effective, and reliable strategies for predicting and preventing preterm labour and birth are urgently needed. Various methods of predicting preterm labour have been studied and are described below. Although multiple methods of predicting preterm birth are available, none of them have been routinely used. There is no standard technique used to predict preterm births or diagnose prelabour rupture in advance. A unique medical device would have to be developed to predict preterm births, and would be especially necessary for predicting prelabour ruptures.

B.1.1. Risk Scoring Systems

Risk scoring systems have been developed in order to identify women at increased risk of preterm delivery. Within these systems there are different ratings for each symptom that can be associated with preterm birth. As it can be understood that there should be some symptoms” to form a risk scoring system. Each symptom, such as a history of preterm birth, multiple pregnancies, race, low socioeconomic class, low body-mass

index, cigarette smoking, drug and alcohol abuse, extremes of reproductive life and numerous obstetric and medical disorders, have their own respective intensity values and are collected from patients by a physician. After that, the scores are calculated by summing the frequency and intensity ratings for each symptom to determine the risk of preterm delivery. However, the risk scoring system performs poorly in practice. They have a low predictive value and show poor reproducibility between different populations (Keirse , 1989).

B.1.2. Home Uterus Activity Monitoring

Home uterus activity monitoring (HUAM) was developed in the 1980s and was suggested for reducing the incidence of preterm birth. It was anticipated that HUAM would provide predictive information about the risk of preterm labour in women already known to be at increased risk of preterm labour (Chuileannain and Brennecke , 1998). HUAM depends on daily uterus self-palpation and weekly telephone contact with trained nursing staff that provide education, support and advice. There has been an argue against its utility in clinical practice and it is thought that the program did not improve pregnancy outcomes, but rather increased the number of unscheduled visits to obstetricians and increased the rate of administration of prophylactic to colytic drugs (Chuileannain and Brennecke , 1999). HUAM is an expensive tool and it requires considerable compliance and dedication on the part of the patient. Well-designed randomized controlled trials are still required to assess the usefulness of HUAM in predicting preterm labour (Chuileannain and Brennecke , 1998).

B.1.2. Cervical Assessment

Cervical dilatation and cervical shortening are clinically relevant to an increased risk of preterm labour. In the past, the cervix was assessed by digital examination and trans abdominal ultrasound but both methods had limitations. Digital assessment of the cervical length is subjective; it varies between examiners, and underestimates true anatomic length. Besides, today's trans abdominal ultrasonography is not recommended to use for cervical length assessment to predict preterm birth. As ultrasonography equipment and techniques have improved, high resolution imaging of the cervix and lower uterus segment has become possible. Use of this technology found that the risk of preterm birth was inversely correlated to the length of the cervix as measured by

ultrasound (Lim, Butt, and Crane , 2011). Nowadays, cervical length evaluated with the use of transvaginal ultrasonography seems to be a useful tool for the prediction of true preterm labour and delivery (Botsis, Makrakis, Papagianni, Kouskouni, Grigoriou, Dendrinou, and Creatsas , 2006;Tsoi, Akmal, Rane, Otigbah, and Nicolaides , 2003). However, cervical length in the general obstetrical population is relatively stable over the first 6 months, with no consensus on the optimal timing or frequency of serial evaluations of cervical length. Furthermore, while transvaginal ultrasounds appear to be safe in preterm premature rupture of membranes, its clinical predictive value is uncertain (Lim, Butt, and Crane , 2011). In conclusion, due to the poor positive predictive values and sensitivities, as well as the lack of proven effective interventions, routine transvaginal cervical length assessments are not recommended for women at low risk (Lim, Butt, and Crane , 2011).

B.1.3. Fetal Fibronectin Test

Remodelling of the extracellular matrix (ECM) of the amnion, chorion, decidua and myometrium occurs prior to the onset of labour. It has been hypothesized that disruption of the chorionic-decidual interface precedes the onset of preterm labour (Lockwood, Senyei, Dische, Casal, Shah, Thung, Jones, Deligdisch, and Garite , 1991). Remodelling may lead to a disruption between the chorionic-decidual interface and the ECM components, like fetal fibronectin (fFN), which can merge in cervicovaginal fluid. At this point, biochemical markers of this disruption may prove to be useful clinical screening tools in the prediction of preterm labour (Chuileannain and Brennecke , 1999). The presence of fFN in cervicovaginal fluid at concentrations higher than 50 ng/ml from 21 to 37 weeks gestation is considered abnormal and indicative of impending preterm labour (Lockwood, Senyei, Dische, Casal, Shah, Thung, Jones, Deligdisch, and Garite , 1991). Therefore, a reasonable conclusion concerning fetal fibronectin in cervicovaginal fluid in the late second and early third trimesters is that it is an important risk factor for spontaneous preterm labour and delivery in asymptomatic women carrying multiple pregnancies (Goldenberg, Iams, Miodovnik, Van Dorsten, Thurnau, Bottoms, Mercer, Meis, Moawad, Das, Caritis, and McNellis , 1996).

B.1.4. Cytokines

The role of inflammatory cytokines such as interleukin-1 β , tumour necrosis factor α , interleukin-6 (IL-6) and interleukin-8 (IL-8) in the initiation of labour both at term and preterm has been studied (Keelan, Coleman, and Mitchell , 1997). Most of the work to date has focused on IL-6. IL-6 helps propagate the local inflammatory cytokines, it stimulates gestational tissues to produce prostaglandin which, in turn stimulates uterus contractions and cervical ripening (Chuileannain and Brennecke , 1999). Elevated amniotic fluid concentrations of IL-6 at the time of amniocentesis in the second trimester are associated with an increased risk of miscarriage or preterm birth (Greig, Murtha, Jimmerson, Herbert, Roitman-Johnson, and Allen , 1997). The clinical utility of measuring amniotic fluid concentrations of IL-6 is limited in clinical practice because of a reluctance to perform amniocentesis in women in preterm labour (Chuileannain and Brennecke , 1999). Limited and conflicting data are available on the clinical utility of measuring cervicovaginal concentrations of IL-6 in the prediction of preterm labour (Chuileannain and Brennecke , 1999).

B.1.5. Matrix Metalloproteinases

The tissue matrix metalloproteinases are a family of zinc-binding endopeptidases that are capable of degrading collagens, which are the main components of the amnion and chorion (Chuileannain and Brennecke , 1999). Increased activity of this family, matrix metalloproteinase-9, has been found to be associated with preterm premature rupture of the membranes and normal labour (Romero, Ceska, Avila, Mazor, Behnke, and Lindley , 1991). The place of these biochemical markers as clinically useful predictors of preterm labour awaits further appropriately designed clinical studies.

B.1.6. Additional Markers

Elevated maternal plasma concentrations of corticotrophin-releasing hormone (CRH), serum ferritin concentrations during the second trimester, serum placental alkaline phosphate concentrations are associated with an increased risk of preterm labour. It is also known that maternal serum activin-A concentrations are elevated in women in preterm labour and unexplained elevations in maternal serum α -fetoprotein are associated with preterm delivery. Premature birth is a sophisticated subject and has yet

to be fully understood. Apart from these, different markers can be determined. Nowadays, there are also some commercial markers on the market whose results are notable. Additional work on all of these potential biochemical markers is required in order to determine their effectiveness in clinical practice.

B.2. Existing Technology That Can Be Used in the Prediction of Preterm Birth

Existing methods are not enough for diagnosing potential pregnancy complications. Physicians need reliable and practical data to make good decisions. New optical imaging technology is aiding physicians in their effort to diagnose and treat patients by providing new options and techniques to analyze tissues. These parameters can be used to design new kinds of medical devices. These devices can be used either for diagnosing or during treatment. These improvements could help physicians make informed decisions.

B.2.1. Optical Techniques

Optical techniques play a significant role in biology, because they supply safe and low-cost solutions to many matters. The following section describes three types of optical techniques used in the laboratory for diagnostic purposes.

B.2.2. Spectrophotometer

During the past 20 years, the use of optical techniques in the biological sciences has grown substantially. The functioning principle of a spectrophotometer is based on the coaction of two instruments, a spectrometer and a photometer (Donald L.Pavia, Gary M.Lampman, George S.Kriz, and James R.Vyvyan , 2000). The spectrometer produces light of multiple wavelengths, and the photometer receives and analyzes this light. The instruments have to be arranged in such a way that a sample, such as a fluid in a cuvette, could be placed in the light beam between the spectrometer and the photometer. The photometer measures the strength and wavelengths of the light which pass through the sample without being absorbed (Donald L.Pavia, Gary M.Lampman, George S.Kriz, and James R.Vyvyan , 2000).

This absorption of light is the primary functioning principle behind spectrophotometers. A light beam consists of photons, which molecules within the tissue sample are capable

of absorbing, depending on the characteristics of the tissue. Every photon that is absorbed reduces the number of photons in the light beam, and thereby its intensity. The photometer receives the light which has penetrated through the sample, and converts this into an analog electric current. This current is then used to create a graph of the absorption characteristics of the tissue at different transmitted wavelengths of light (Donald L.Pavia, Gary M.Lampman, George S.Kriz, and James R.Vyvyan , 2000;Joseph R.Lakowicz , 2010).

A fundamental aspect of spectroscopy is the measurement of light absorption. The basic principle of light absorption is based on the Lambert-Beer law (Donald L.Pavia, Gary M.Lampman, George S.Kriz, and James R.Vyvyan , 2000;Joseph R.Lakowicz , 2010). This law says that there is a linear relationship between absorbance of light, and the concentration of the absorbing sample that can be measured.

Lambert-Beer law:

$$A = \epsilon(\alpha) \times b \times c$$

A: absorbance, $\epsilon(\alpha)$: molar absorptivity [L/(mol·cm)], b: path length of the cuvette in which the sample is contained [cm], c: concentration of the compound solution [mol/L].

Using Beer's law, the concentration of absorbing material or solute present can be calculated by determining the amount of light absorbed by the sample. Spectrophotometry uses a given wavelength of light, typically between 190 and 900 nm and can be used to determine the color property of the amniotic liquid in vivo.

B.2.3. Autofluorescence

Autofluorescence diagnosis is an optical process which is based on the detection of a fluorescent endogenous spectrum in the tissues of the body (Vladimir N.Uversky and Eugene A.Permyakov , 2007;Kakizoe, Kobayashi, Shimoura, Hattori, and Jidoi , 1992). Fluorescence is a kind of luminescence and occurs if a molecule, atom or nanostructure relaxes to its ground state after being electrically excited. This excitation could be introduced by electric fields (electroluminescence), chemical reactions (chemiluminescence, bioluminescence) or by optical stimuli (photoluminescence) (Vladimir N.Uversky and Eugene A.Permyakov , 2007). Photoluminescence can be

classified into fluorescence and phosphorescence. The Jablonski energy level-diagram illustrates the fluorescence emissions; the phosphorescence is of no importance for this example and can be neglected (Figure 10).

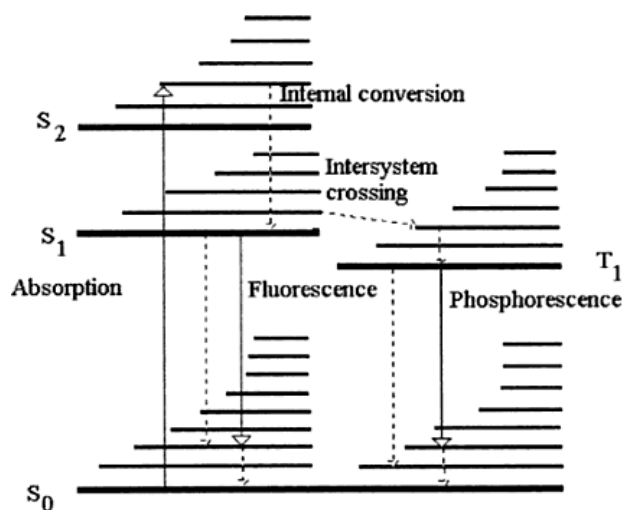


Figure 10: Jablonski scheme of fluorescent and phosphorescent energy levels in multiatomic molecules, with transitions shown (Tang, Zeng, Savage, Ho, and Alfano , 2000).

Absorption of light quantum elevates the energy level of a molecule from the ground state S_0 to one of the vibration levels of the excited states S_1 , S_2 , and so on. In a condensed medium, the energy of the excited state S_2 or any other higher states rapidly dissipates due to inelastic collisions, depleting the energy level of the molecule until it reaches the zero vibration level of the state S_1 , without emitting of light (Wiemer , 2009). The radiationless transitions between electronic states of the same multiplicity are called internal conversion. Fluorescence occurs if a molecule in electronically excited state can reach its ground state due to spontaneous or forced emission of a light quantum. The forced emission requires the presence of an external electromagnetic field affecting the molecule. This method is used to measure the spectrum of light emitted by the tissue and is different from spectrophotometric measurements which, measures the light passing through the tissue. In other words, autofluorescence measures the light emission spectrum of a tissue sample (Kakizoe, Kobayashi, Shimoura, Hattori, and Jidoi , 1992; Kimura, Tsushima, Yoshizaki, and Nakayama , 1988).

B.2.3.1. Special Autofluorescence Characteristics of Collagen

As was previously described in section A.2.4., the important type of collagen for the stability of the fetal membranes is collagen type I in the amniotic layer (Wiemer , 2009). Thus it is important to know the autofluorescent characteristics of type I collagen, in order to identify the wavelength-peaks during fluorescent excitation and emission spectra of type I collagen in tissue samples.

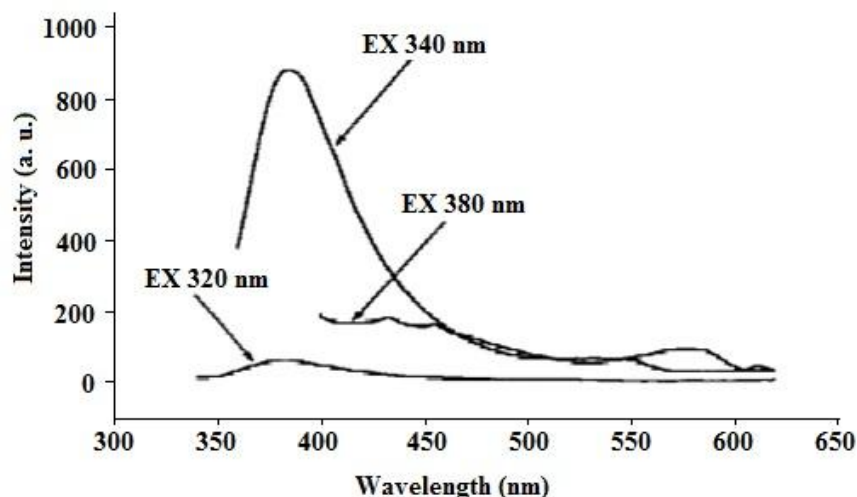


Figure 11: *Fluorescent emission of pure collagen type I at different excitation levels, using a high-pressure xenon lamp (Wiemer , 2009).*

As figure 11 demonstrates, a fluorophoric substance like collagen can have different absorption-maxima at variable wavelengths of excitation. We can see three graphs of pure collagen type I with different maxima of emission, which are created at 320nm, 340nm and 380nm of excitation.

It is obvious that the most intensive fluorescent emission occurs at an excitation wavelength of 340nm. A strong, but very narrow emission peak for this graph can be found at 390nm. Outside of this range, the intensity decreases rapidly. The third graph with 380nm of excitation is five times weaker than the second one at 340nm, but it has 3 small local maxima at 400nm, 430nm and 460nm, which broadens the bandwidth. The first graph with 320 nm also has just one peak which, is close to the peak-wavelength of the second graph. However, this frequency produces the weakest intensity of all, and

therefore was neglected as a choice of final excitation wavelength. As a result of these graphs, there are two possible excitation wavelengths for fluorescence measurements.

The first wavelength for excitation is at about 335/340 nm and has a strong and sharp emission at 390 nm.

The second wavelength for excitation is at about 370 nm and has a broader, but less intensive emission at 440 nm.

B.2.4. Optical Coherence Tomography

Optical coherence tomography (OCT) is an emerging imaging technology in the biomedical science and medicine fields. OCT performs high resolution, cross-sectional imaging of biological tissues by measuring echoes of backscattered light (Huang, Wang, Lin, Puliafito, and Fujimoto , 1991). Tissue pathology can be imaged in situ and in real time with resolutions of 1–15 μm , one to two orders of magnitude finer than conventional ultrasound. The unique features of OCT make it a powerful imaging technology, which promises to enable many fundamental research and clinical applications (Drexler and Fujimoto , 2008).

OCT technology is similar to ultrasound technology however, it uses low coherence light instead of sound (Mark Brezinski , 2006). OCT techniques enable high-resolution, non-invasive (without touching the surface) in-vivo imaging, so it is possible to examine microstructures of tissues up to depth of 2 mm. The depth of imaging is naturally dependent upon the type of tissue being examined, due to reflective indexes.

“OCT performs cross-sectional imaging by measuring the magnitude and echo time delay of backscattered light. Cross-sectional images are generated by performing multiple axial measurements of echo time delay (axial scans or A-scans) and scanning the incident optical beam transversely, as shown in Figure 12. This produces a two-dimensional data set, which represents the optical backscattering in a cross-sectional plane through the tissue. Images, or B-scans, can be displayed in false color or grey scale to visualize tissue pathology. Three-dimensional, volumetric data sets can be generated by acquiring sequential cross-sectional images by scanning the incident optical beam in a raster pattern. Three-dimensional OCT (3D-OCT) data contain

comprehensive volumetric structural information and can be manipulated similar to MR or CT images.” (Drexler and Fujimoto , 2008).

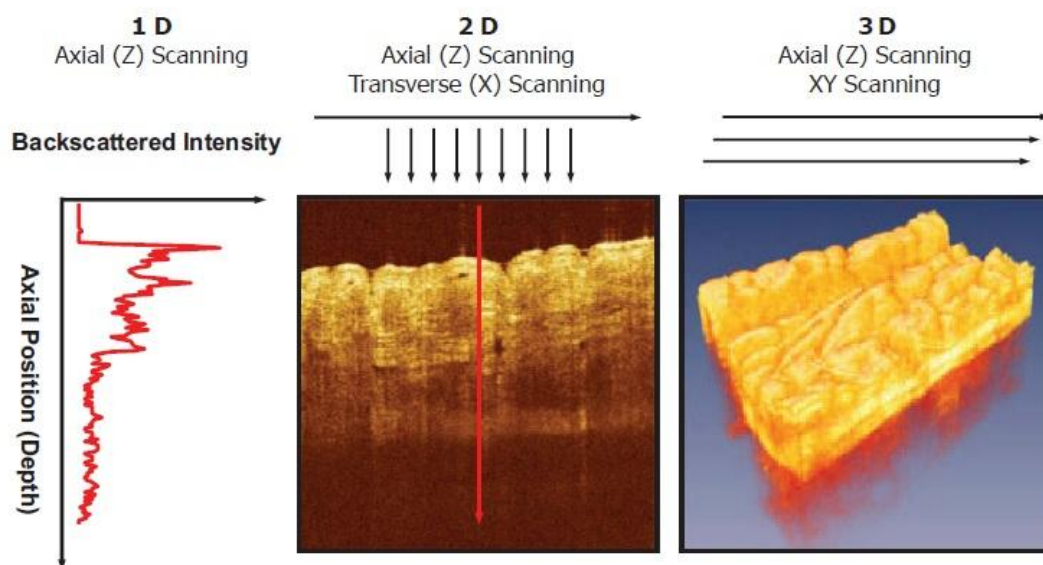


Figure 12: “OCT generates cross-sectional or three-dimensional images by measuring the magnitude and echo time delay of light. Axial scans (A-scans) measure the backreflection or backscattering versus depth. Cross-sectional images are generated by performing a series of axial scans at different transverse positions to generate a two-dimensional data set (B-scan), which is displayed as a grey scale or false color image. Three-dimensional data sets (3D-OCT) can be generated by raster scanning a series of two-dimensional data sets (B-scans).” (Drexler and Fujimoto , 2008).

OCT is a powerful imaging technology in medicine because it performs “optical biopsy;” the real time, in situ visualization of tissue microstructure, without removing and processing specimens (Fujimoto, Brezinski, Tearney, Boppart, Bouma, Hee, Southern, and Swanson , 1995;Brezinski, Tearney, Bouma, Izatt, Hee, Swanson, Southern, and Fujimoto , 1996). Due to the fact that optical interferometry has become one of the favorite tools used by the scientists to solve many problems (Mark Brezinski , 2006). Over the last decade, the field of medicine has been supported by a multitude of low coherence imaging technologies, broadly sorted under the terms ‘low coherence interferometry’ or ‘optical coherence tomography (OCT).

Interferometry is a powerful technique in the measurements of the magnitude and echo time delay of backscattered light with very high sensitivity (Drexler and Fujimoto , 2008). OCT is based on a low-coherence interferometry, or white light interferometry,

first described by Sir Isaac Newton. Low-coherence interferometry was used in photonics to measure optical echoes and backscattering in optical fibers, and was also used in waveguide devices in the 1980s (Drexler and Fujimoto , 2008;Takada, Yokohama, Chida, and Noda , 1987;Youngquist, Carr, and Davies , 1987).

Interferometry techniques correlate the interference between light that is backscattered from the tissue to the light that has traveled a known distance or time delay through a reference path, to perform an analysis of the sample. Interferometry measures the field of the light rather than its intensity (Drexler and Fujimoto , 2008).

Spectral/Fourier domain OCT detection uses a broad-bandwidth light source and detects the interference spectrum from the interferometer, using a spectrometer and a line scan camera (Wojtkowski, Leitgeb, Kowalczyk, Bajraszewski, and Fercher , 2002;Drexler and Fujimoto , 2008;Youngquist, Carr, and Davies , 1987). The system uses Fourier-Domain technology to determine the optical properties of a sample by analyzing the back reflected and scattered light from an illuminated volume of the sample. The light of a broadband light source is guided nearly perpendicular to the sample, using a narrow focus to achieve an illuminated volume with a small lateral dimension. This leads to a good lateral measurement resolution. The returning light signal travels to the spectrometer and the depth information is processed via a Fast-Fourier-Transformation (FFT).

The two main properties of the scanned image are the axial and lateral resolutions. The axial resolution is not dependent on the optics; it is driven by the spectral bandwidth of the light source and is therefore in the range of less than 10 μm . The lateral resolution on the other hand, is affected by the chosen optical setup and the numerical aperture of the application optic. Figure 13 describes the basic working principle of the OCT. Light is generated by a low coherence light source and directed to a fiber optic coupler. The coupler is assumed to split the incident optical power evenly into two halves by a beam splitter. One half is directed onto a sample and the other half of the light is directed to the reference arm. Then these lights are reflected back by mirrors and recombined by a beam splitter and directed at the detector. If the path lengths match to within a coherence length, interference will occur (Mark Brezinski , 2006). OCT measures the intensity of interference and uses it to represent back reflection intensity (Mark Brezinski , 2006).

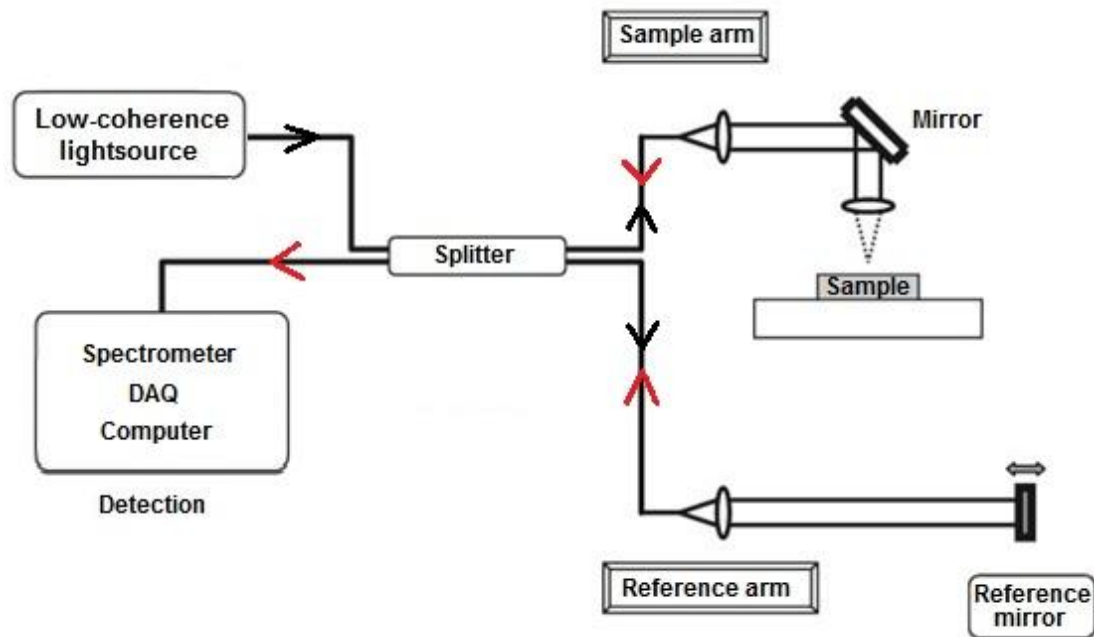


Figure 13: A simplified schematic of an interferometer. The source light is divided into two parts by a beam splitter. Half of the light is directed onto a sample via the sample arm, while the other half of the light is directed into a mirror attached to the reference arm. Light is reflected back from both arms by mirrors (from the sample and reference arms) and are recombined at the beam splitter. Part of the light is then directed into a detector (Mark Brezinski , 2006).

The OCT system can be used to noninvasively assess normal and abnormal tissue in vivo. The use of noninvasive OCT imaging could have broad applications for screening, detection, and surgical-margin planning, including allowing surgeons to identify margins in vivo without obtaining frozen sections. OCT is one of many promising optical techniques for the early detection of biological disorders, and can be used for diagnosing prelabour ruptures at birth.

C. Purpose, Questions, Tasks and Suggestions of This Study

Identifying the mechanical characteristics of fetal membranes which ruptured after the onset of labour may help to improve our understanding of the mechanisms involved in rupture before the onset of labour. This knowledge is also essential in order to understand how changes in the fetal membrane can influence the likelihood of prelabour rupture.

The focus of this work was to investigate the mechanical properties of different types of FM, obtained directly after birth. In this study, the mechanical properties such as thickness, bursting pressure, and average stress-strain ratio of the fetal membranes were measured in-vitro using engineering approaches in all birth types, including: normal birth (NB), preterm birth (PRB), prelabour rupture of membrane birth (PROMB) and preterm prelabour rupture of membrane birth (PPROMB).

The physical sample sizes of the FM were minimized (8cm X 8cm) to allow multiple experiments to be conducted on each FM. Sample sizes were also reduced to promote the mapping of the membrane, in order to find out if there is any relation between the location of the sample and the mechanical stability and properties.

A unique device called DIMPAST (**D**evice for the **I**nvestigation of the **M**echanical **P**roperties of the **A**mniotic **S**ac **T**issue) was designed and used to measure all of the mechanical properties of the FM. Its functioning principle is based on Cell-Drum technology, which was developed and presented in previous studies (Linder, Trzewik, Ruffer, Artmann, Digel, Kurz, Rothermel, Robitzki, and Temiz , 2010). In this way, the mechanical parameters of the fetal membranes were assessed while the physiological conditions were simulated. The results were then used to design a new, technologically advanced diagnostic tool which included a fiber optic fluorescence, and a fiber optic OCT probe.

The first version of the diagnostic tool, which contains a fiber optic probe, was produced and tested to obtain preliminary data for the future scope. This data will be used to detect and correct errors on the current version of the diagnostic tool, as well as to develop a better diagnostic tool for the in-vivo examination of patients. The final version of the diagnostic tool, which will be looked like a prediction probe, will be a combination of the OCT and fluorescence probe.

In-vivo examination process may help to more accurately determine the risk of a prelabour rupture during pregnancy. This would also assist in defining the critical parameters needed to design a specialized in vivo probe. Depending on the development of the instrumentation and data, we will apply for research grants and continue our industry contacts.

3 Methods

3.1 Device for the Investigation of the Mechanical Properties of the Amniotic Sac Tissue (DIMPAST)

3.1.1 Measurement Principle

The main idea was to apply a load to our tissue samples that mimics physiological conditions. Thus, the methods known from regular material science – for instance uniaxial stretching – were not applicable. Additionally, other methods used before – like penetration with a defined probe – did not accurately simulate physiological conditions. Therefore, it was decided that a balloon like system based on the Cell Drum technology would be used, since it more accurately mimics physiological conditions (Linder, Trzewik, Ruffer, Artmann, Digel, Kurz, Rothermel, Robitzki, and Temiz , 2010). The first step when preparing for a test using this technology is to place the tissue in the tissue holder, and stabilize it with a tissue fixing ring (Figure 14A). This forms a tissue chamber (Figure 14B).

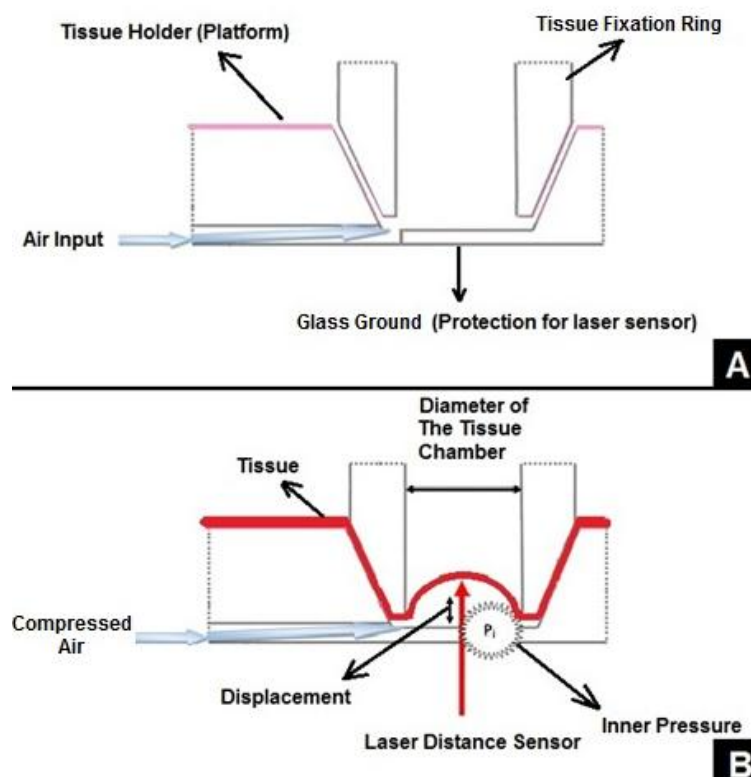


Figure 14: Sketch of the Cell Drum-like measurement principle.

Then air is pumped into this chamber, and a laser sensor is used to measure the deformation of the tissue surface. A glass window is used to protect the laser sensor. Air pressure sensors are used to measure the pressure within the chamber (Figure 9B). This data allows the mechanical properties to be calculated. Additionally, the maximum load, which the tissue can withstand, can be found by increasing the pressure until a rupture occurs. All these information were used to interpret the stability of fetal membrane according to birth types.

3.1.2 Components and Technical Design for In-Vitro Measurements

Laser-triangulation-sensor

A laser-triangulation-sensor (Keyence, model LK-G 3001P, Figure 15A) with a measuring head (LK-G 32, 15B) used in this study. A resolution was $0.05\ \mu\text{m}$ and a measurement range was 1 cm. First, a laser beam is projected orthogonally to the surface of the sample. This projection is observed by a CCD-chip at an angle of approximately 40° (Figure 10c, d). Laser sensor was used to measure the displacement of the membrane during pressure-change in the measurements. The thickness of the membrane can be measured, when the laser sensors are applied from both sides with a defined distance.

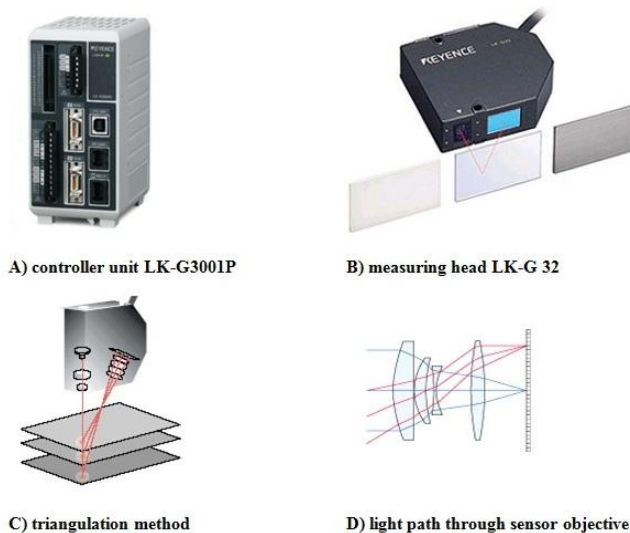


Figure 15: A: laser-triangulation-sensor (Keyence, LK-G 3001P, Osaka, Japan) and B: measuring head (Keyence, LK-G, Osaka, Japan).

Air Pumping Unit

A syringe was modified to use as a pump which is moved by a linear bearing and a stepper-motor (Figure 16). An advantage of this system is that the resolution can be adjusted simply by changing the size of the syringe. The stepper-motor is controlled by the computer so that pumping and data acquisition can be synchronized. The resolution of this pump with a 10 ml syringe is 3 μl per step. The pressure tubes are connected by Luer-locks which provide an air-tight and secure connection. These tubes can easily be replaced if contamination occurs.

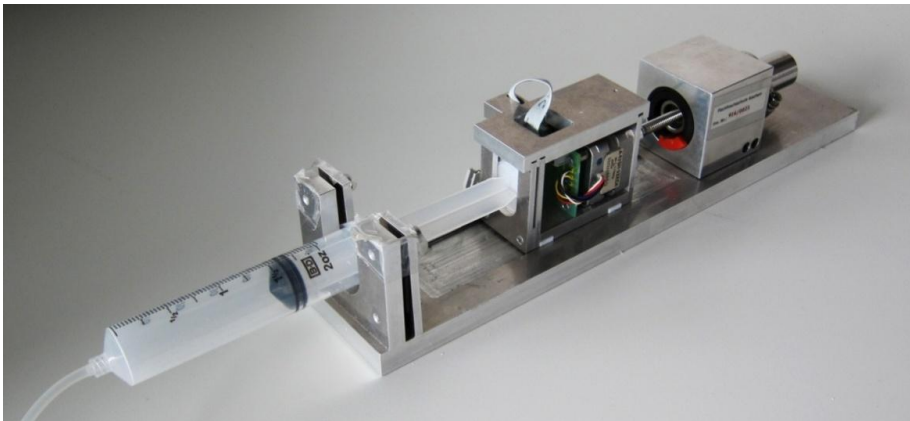


Figure 16: *Syringe Pump System.*

Pressure sensor

The pressure sensor is from the Keyence company (Figure 17). The AP-40W has a range from -101.3 kPa to 101.3 kPa with a maximum resolution of 0.02 kPa. Electronically controlled magnet-valves close the connections to the measuring heads as soon as their limits are reached to avoid sensor damage.



Figure 17: *Pressure sensor (Keyence, AP-C40W, Osaka, Japan).*

Tissue Chamber

The tissue chamber (Figure 18A) has a circular design to enable a balloon-like strain distribution, similar to the cell-drum principle (Linder, Trzewik, Ruffer, Artmann, Digel, Kurz, Rothermel, Robitzki, and Temiz, 2010). The bottom had to be transparent to enable laser-triangulation-measurements. Therefore, the bottom of the chamber was closed by a special glass (Index 1). The surrounding plateau supports the precise alignment of the sample. The tissue chamber, which can be also called a measurement chamber, must keep the membrane in a fixed position to prevent overlapping material from being pulled inside, which would change the results. A fixing ring (Figure 18B) squeezes the tissue against the tissue holder platform. Its edges are rounded up to avoid damage of the membrane. When the fixing ring is in place, the gap between sample and bottom surface of the fixing ring is approximately 1 mm. There is an additional silicon layer between the tissue and the fixing ring, which functions as a sealing ring. A hole drilled horizontally into the chamber directly above the bottom is used to connect the pressure system, via a Luer connector. Air is applied to the chamber through that drilled hole. The white part seen in figure 18 is a Teflon layer that allows tissues to slide easily for positioning. Three clamps are applied to the top of the fixing ring to produce a force strong enough to keep the tissue in the correct position, and also prevent any air escaping from the chamber. These clamps were found to work well, even during high chamber pressure measurements (Figure 18C).



Figure 18: *Tissue Chamber (A) with fixing ring (B) fixed by clamps (C).*

Data Interface

All measured data was transferred to a computer by a NI-USB 6251 DAQ (National Instruments, Texas) (Figure 19) which also controlled the stepper motor of the syringe pump. The communication with the computer was completed using a USB connection. The integration was completed using the libraries provided in the Labview-software.



Figure 19: NI-USB 6251 Data-Acquisition Unit (National Instruments, NI-USB 6251 DAQ, Austin, USA).

3.1.3 Construction of the Experimental Device (DIMPAST)

The entire assembly (Figure 20), that holds the laser-sensors and the tissue-chamber, is made of aluminum. This ensures the possibility to clean and sterilize all parts using different methods (heat, chemicals, etc.). The dimensions were made robust to avoid errors caused by any vibrations or displacements, including a large supporting base plate.

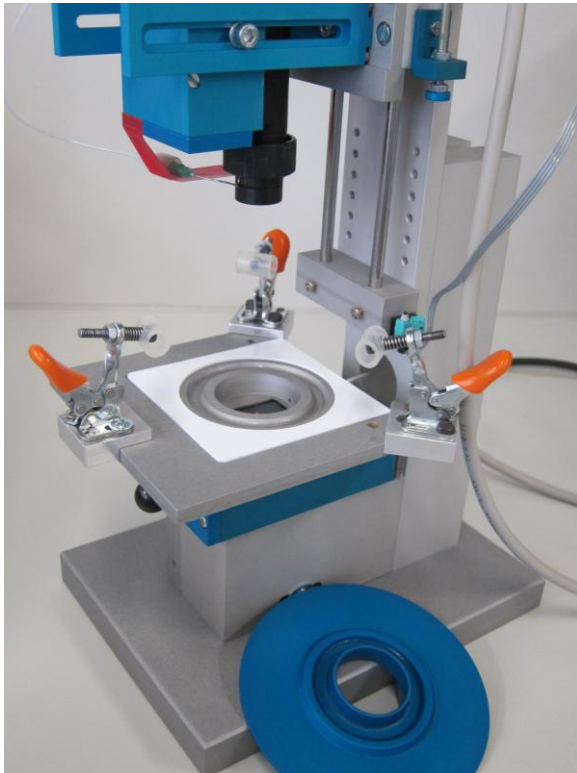


Figure 20: *Aluminum Construct containing laser sensor and OCT.*

3.1.4 Software

The operating software for this test was written by using Labview™ 2009 (National Instruments, Austin, USA). The measurements essentially consist of two separate parts, which can be accessed by the control tab at the top.

OCT Control Window

The first tab (Figure 21) is for controlling the OCT unit by a stepper motor. This part of the software grants the opportunity to perform separate measurements with only the OCT unit.

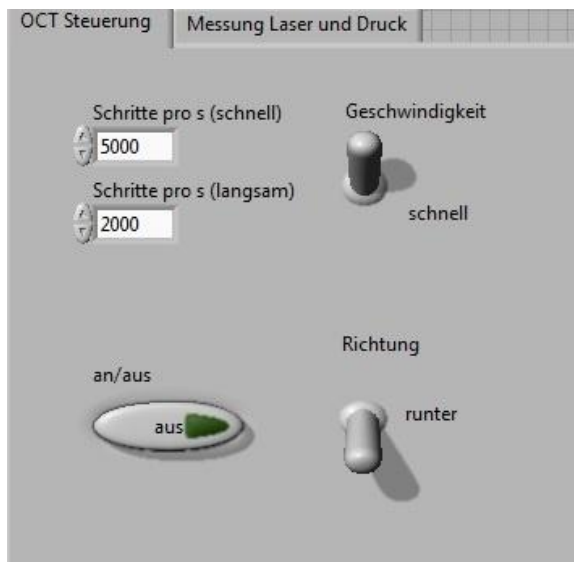


Figure 21: *OCT control part of the operating software.*

Data Acquisition Window

Figure 22 shows the data acquisition window and points out all of the important information during the experiments.

The pressure inside the chamber and the deflection of the membrane are shown as digital values, as well as in a chart. This control menu has five different sub-control steps (Figure 22B) to control different parts of the measurements. These sub-controls control the following functions: filling the pump with air while the experiment is running, stopping the air pump either at a certain inner pressure level or at a certain

deflection of the membrane surface, pausing the experiment when is something wrong, and conducting bursting measurements.

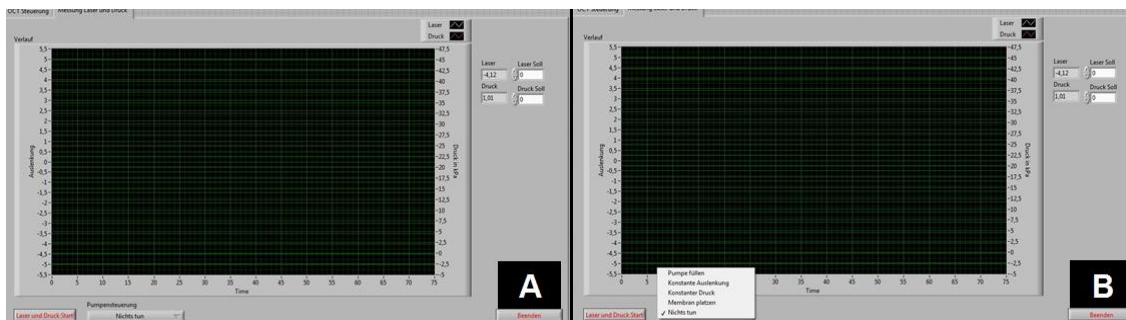


Figure 22: Data acquisition view. (A) General view of the main control window and (B) control menu of the software.

A part of the software's block diagram can be also seen in figure 23.

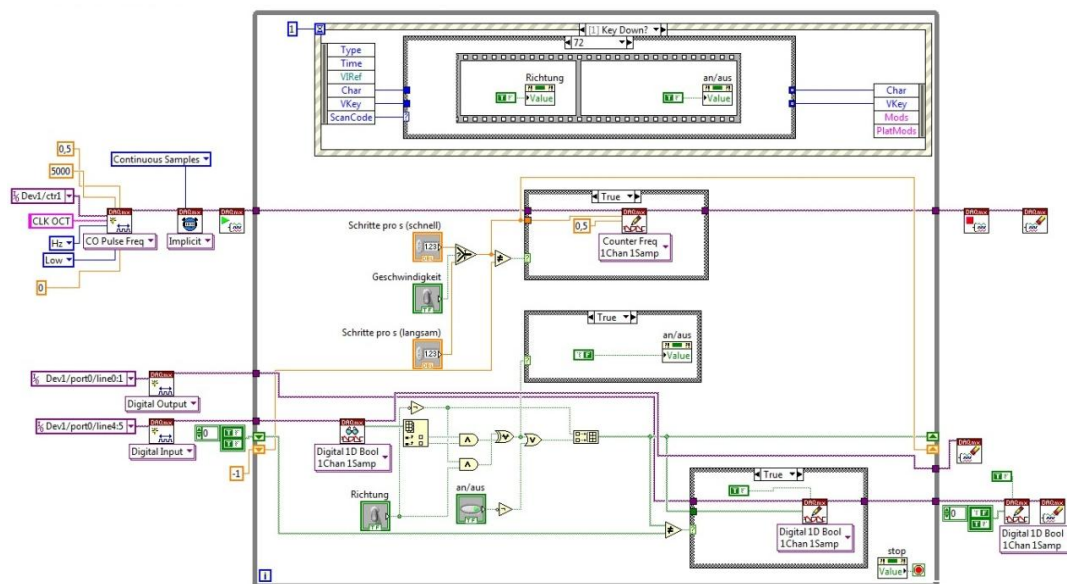


Figure 23: A part of the block diagram.

3.2 Sample Collection

A total of 87 fetal membranes were collected and analyzed before designing a new probe in this study.

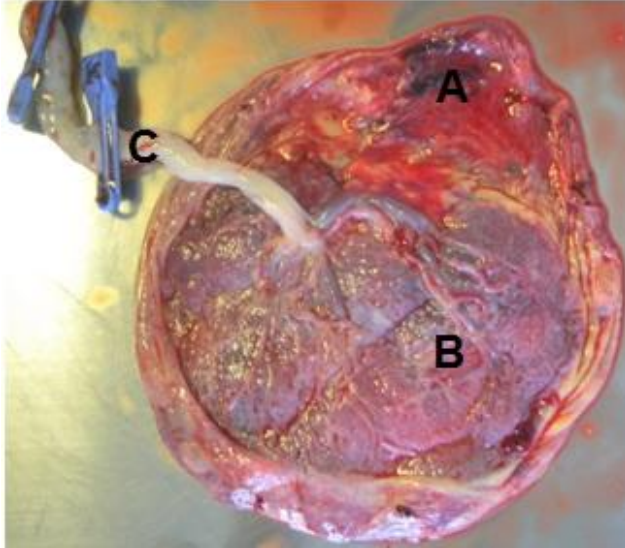


Figure 24: *View of the amniotic sac tissue. The fetal membrane (A) and the placenta (B) are connected to each other. The Umbilical cord (C) connects the fetus to the placenta.*

The pregnancies were randomly selected after serologic tests for human immunodeficiency, hepatitis B, C viruses, Streptococcal infection, Rubella and Toxoplasmosis were confirmed negative. The selected women had no history of diabetes, connective tissue disorders or hypertension.

Samples from 45 FMs were fixed in a formaldehyde solution (3.7 %) and stored at 4 °C until they were tested later that day. They were used for comparing the thickness between histological and OCT methods to prove the OCT's reliability. Histological tests were conducted by Serap Cilaker Micili at the department of histology and embryology, medical school of Dokuz Eylul University in Izmir – Turkey.

Then the other 42 FM samples used for the evaluation of mechanical properties were prepared and stored at 4 °C before being tested.

3.3 Sample Preparation

Amniotic sac tissues were collected (Figure 25A) from the Department of Obstetrics and Gynecology, Faculty of Medicine, University of Cologne, Germany, and transported to the Laboratory for Medical and Molecular Biology at Aachen University of Applied Sciences Institute of Bioengineering. Before measurements were made, the placenta was removed (Figure 25B), and the fetal membrane which can be seen on the right hand side of figure 25C (the amnion and chorion) was washed with an isotonic NaCl solution (a saline solution 0.9%). Afterwards the fetal membrane was prepared for mapping (Figure 25D, E). The round form of the membrane was made flat by cutting the connection parts as shown in figure 25D. Next, small pieces of fetal membranes (8cm X 8cm) were prepared in accordance with the size limits of the OCT tissue chamber (Figure 25F). Finally, the fetal membranes were signed and mapped (Figure 25G). The weak parts of the membrane, where the amnion and chorion were detached from each other, were marked on the fetal membrane mapping with X. These parts were not included in the measurements, as they could distort the results.

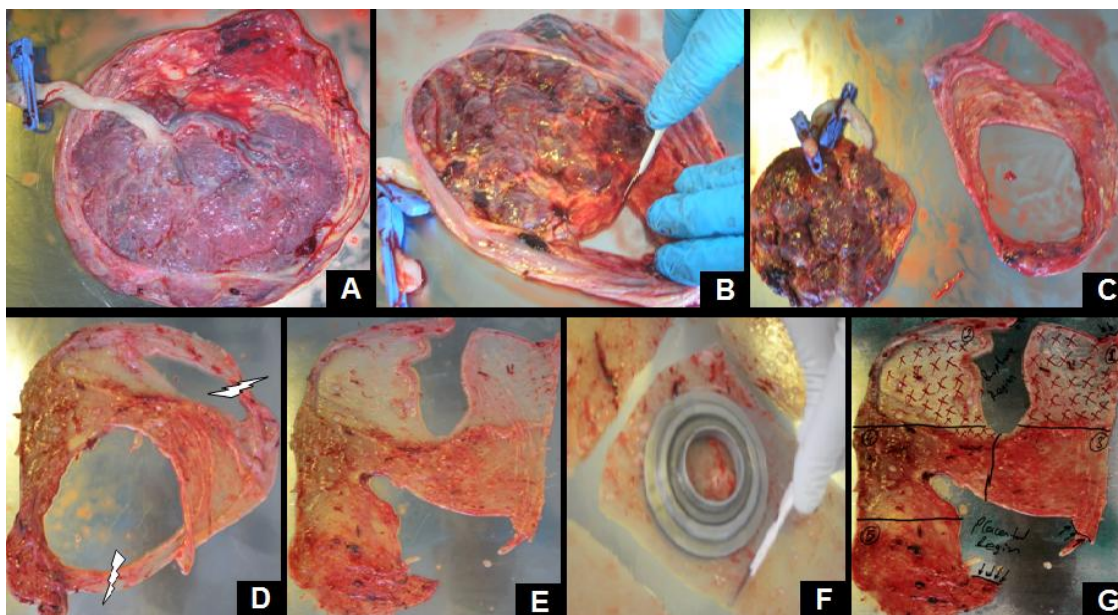


Figure 25: Mapping the fetal membrane. Fetal membrane with placenta (A), separation of the placenta from the fetal membrane (B), the placenta and fetal membrane respectively from left to right hand side (C), cutting the edges of the fetal membrane to flatten it (D), flattened view of the fetal membrane (E), sample preparation of the fetal membrane (F), mapped view shows samples` location on the fetal membrane (G).

The histological samples were prepared in a same way as above mentioned. However, histological samples were adjusted to 10mm X 10mm, and set in paraffin wax after the samples were fixed with a formaldehyde solution (3.7 %) for one day.

3.4 Measurements

A piece to piece comparison of the fetal membrane was performed in this study, since previous studies confirmed that mechanical properties vary significantly from piece to piece (Lavery and Miller , 1979;Lavery, Miller, and Knight , 1982;Moore, Mansour, Redline, Mercer, and Moore , 2006;Lavery and Miller , 1977). As a result, it was possible to test more than one piece from a single membrane (Lavery and Miller , 1979;Lavery, Miller, and Knight , 1982;Moore, Mansour, Redline, Mercer, and Moore , 2006;Lavery and Miller , 1977).

3.4.1 Thickness Comparison Between Histological Technique and OCT

A. Data Groups:

This part of the study compared data obtained from the Histological analysis of the samples, to data collected during OCT analyses. In this part of the study, three sub-groups were formed according to birth type: (NB), (PRB), and PROMB (Table 3). The rupture side, mid-zone, and placental edge of the fetal membrane were of special interest in this study, and analyzed independently for each birth type. All fetal membranes were obtained immediately after delivery, and washed with 0.9% saline solution. This procedure cleaned the membrane and aided the visual investigation of the rupture side. Tissues from patients with documented inflammation and/or infection, as evidenced by neutrophil infiltration, were excluded after histological examination.

Experimental Groups		Total Thickness	
		OCT n / s	Histology n / s
Types of birth	NB (I)	24 / 124	3 / 27
	PRB (II)	4 / 21	3 / 27
	PROMB (III)	8 / 55	3 / 27

Table 3: Data groups. Normal Birth (NB); Preterm Birth (PRB); Premature Rupture of Membrane Birth (PROMB, number of membranes (n), number of samples (s)).

B. Measurement Technique:

The aim was to assess if Optical Coherence Tomography (OCT) was accurate enough to be used for clinical investigations of high risk pregnancies. To validate this technique, fetal membranes were examined using both OCT and histological techniques in parallel.

B.1 Thickness Measurements with a Histological Method:

Prior to processing and mounting the tissues in Paraffin wax, the fetal membrane samples that contain amnio-chorionic tissues needed to be biologically stabilized. This task was completed by submersing the tissue samples in a neutral formalin solution for 24-48 hours. Next, a microtome (RM 2255 Leica) was used to create 4 μm thick samples (Figure 26A), which were transferred onto glass slides. These samples were then prepared in a water bath (Figure 26B), and then dried at room temperature (Figure 26C). After that, they were stained according to the Periodic Acid Schiff Stain (PAS) method (Figure 26D), and mounted in Entellan® mounting medium (Figure 26E). After all these steps, the sample was ready for evaluation (Figure 26F). The samples were examined under a light microscope.

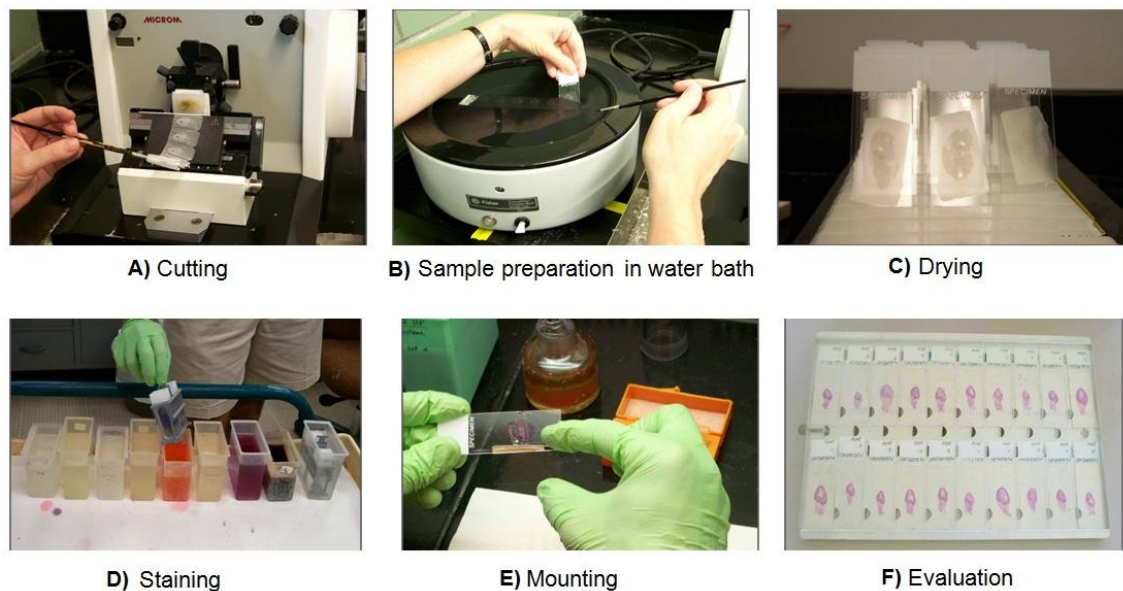


Figure 26: *Histological evaluation method* (Serap Cilaker Micili , 2011).

Process	Material	Period of Time
Deparffinization	60°C incubator	1 Night
Deparffinization	1 (incubator)	1 hour
Deparffinization	2-3 (Room Temp.)	30 minutes
Rehydration	% 100-100-96-80-70 Alcohol	Shaking
Lavation	Distilled Water	10 minutes
Dyeing	Periodic Acid	3-5 minutes
Lavation	Stream	1 minute
Dyeing	Schiff	20-25 minutes
Lavation	Stream	1-2 minutes
Dyeing	Hematoksilen	2 minutes
Lavation	Stream	5 minutes
Dehydration	% 60–70–80–96-100 Alcohol	Shaking
Trasnparent	Xylene 1–2–3	20 minutes per each
Sealing	Entellan	

Table 4: *PAS staining method. Entellan (Merck 1.07961.0100, Darmstadt, Germany), Lamel (Isotherm 76X26 mm), Light microscope (Olympus DP70), Microtome (RM 2255, Leica), Digital camera (Olympus DP71), Computer Analysis system Image Tool software (Uthscsa-version 3.00 for Windows).*

B.1.1 Light Microscopic Examination

The light microscope was connected to an image capturing system. Five fields were selected from each section of each sample in a automated random pattern (Figure 27). Average values of these 5 measurements were recorded. Images were taken and examined with Image Tool software (Uthscsa-version 3.00 for Windows).

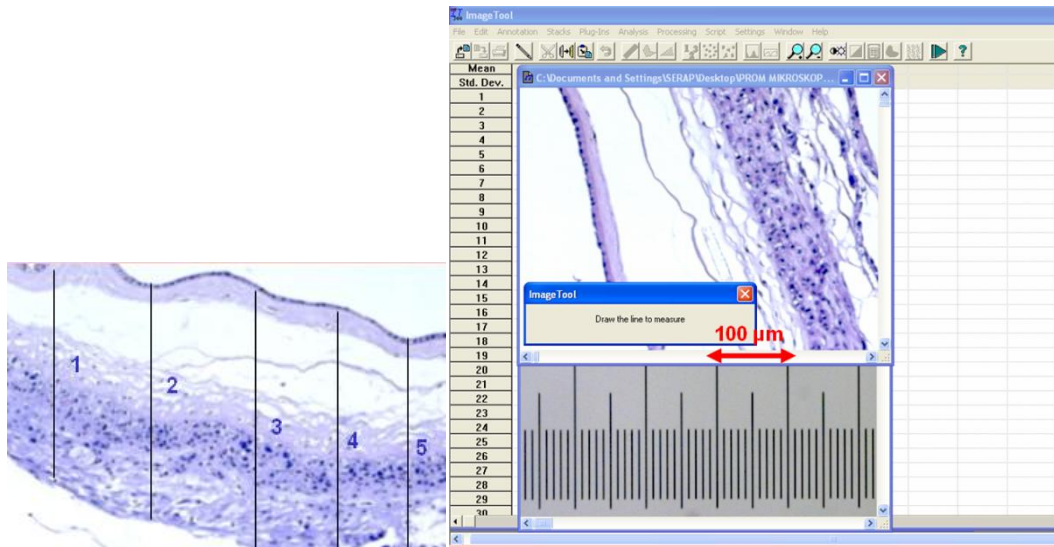


Figure 27: Figure on the left hand side; Measurement zones on the same sample. Figure on the right hand side; A view of Image Tool Software (Uthsca-version 3.00 for Windows) and scale is seen for both figures.

Finally, the total thicknesses of the fetal membranes (amnion, chorion and subgroups) were measured. Measurements were taken from the section vertically, and the layers of the fetal membrane were defined according to Bourne (Bourne, 2011). All layers of the fetal membrane can be seen in Figure 28.

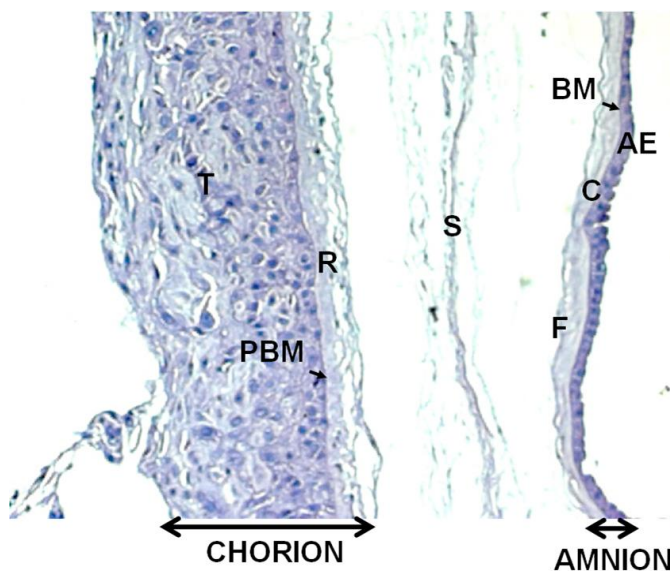


Figure 28: Light micrograph of the fetal membrane (haematoxylin and eosin stained). It shows the different layers of the amnion-chorion and decidua. (AE) A single layer Amniotic cuboidal Epithelium, (BM) amniotic Basal Membrane, (C) Compact layer, (F) Fibroblast layer, (S) Spongy layer, (R) Reticular layer, (PBM) Pseudoasal Basal Membrane, (T) Trophoblast layer. Magnification is X400.

B.2 Thickness Measurements with OCT:

Thickness measurements of the FM were also made using OCT. The OCT was mounted on the DIMPAST device as shown in figure 29A. DIMPAST has a working surface for positioning and fixing the tissue in a certain location. The tissue was placed on this surface (Figure 29B), and then a round mounting fixture was used to stretch it to the target position (Figure 29C). Three additional clamps were used to compress the round mounting fixture and prevent sliding of the sample between the working surface and the mounting fixture (Figure 29D). Finally, a stepper motor (controlled with Labview software) was used to position the OCT over the tissue to capture a cross-sectional view of the tissue (Figure 29E). The OCT results were compared with the histological microscopic results to check if OCT technology is reliable to predict premature births according to thickness properties.

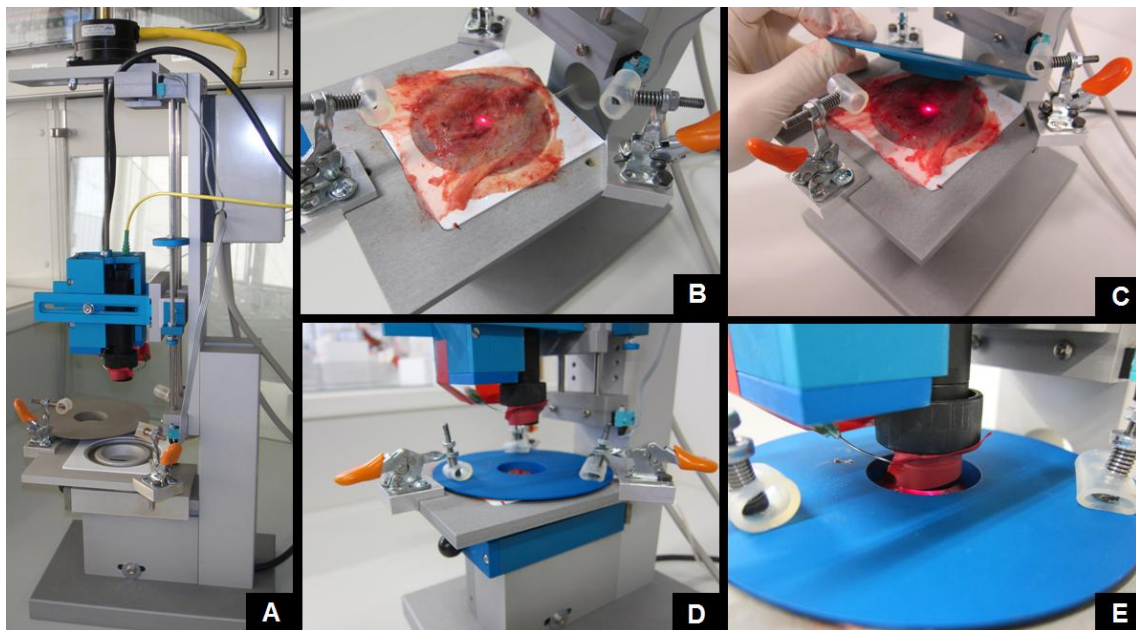


Figure 29: *OCT setup and steps for making OCT measurements. An additional device needed to conduct the OCT measurements was designed and manufactured in the period of this study (A), sample is positioned on the OCT working surface(B), the round platform stretches tissue into the target position (C), 3 clamps are applied to compress the round platform with constant force (D), OCT position controlled with a stepper motor via Labview software (E).*

3.4.2 Evaluation of Mechanical Properties of FM with the DIMPAST

The evaluation of the mechanical properties of the FM was performed by the DIMPAST. Table 5 lists all groups and shows the number of experiments in each group, with and without consideration of the birth type.

Experimental Groups		Number of Fetal Membranes	Number of Samples for Each Measurement Technique		
			Thickness	Bursting Pressure	Stress-Strain Ratio
Type of birth	NB	24	93	139	114
	PRB	4	13	19	17
	PROMB	8	37	37	43
	PPROMB	6	25	33	33
Total		42	168	208	207

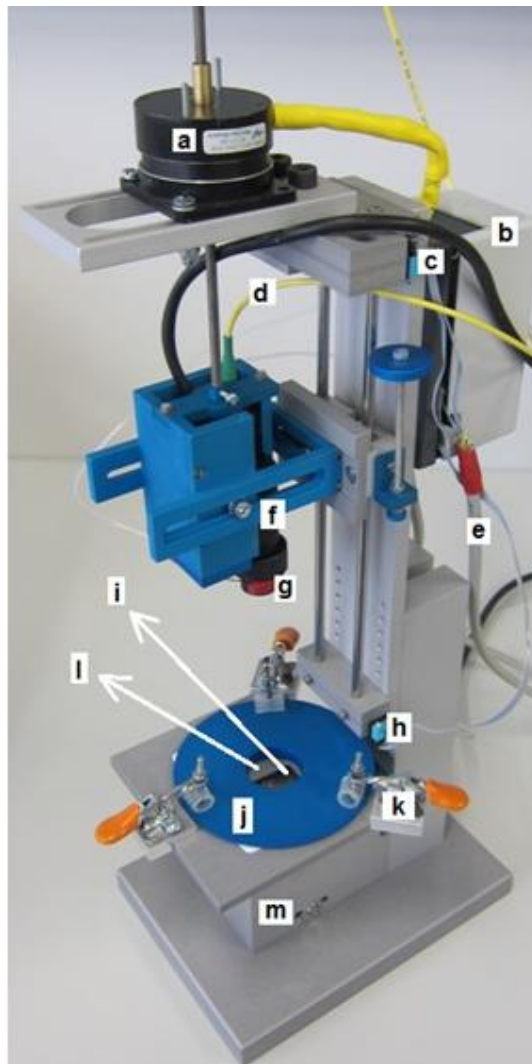
Table 5: *The number of experiments made for each group during the evaluation of mechanical properties, with and without consideration of birth type.*

A. Data Groups:

The data were divided into four groups: NB, PRB, PROMB and PPROMB (Table 5). Three different measurements were conducted on each group. These measurements were the thickness measurements, determination of the bursting pressure by application of air pressure, and Stress-Strain measurements. However, some measurements failed because of inconvenient samples. For instance, bursting pressure measurements could not be performed when the sample size was so small due to the close proximity of the rupture zone on the membrane, so the amount of samples was not equal for all measurement techniques.

B. Measurement Technique:

The DIMPAST (Figure 30) uses different measurement techniques such as laser triangulation, air pressure measurement, and optical coherence tomography (Type OCP930SR, Thorlabs GmbH, Dachau/Munich, Germany).



- (a) Stepper motor (OCT position control)
- (b) electrical circuit box
- (c) up switch (max. distance control)
- (d) fiber optic cable
- (e) data cables (DAQ-pad communication)
- (f) OCT
- (g) special designed OCT tip (to apply air flow)
- (h) down switch (min. distance control)
- (i) glass window (for laser beam)
- (j) tissue fixing ring
- (k) spring clamp (constant compressive force)
- (l) tissue chamber (seal with tissue sample before pressurizing)
- (m) laser sensor chamber.

Figure 30: *Measurement technique and the DIMPAST (Device for the Investigation of the Mechanical Properties of Amniotic Sac Tissue).*

The DIMPAST creates a closed chamber (Figure 30, l) by fixing the tissue between the OCT and the glass window (Figure 30i). That glass window also protects the laser sensor (Keyence, LK-G32) which is located inside another chamber (Figure 30m). The DIMPAST uses a platform and a tissue fixation ring (Figure 30j) to fix the membrane on the device. Two constant force spring clamps (Figure 30k) are applied to the tissue fixation ring to ensure that there is no air leakage from the chamber. An air pump system (Figure 31t) is used to pump air into the tissue chamber to increase the inner pressure of the chamber until the membrane ruptures. This measurement principle is based on the Cell Drum technology (Linder, Trzewik, Ruffer, Artmann, Digel, Kurz,

Rothermel, Robitzki, and Temiz , 2010) which had been developed and published before by the Laboratory of Cell Biophysics at the Aachen University of Applied Sciences Institute for Bioengineering. While the air is being pumped into the tissue chamber, the laser sensor is measuring the displacement of the tissue surface. This step is necessary because the tissue deforms during the inflation test. The measurement technique of the laser sensor is based on laser triangulation, and inner pressure differences of the tissue chamber are recorded simultaneously by a pressure sensor (Keyence, AP-C40W) which is placed inside the DIMPAST control unit (Figure 31s). Furthermore, the thickness of the membrane is measured by an OCT. A stepper motor (Figure 30a) controls the position of the OCT unit, which maintains a constant distance from the membrane surface while the membrane is inflating.

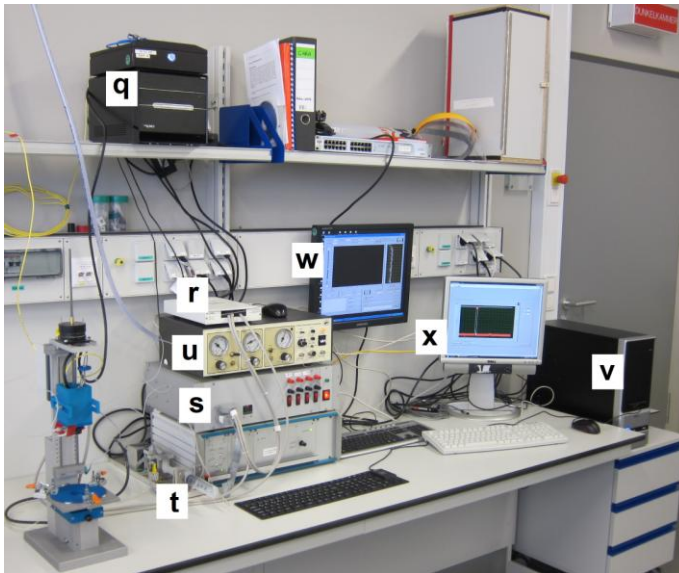


Figure 31: *Measurement setup. (q) OCT control unit, (r) DAQ-Pad, (s) DIMPAST control unit, (t) air pump system, (u) air generator, (v) computer, (w) OCT view (cross-sectional view of the membrane), (x) labview view (part of the software to control the DIMPAST and read the values on sensors).*

All data is collected by a data acquisition unit (NI USB-6251, National Instruments, Austin, USA) (Figure 31r). The operating software was written in Labview 2009 (National Instruments, Austin, USA).

B.1 Thickness measurement:

Optical techniques play an important role in medicine because they promise a safe and low-cost solution. Optical interferometer has traditionally been one of these favorite techniques. OCT is a new investigational imaging modality that uses near infrared light to produce real-time, high resolution (1 to 10 μm), cross-sectional images of the microstructure of in-vivo tissues (Huang, Swanson, Lin, Schuman, Stinson, Chang, Hee, Flotte, Gregory, Puliafito, and . 1991). One of the aims of this study was to use OCT imaging techniques to diagnose preterm births and premature ruptures in-vivo. Therefore, OCT measurement techniques were applied to in-vitro tissue samples. DIMPAST has a chamber which positions the OCT directly over the inspected surface of the sample.

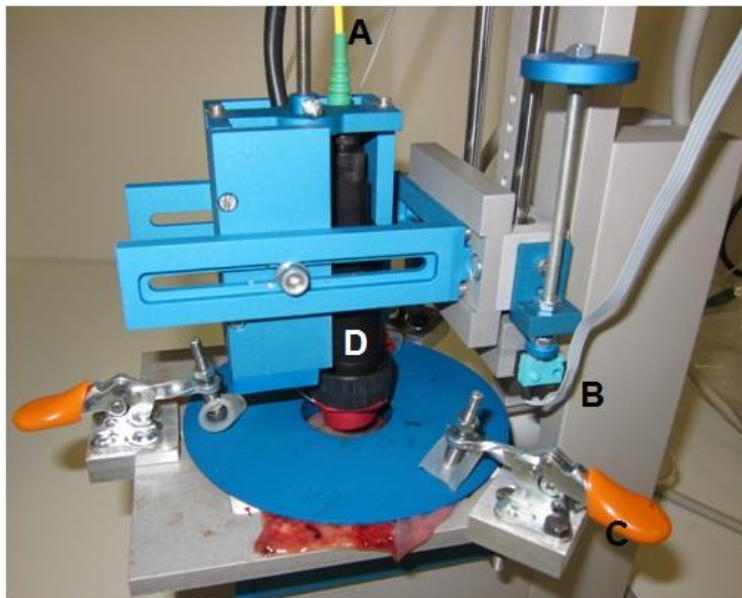


Figure 32: *OCT chamber of the DIMPAST holds the hand-held part of the OCT (D), over the sample. OCT works near infra-red zone and the light is transmitted by a fiber optic cable (A). The height position of the OCT is controlled by a stepper motor and it stops at a lower switch level (B). The 3 clamps (C) stretch the sample under the fixing ring.*

Figure 33 shows the cross-sectional view of the fetal membrane. The fetal membrane is composed of two main layers, the amnion and the chorion. There are many different sub-layers within those two main layers, with an additional layer in between these two primary layers, called the spongy layer. This spongy layer can be detected as it is seen

as a gap between the amnion and the chorion layers (Figure 33). The total thickness was considered as the sum of all these layers, as shown in the figure 33. The surface of the tissue was not flat, so three thickness measurements were recorded from left, right, and a middle part of this cross-sectional view. The average thickness was calculated and used in this study.

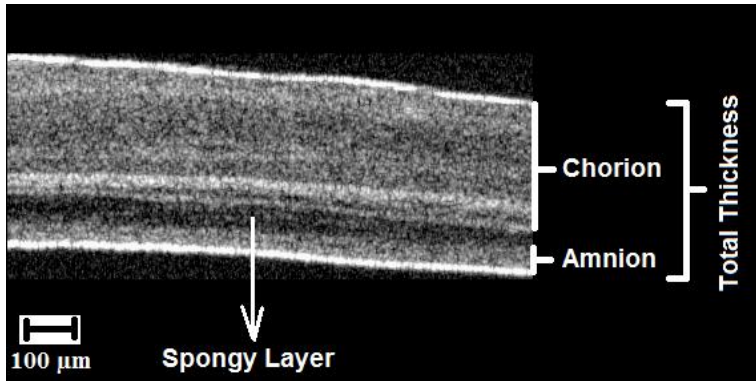


Figure 33: *Cross-sectional view of the fetal membrane. This view was captured with the Optical Cohorence Tomograpy (OCT). The amnion and chorion layers are easily identified, and the spongy layer is obvious.*

Sometimes the amnion and the chorion were detached from each other, as the chorion was sliding over the amnion. The thickness of these particular samples was not measurable because there was a gap between two main layers, which affected the thickness. Figure 34 shows an example of such a sample. The gap between these layers is thicker than the total thickness of these two layers. Blood and some amniotic fluid filled the void between the layers.

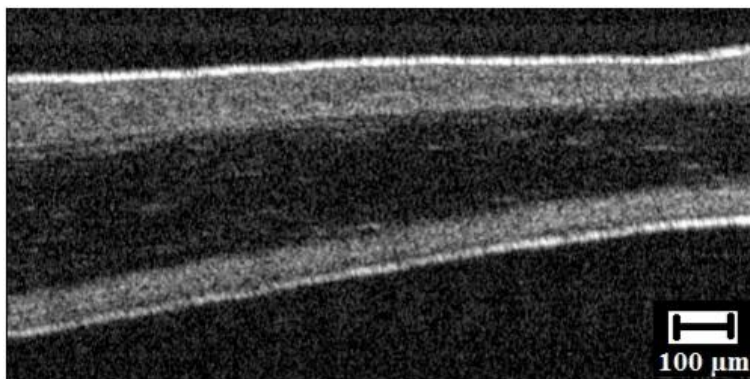


Figure 34: *Visible gap between the amnion (upper layer) and chorion (lower layer).*

B.2 Bursting pressure measurement:

Bursting pressure measurements were also performed with the DIMPAST device. A piece of fetal membrane was stretched over the tissue chamber as seen in Figure 35A. Then, the tissue was fixed with a fixing ring (Figure 35B), which uses clamps to press the membrane on three sides. This prevents any air leakage from the inner part of the tissue chamber to the atmosphere (Figure 35C).

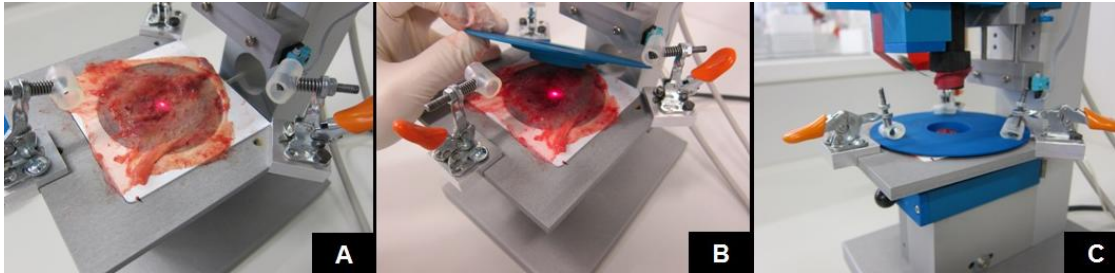


Figure 35: *Positioning of the sample on the tissue chamber.*

After forming the tissue chamber between the OCT and the laser protective glass floor, the air pump system (Figure 36) was used to inject air into the chamber and inflate the membrane.



Figure 36: *Air pump system.*

Air was pumped into the tissue chamber until the tissue ruptured at the bursting pressure measurement. The pressure in the chamber and the position of the membrane surface were recorded simultaneously with the pressure and the non-contact laser displacement sensors. First the chorion ruptured in in-vitro experiments, followed by the amnion as shown in Figure 37.

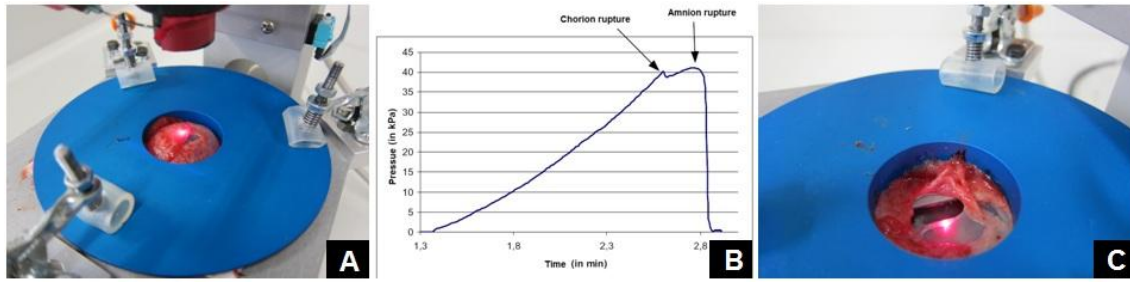


Figure 37: Bursting of the fetal membrane. First the chorion ruptured (A), then the amnion burst (C). The graph (B) shows the relation between inner pressure of the tissue chamber and the tissue's strength.

B.3 Stress-Strain Ratio:

The Stress-strain ratio of the fetal membrane was measured using the DIMPAST, and calculated by using the pressure-strain data. As it was previously mentioned, the inner pressures and the deformations were recorded simultaneously with two sensors. Air was pumped into the chamber to inflate the fetal membrane. The inflation was stopped at a constant deflection ($h_{\max} = 8\text{mm}$) of the membrane surface in order to calculate the Stress-strain ratio before continuing to the bursting pressure. The spherical segment was formed while the membrane was being inflated, and all fibers were assumed to deform equally (Figure 38A). As it is depicted in figure 38A, the longitudinal fibers were considered when calculating the Stress-Strain ratio. The initial length of those longitudinal fibers' was equal to the diameter of the tissue chamber at start position ($L_0=34\text{mm}$). The vertical deflection (h) was observed and controlled by the laser sensor, with the final vertical deflection being 8mm in all measurements (Figure 38B). Those values (L_0 and h) belonged to the spherical segment which was formed by the membrane. The arc length of this circular segment is illustrated as 'L' in figure 38C.

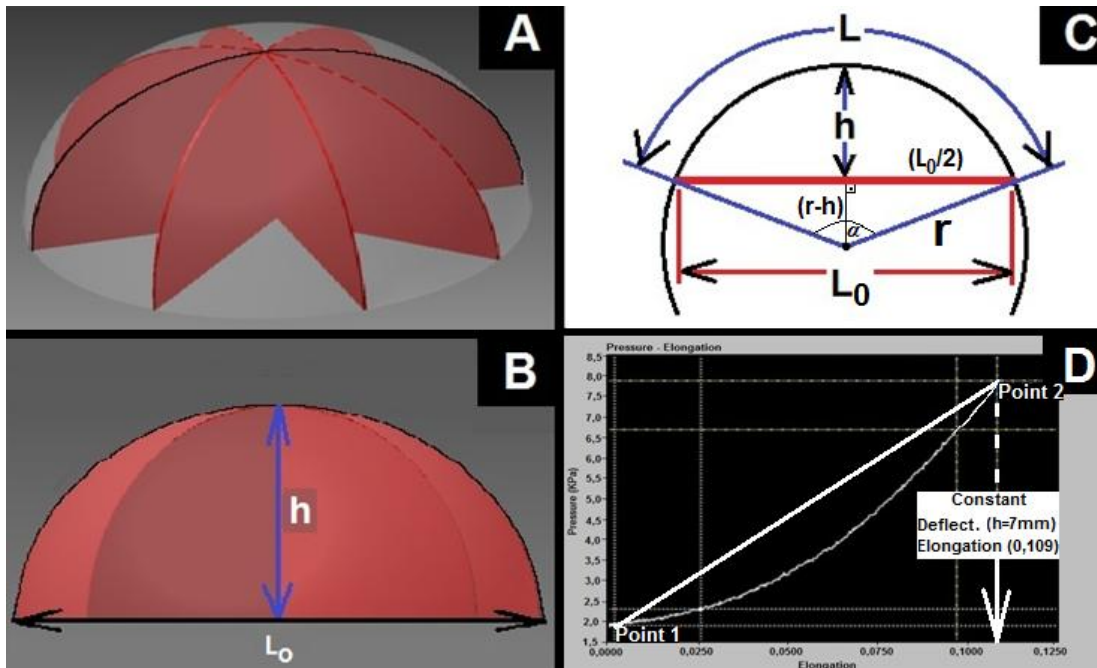


Figure 38: This figure clarifies the calculation of the average Stress-Strain Ratio of the fetal membrane. (A) The piece of fetal membrane was inflated until a constant deflection of $h_{max}=8mm$ was achieved, forming a spherical segment over the chamber. (B, C) The height of this spherical segment was equal to the deflection value (h) which increased up to 8mm. The bottom diameter was equal to the chamber diameter ($L_0=34mm$). (D) The elongation (ϵ) values were calculated for every point of the Pressure – Deflection curves to derive the Pressure (kPa) – Elongation (ϵ) curve.

The arc length of this circular segment is equal to the final length of the fibers in the membrane, so the elongation of the fibers was calculated using the following equation:

$$\text{Elongation } (\epsilon) = \frac{L - L_0}{L_0} \quad (1)$$

The important point was to calculate the arc length (L) of the circular segment. It was calculated by using the following equation:

r : radius of the circle which was formed by L_0 and h .

$$L = r \times \alpha \quad (2)$$

$$\alpha = 4 \times \tan^{-1} \frac{2 \times h}{L_0} \quad (3)$$

$$r^2 = (r - h)^2 + \left(\frac{L_0}{2}\right)^2 \quad (4)$$

$$r = \frac{L_0^2 + 4 \times (h)^2}{8 \times h} \quad (5)$$

$$L = \frac{\tan^{-1}\left(\frac{2 \times h}{L_0}\right) \times (4 \times h^2 + L_0^2)}{2 \times h} \quad (6)$$

The elongation (ϵ) of the longitudinal fibers can be calculated by using these equations. This calculation was applied at each pressure level to derive the pressure vs. deflection and pressure vs. elongation graphs (Figure 38D). Two points were taken at the beginning and end of the curve to calculate the slope, which represents the average Stress-strain ratio of each longitudinal fiber in the fetal membrane sample (Joyce, Moore, and Sacks, 2009).

$$\text{Stress - Strain ratio (kPa)} = \frac{\text{Pressure (kPa)}}{\text{Elongation (\%)}} \quad (7)$$

Since failure always originates from the weakest point, each fiber's average Stress-strain ratio can be assumed to be the same as the Stress-Strain ratio of the fetal membrane, which allows it to be used as a comparison factor between each type of membrane.

3.4.3 Extra Measurements for In-Vitro Probe Designing

The following measurements and their results are not for the statistical evaluation. They were conducted to generate design ideas for a specialized diagnostic probe.

A. Deflection Measurements

Deflection measurement is important for designing a probe because this measuring technique can be applied to in-vivo measurement probes. The technique uses a constant pressure air flow which is directed at the surface of fetal membrane. This air stream causes the membrane to deflect, relative to the inner pressure of the chamber, and is measured using non-invasive optical methods. OCT device has a specially designed tip

to direct air flow as well to measure the deflection of the tissue surface (Figure 39A-g). That OCT tip has two extra air channels for the air flow. Those two channels are focused on the same point as the OCT head, so it is possible to direct a constant pressure air stream at the surface of the tissue from a distance of about 2 mm. The deflection of the fetal membrane surface was observed and recorded when the air stream was applied through those air channels. The pressure of this air stream was controlled by a pressure generator (Figure 31u).

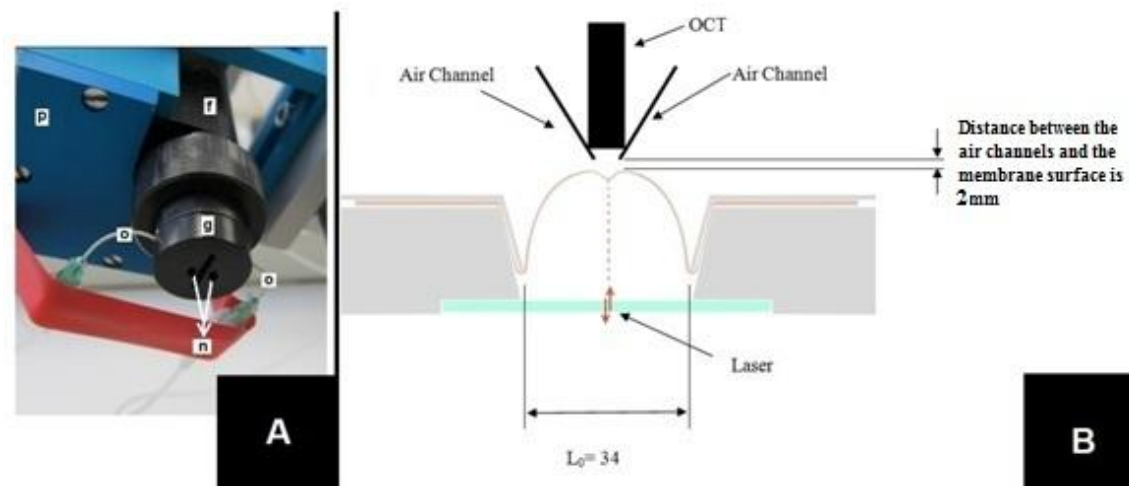


Figure 39: OCT tip for the deflection measurement (A), and a sketch of the process (B).

Deflection measurements were conducted to check if it is possible to measure the deflection of the fetal membrane by applying an air flow. The fetal membrane was inflated until a certain inner pressure level, and then an air flow was applied on the membrane's surface. Air flow was controlled with an air generator which provided a constant flow pressure. This method more accurately mimicked the biological environment and gave some ideas towards the design of a new in-vivo probe, since this method could also easily be applied in-vivo with the help of a specialized diagnostic probe. It will also solve the subjectivity problem of palpation technique.

B. Spectral Absorbance Measurements

In addition to deflection measurements, spectral absorbance measurements were also conducted on FM samples to generate useful ideas for the design of a new diagnostic probe. Absorption means that the intensity of light decreases in matter, because matter absorbs a part of the light. Thereby light quanta are captured by molecules or atoms and the energy in the light quanta are converted into atomic excitation energy, which will be transformed for example into heat-energy or fluorescent light.

Spectral absorption is the energy capability of tissue-characteristic substances and it is related to the wavelength.

The therapeutic window (or optical window) describes the absorption-range of wavelengths from 650 nm to 1.3 μm . This is the range in which the light has the maximum penetration depth in tissue, based on favorable conditions for scattering and absorption, and is used in medical diagnostic applications like the coherence tomography. However, the fluorescent microscopic measurements in this range are irrelevant, because an excitation wavelength of 340 nm is used and the expected fluorescence light is approximately 390 nm.

C. Autofluorescence Measurements

One of the other measurement techniques is fluorescence measurements. This technique was also used to stimulate ideas about designing a diagnostic probe. A Keyence fluorescence microscope (Keyence BZ 8100, Japan) was used and two different kinds of filters were chosen; low-pass 360 nm (FWHM: 40 nm) and high-pass 400 nm (FWHM: 50 nm). This method was first applied on the raw collagen fibers (Figure 40A), and then later was applied to the fetal membrane samples (Figure 40B). The fetal membrane's fluorescent properties at a certain range of wavelengths were compared with the collagen fibers's response. It was thought that it would be possible to detect the amount of collagen in the fetal membrane using these fluorescent measurements.

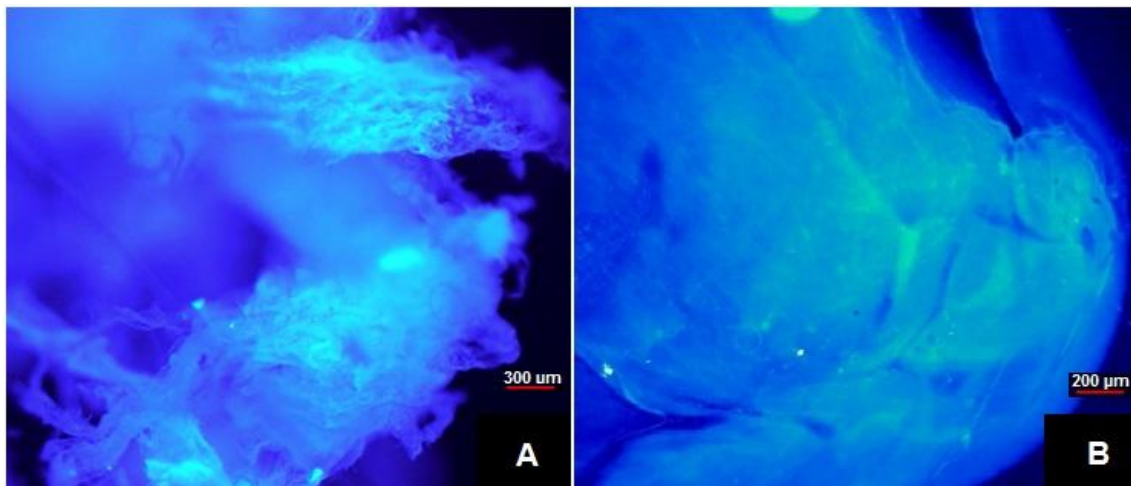


Figure 40: *Fluorescence response of the dried collagen fibers (A) and the fetal membrane (B) (Keyence, BZ 8100, Osaka, Japan).*

3.5 Statistical analysis:

The results are presented as the mean with 95% confidence intervals. Significance was calculated with the Mann-Whitney Rank sum test (SigmaPlot 11.0)

4 **Results**

The results from this study, which were statistically evaluated, are divided into two main parts. The first of them is the result of the thickness comparison work between OCT techniques and histological methods. This part was necessary to prove if OCT would be a useful diagnostic tool in this field. The second part of the results summarizes the mechanical properties of the fetal membrane. This information was required to design a new diagnostic probe. Following the acquisition of this data, a preliminary version of a specialized OCT probe was designed and produced, however it is presented in a separated caption of this thesis.

4.1. Comparing the OCT Technique with the Histological Technique

As it was previously mentioned, the thickness of the fetal membranes was measured using both OCT, and histological methods. OCT worked well and images were successfully obtained from all fetal membrane samples. The amnion-chorion layers are visible and the total thickness of the fetal membranes was measured (Figure 41).

As the figure depicts, the separation of the amnion and the chorion layers was detectable. The CCD camera view, shown in the lower left-hand corner of Figure 41, is used for positioning the OCT head over the inspection area. The Amniotic cuboidal Epithelium (AE), the Spongy layer (S) and the Reticular layer (R) were vaguely detected using OCT. However, all layers of the fetal membrane were easily distinguishable in the histological images (Figure 42). Of course microscopic evaluation is better at detecting the sublayers, but for the total thickness measurements, the OCT is sufficient and is better suited for the biological cases in-vivo. If the image resolution of the OCT can be improved, then the sublayers of the fetal membrane could be more easily detected.

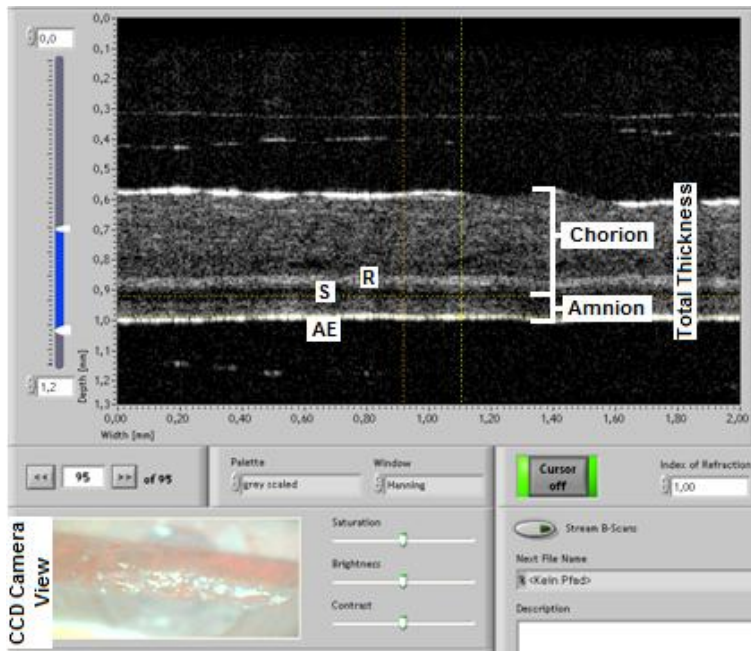


Figure 41: OCT view of the fetal membrane. The CCD camera view can be seen in the lower left-hand corner, and is used for positioning the OCT head over the inspection area. Total thickness, as well as the amnion and chorion can be easily detected. (AE) Amniotic cuboidal Epithelium, (S) Spongy layer, (R) Reticular layer.

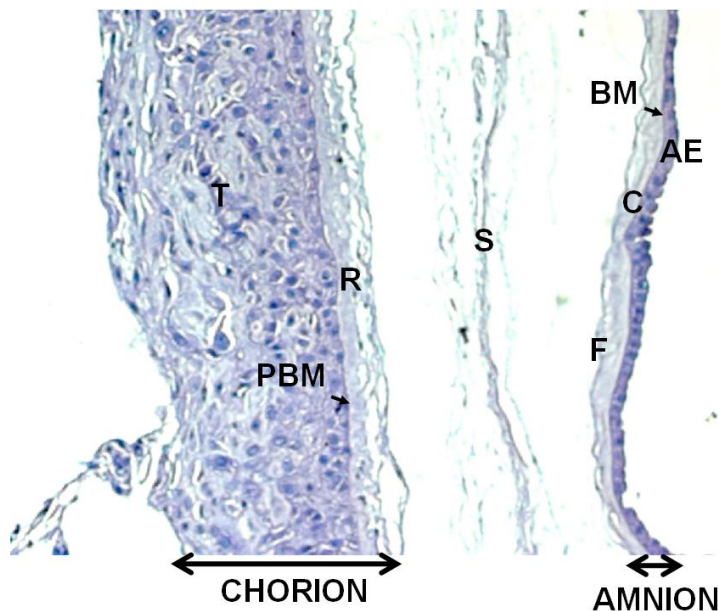


Figure 42: Light micrograph of the fetal membrane (haematoxylin and eosin stained). It shows the different layers of the amnion-chorion and decidua. (AE) a single layer Amniotic Cuboidal epithelium, (BM) amniotic Basal Membrane, (C) Compact layer, (F) Fibroblast layer, (S) Spongy layer, (R) Reticular layer, (PBM) Pseudoasial Basal Membrane, (T) Trophoblast layer. Magnification X400.

Data showed that the fetal membranes were thickest in NB (I), and thinnest in PRB (II). The thickness of the fetal membranes in the PROMB group (III) is between the values for NB (I) and PRB (II) respectively. The OCT analysis determined that the difference in membrane thickness between the NB (I) and PROMB (III) classifications was insignificant. However, the difference between NB (I) and PRB (II) was significant at a p-level of $p=0.039$. The microscopic analysis determined that the difference between the NB (I) and PROMB (III) was significant at a p-level of $p=0.001$ and the difference between NB (I) and PRB (II) was also significant at a p-level of $p=0.001$. The histological and OCT analysis both produced similar results. However, thicknesses measured by OCT were always smaller (Table 6).

Total Thickness					
Experimental Groups		OCT		Histology	
		n / s	Mean \pm SD (μm)	n / s	Mean \pm SD (μm)
Types of birth	NB (I)	24 / 124	313.9 \pm 72.2	3 / 27	383.8 \pm 19.2
	PRB (II)	4 / 21	270.2 \pm 66.1*	3 / 27	324.6 \pm 14.4**
	PROMB (III)	8 / 55	302.7 \pm 99.7	3 / 27	343.1 \pm 21.2***

Table 6: Comparing the total thickness of the fetal membranes. OCT data vs. Histological data.

Next, subgroup thicknesses of the rupture side, mid-zone and the placental edge were determined and compared for the same type of birth. Results are as follows:

NB- OCT showed statistically significant differences between the rupture side and the placental edge ($p=0.001$) as well as between mid-zone and placental edge ($p=0.005$), respectively. Although the thickness of the rupture side was less than the one at the mid-zone, there was still no significant difference found. Although histological data showed same tendency, however there was not any statistical significant difference between the subgroups in NBs (Table 6).

PRB- According to OCT, there were significant statistical differences between the rupture side and the mid-zone ($p=0.048$), as well as between the rupture side and the placental edge ($p=0.003$). The thickness of the mid-zone was less than the thickness of

the placental edge however, it was not statistically significant. Interestingly, the histological analysis showed that there were significant statistical differences between the rupture side and the mid-zone ($p=0.015$), as well as between the rupture side and the placental edge ($p=0.002$). The thickness of the mid-zone was less than the thickness of the placental edge, with no statistical significance (Table 7).

PROMB- OCT results showed that there were statistical significant differences between the rupture side and the placental edge ($p=0.001$) and between the mid-zone and the placental edge ($p=0.012$). The thickness of the rupture side was less than the thickness of the mid-zone however, it was not statistically significant. The histological results showed that all differences between all three sub-groups in the main group of PROMB were statistically significant (Table 7).

		Total Thickness			
		Piece location on the fetal membrane			
Observational Technique	Kind of birth	n	Rupture	Middle	Placental
			Mean \pm SD (μm) / s		
OCT	NB	24	269.9 \pm 143.8 / 30	321.6 \pm 116.7 ^{#1} / 39	366.8 \pm 112.9 ^{¥1} / 55
	PRB	4	181.4 \pm 70.5 ^{*1} / 8	273.3 \pm 18.6 / 3	345 \pm 89.8 ^{¥2} / 10
	PROMB	8	233.6 \pm 112.5 / 21	280.3 \pm 100.4 ^{#2} / 11	400.8 \pm 132.1 ^{¥4} / 23
Histology	NB	3	356.2 \pm 48.7 / 9	368.6 \pm 34.7 / 9	386.4 \pm 15.4 / 9
	PRB	3	305.9 \pm 11.0 ^{*2} / 9	325.7 \pm 18.5 / 9	354.2 \pm 13.1 ^{¥3} / 9
	PROMB	3	315.1 \pm 11.4 ^{*3} / 9	352.7 \pm 14.1 ^{#3} / 9	385.7 \pm 28.0 ^{¥5} / 9

Table 7: Comparison of the total thickness of the fetal membranes in subgroups. OCT data vs. Histological data.

n: number of the fetal membranes; *s*: Number of samples (pieces)

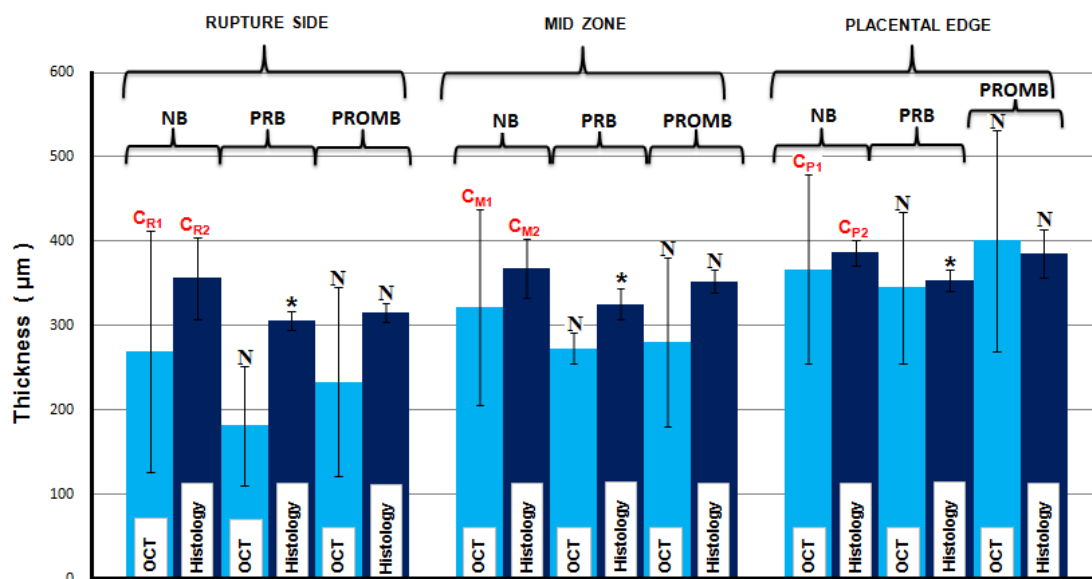
Mann Whitney U test was performed and the difference was statistically significant for these subgroups;

*: Rupture side vs. Mid zone, ^{*1}: $p=0.048$, ^{*2}: $p=0.015$, ^{*3}: $p=0.004$ etc.

¥: Rupture side vs. Placental edge. ^{¥1}: $p=0.001$, ^{¥2}: $p=0.003$, ^{¥3}: $p=0.002$, ^{¥4}: $p=0.001$, ^{¥5}: $p=0.002$ etc.

#: Mid zone vs. Placental edge, ^{#1}: $p=0.005$, ^{#2}: $p=0.012$, ^{#3}: $p=0.041$ etc.

Finally, the results of the OCT analysis were compared to results of the histological analysis with consideration for the birth type and location (rupture side, mid-zone and placental edge). This comparison is different from the first focal point of the study because this analysis compared the birth types according to the piece location, instead of the average thickness values of complete membranes. According to the OCT results, there were no statistical significant differences between birth types at the same location however, the NB membranes were thicker than the PRB in all locations. Histological analysis of the samples determined that thickness differences between the NBs and PRBs in all locations was statistically significant ($p=0.032$ in rupture side; $p=0.018$ in mid-zone; $p=0.016$ in placental edge) according to the histological results. Both methods determined that there were no significant statistical differences between the NB and PROMB in all locations. Graph 1 shows the comparison of the birth types in each location. The normal birth was chosen as the control group in each location and in each measurement type independently.



Graph 1: Fetal membrane thickness at different membrane locations: C, Controls of normal birth. indices: P, Placental edge, R, Rupture side, M, Mid-zone etc.; index numbers: 1, OCT data, 2, histological data.

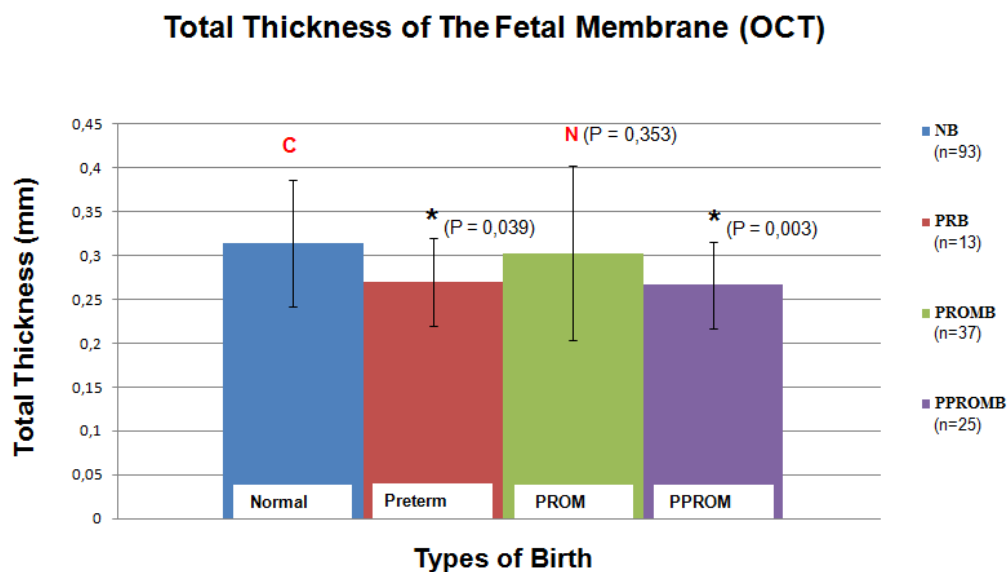
4.2. Mechanical Properties of the Fetal Membrane

This part focused on detecting the mechanical properties of the fetal membrane, which were necessary when designing a new diagnostic probe.

The results of this part of the study showed three important points. Results from the three different measurement methods for each type of birth were summarized to draw conclusions. The three primary interests of this part of the study were the total thickness, the bursting pressure, and the average Stress-strain ratio for each type of fetal membrane. Many interesting points were observed after analyzing the results and 3 graphs show the comparison of all four main groups. The membranes from the NB group were used as a control group to compare with membranes from the other 3 kinds of birth.

4.2.1. Thickness Results:

Graph 2 shows the comparison of the thickness results of all four main groups, and shows the number of measurements in each group. There are statistically significant differences between NB and PRB ($p=0,039$) and between NB and PPROMB ($p=0,003$). Although the NB's membranes were thicker than PROMB's, the difference between them was not statistically significant ($p=0,353$). Four groups were aligned from the thickest to the thinnest: NB (0,314mm), PROMB (0,303mm), PRB (0,270mm) and the PPROMB (0,267mm).



Graph 2: Total thickness comparison;

C; The control group

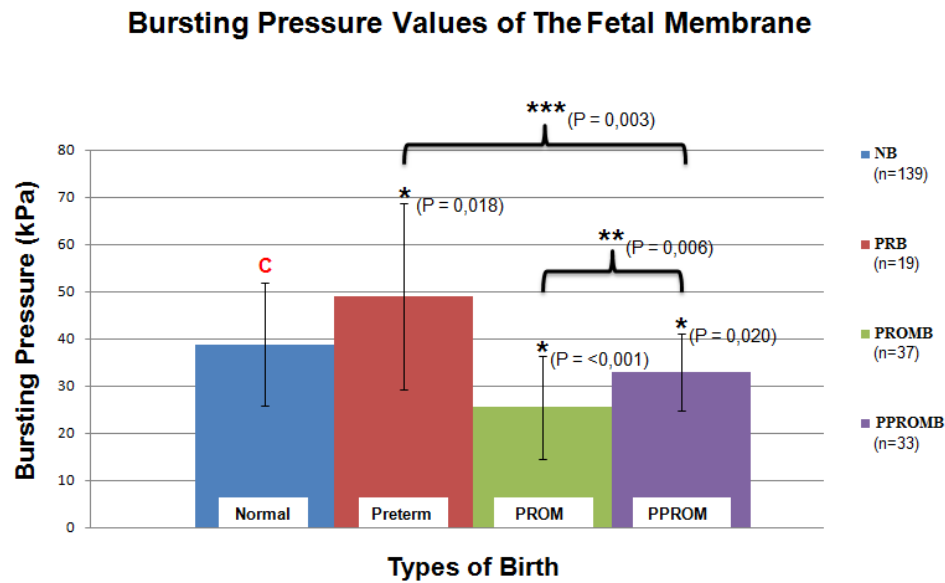
**;The difference with respect to the Control Group is statistically significant.*

N; There is no significant statistical difference

(According to the Mann-Whitney Rank Sum Test)

4.2.2 Bursting Pressure Results:

The results from the bursting pressure tests show that the chorion normally ruptured first, followed by the amnion as shown in figure 37. Graph 3 shows the comparison of the bursting pressure for all groups, and gives the number of measurements in each group. There are statistical significant differences between NB and PRB ($p=0,018$), between NB and PROMB ($p=<0,001$) and between NB and PPROMB ($p=0,020$). The Four groups when categorized from strongest to weakest appear as follows: PRB (49kPa), NB (38,9kPa), PPROMB (33kPa) and PROMB (25,5kPa). Additionally, Graph 3 shows two more results: the comparison between PROMB and PPROMB ($p=0,006$), and the comparison between PRB and PPROMB ($p=0,003$). Both differences were statistically significant.



Graph 3: *Bursting pressure comparison;*

C; The control group

**; The difference with respect to the Control Group is statistically significant.*

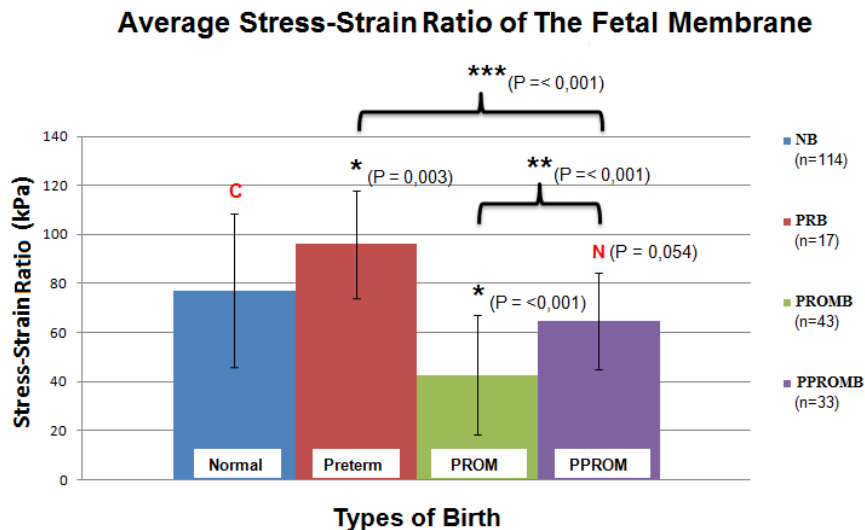
***; The difference between PROMB and the PPROMB is statistically significant*

****; The difference between PRB and the PPROMB is statistically significant.*

(According to the Mann-Whitney Rank Sum Test)

4.2.3. Stress-strain ratio Results:

The results of the average Stress-strain ratio of all four groups are compared in Graph 4, which also provides the number of measurements in each group. Significant statistical differences exist between NB and PRB ($p=0,003$) and between NB and PROMB ($p<0,001$). Although the average Stress-strain ratio of the NBs' membranes were higher than PPROMBs', the difference between NB and PPROMB was not statistically significant ($p=0,054$). The four groups when aligned from the highest average Stress-strain ratio to the lowest appear as follows: PB (96,2kPa), NB (77,2kPa), PPROMB (64,7kPa) and PROMB (42,8kPa). Additionally, Graph 4 shows two more results: the comparison between PROMB and PPROMB ($p<0,001$) and the comparison between PRB and PPROMB ($p<0,001$). Both differences were statistically significant. These results supported the bursting pressure results.



Graph 4: *Stress-Strain Ratio comparison;*

C; The control group

**; The difference with respect to the Control Group is statistically significant.*

***; The difference between the PROMB and the PPROMB is statistically significant*

****; The difference between the PRB and the PPROMB is statistically significant.*

N; There is no significant statistical difference

(According to the Mann-Whitney Rank Sum Test)

4.3. Extra Results for In-Vitro Probe Designing

Additional experiments were conducted during the study such as deflection measurements of the FM, spectral absorbance measurements of the FM, and autofluorescence measurements of the FM. These extra measurements were administered in order to generate ideas about how best to design an in-vivo measurement probe which could be applied in the field.

4.3.1. Deflection Results

As it was previously explained, the technique uses a constant pressure air flow which is directed at the surface of fetal membrane.

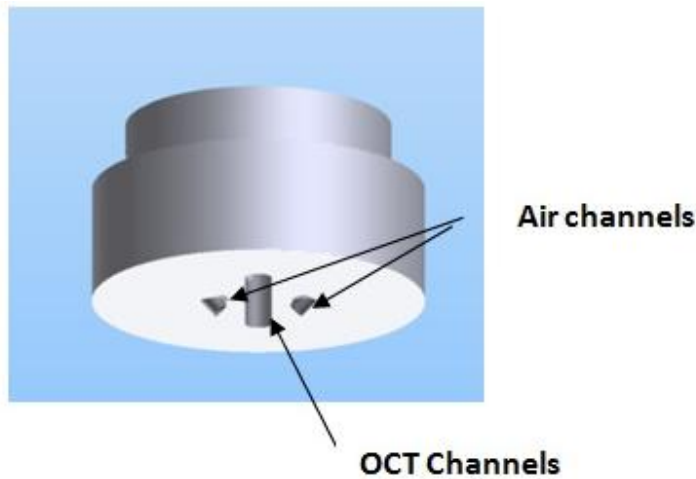


Figure 43: A special OCT tip for the deflection measurements in-vitro. Air channels are positioned at an approximate angle of 70° from the horizontal axis and focus the air stream at the surface examined by OCT. OCT scans the surface to detect the structures of the cross-sectional plane.

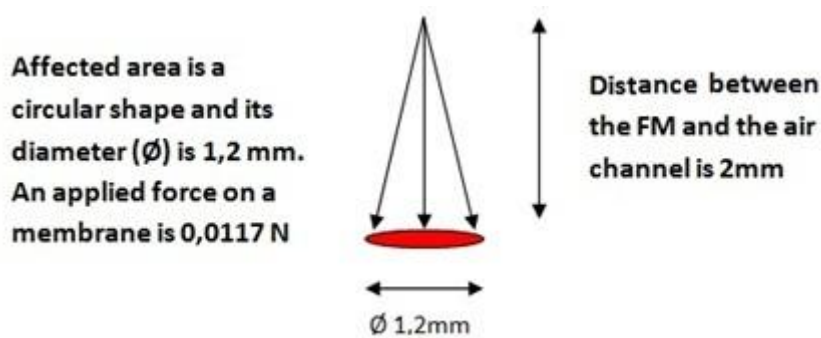


Figure 44: Application parameters of the new OCT tip. When air flow is applied from a distance of 2mm, an affected area's diameter is 1,2mm.

Many measurements were performed on human fetal membranes with the new OCT tip to determine an efficient air flow pressure, with consideration for the different inner pressure values of the membrane chamber. Figure 45 and figure 46 show the deflection results in various inner pressure values.

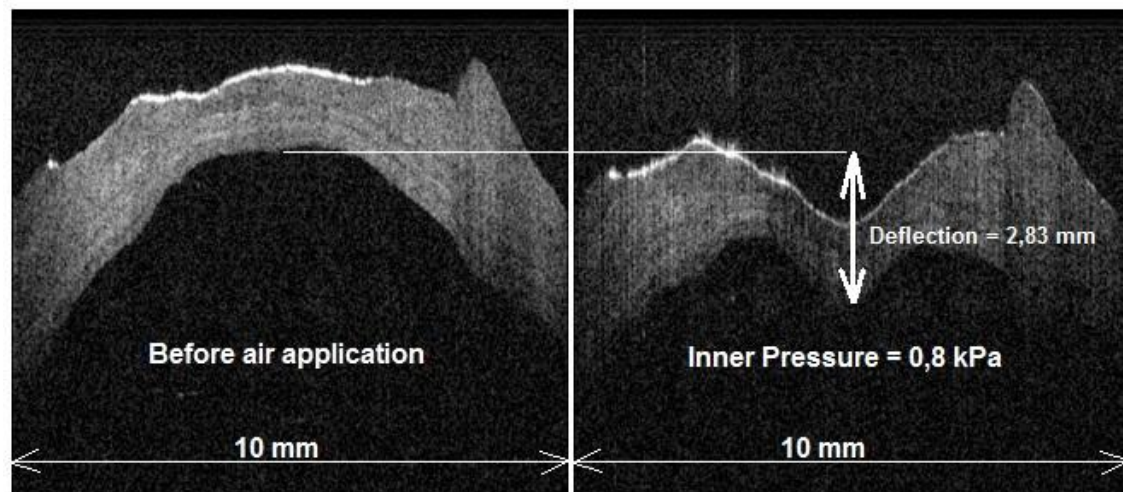


Figure 45: A view of the FM before and after the air application. Structures and the thickness of the FM can be easily examined. The deflection is 2,83 mm when the inner pressure of the membrane chamber is 0,8 kPa.

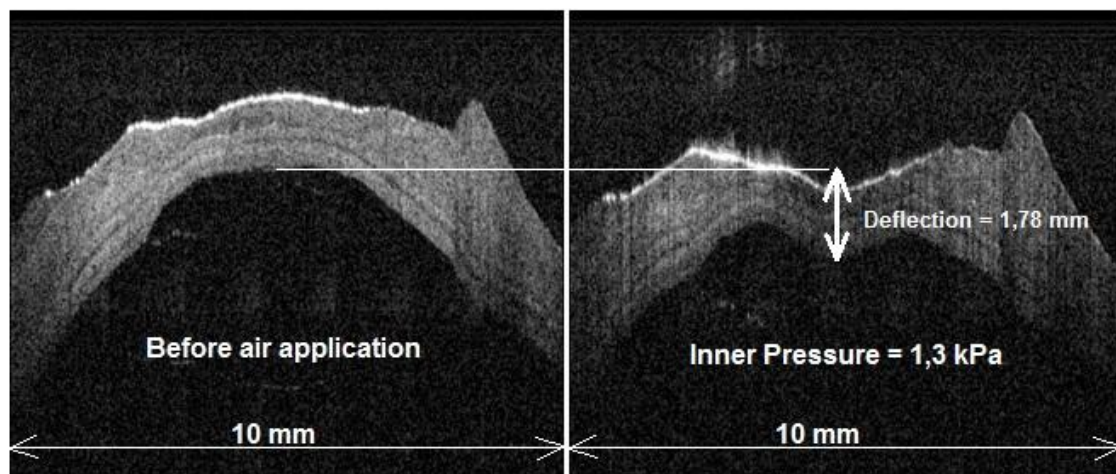


Figure 46: A view of the FM before and after the air application. Structures and the thickness of FM can be easily examined. The deflection is 1,78 mm when the inner pressure of the membrane chamber is 1,3 kPa.

The biological inner pressure of the fetal membranes varies between 0,15 kPa and 1,75 kPa (Fisk, Ronderos-Dumit, Tannirandorn, Nicolini, Talbert, and Rodeck, 1992), so the measurements were applied between these two inner pressure limits, then the air flow was applied onto the membrane. The deflection test conducted under constant air flow (0,0117 N from the distance of 2 mm with an 1,2 mm affected area's diameter) produced deflection results varying between 0,1 mm and 3 mm, with respect to the inner pressure. These parameters are convenient for OCT measurement principles. The

technology can be applied on a handheld probe and the measurement can be performed in-vivo by transmitting the data with fiber optic cables.

4.3.2. Spectral Absorbance Results

Spectrum measurement is an alternative method used to detect some structures and substances in biology since all the biological substances have different optical responses. This method is important for the current study to detect collagen amounts in the FM. Collagen is a kind of protein and supports the structure of the FM. Collagen is a focal point in detecting of premature ruptures because it has been proved that membranes which ruptures before onset of labour are weaker than membranes which ruptures after onset of labour (assuming the same pregnancy duration). If collagen amounts can be detected in the FM, then diagnosing premature ruptures will be possible.

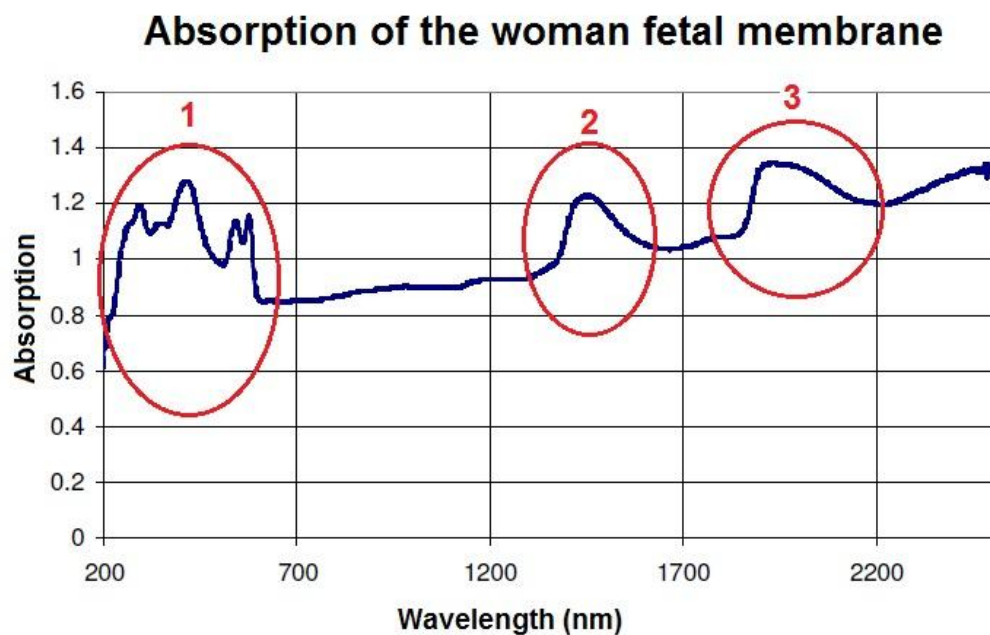


Figure 47: Absorption of the FM. Three strong absorption zones exist.

Figure 47 shows the absorbance measurement of the fetal membrane under a light spectrum of 200nm to 2500nm. The applied spectrum was wide to detect all peaks. Three different zones were detected. The first peak was at the spectrum of light between 250nm and 600nm. The strongest absorption in the first zone was at 415nm. This

wavelength is close to hemoglobin's wavelength, so probably collagen's wavelength interferes with hemoglobin. The second peak (at 1450nm) and the third peak (1900nm) belong to water molecules.

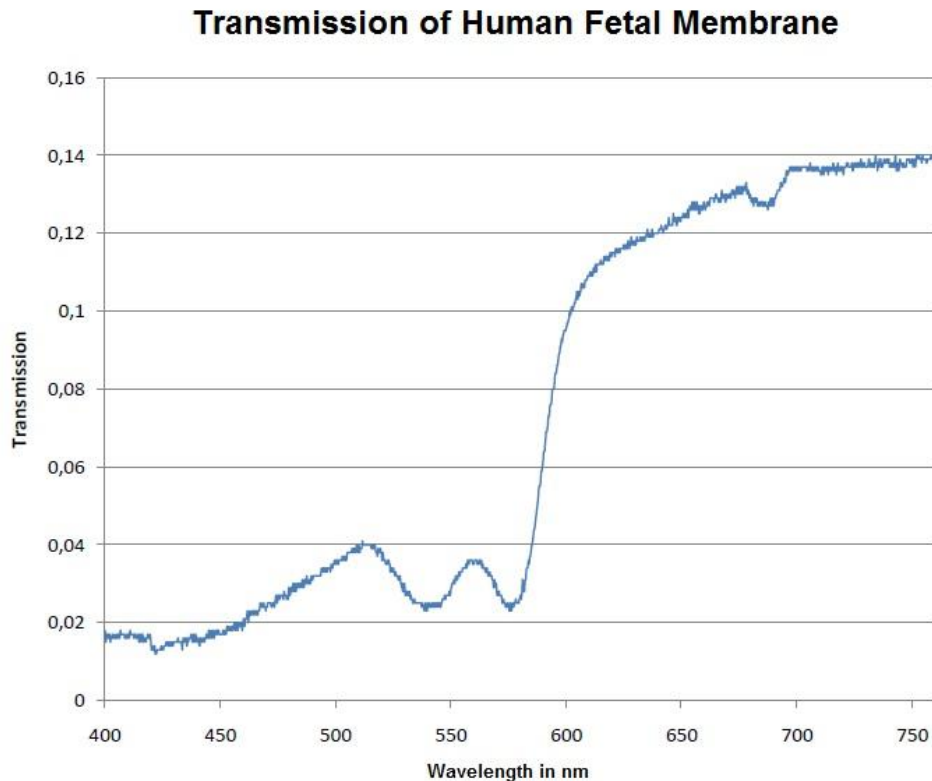


Figure 48: *Transmission of the FM. Spectrum of light at between 400nm – 750nm.*

Figure 48 shows the results of transmission measurements on fetal membranes. This time the spectrum of light applied is at between 400nm and 750nm. These figure shows that the structure of the FM can not be detected separately. The total absorbance zone can be found, however it can not be used to interpret the amount of collagen. Therefore, autofluorescence measurements would be better option than the spectrum absorbance measurements.

4.3.3. Autofluorescence Results

Autofluorescence measurement techniques are similar to spectrum absorbance techniques. The difference is the light source that is fixed at a certain wavelength is used for excitation instead of a light spectrum. This time emissions were measured instead of measuring the absorbance and the transmission of the light source.

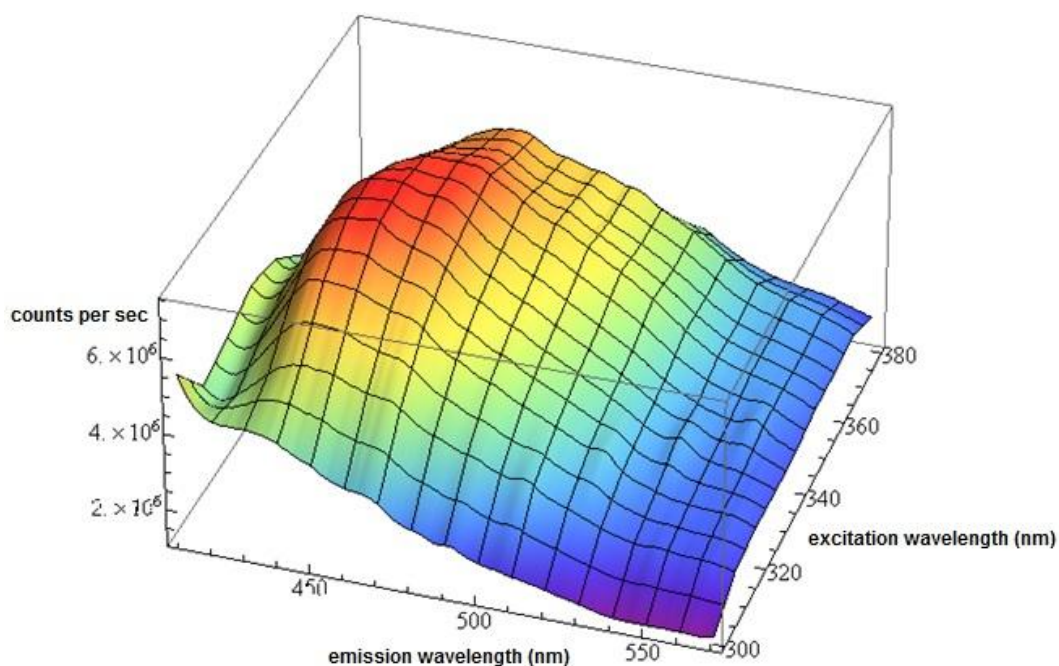


Figure 49: *Autofluorescence measurement. Excitation and emission values are at the same graph.*

A maximum emission was observed when the excitation wavelength used was between 340nm and 360nm, which is the ultraviolet (UV) range. The maximum emission is around the range of 450nm. The results of the Autofluorescence tests were promising, suggesting that this method might be able to detect the structure of the FM in vivo.

5 Discussion

To our knowledge, this study is the first one that examines the thickness, the bursting pressure and the average Stress-strain ratio of human fetal membranes in relation to the birth types. Additionally, this study analyzed the differences in the mechanical characteristics of ruptured fetal membranes. The aim was also to compare the thickness results, to find out if the thicknesses for births occur after 37 weeks of gestation (at fullterm) are thicker than the births which occur before 37 weeks of gestation (at preterm). Equal consideration Of interest was if the membranes that rupture before labour starts (premature rupture) are thinner than the membranes that do not rupture before labour starts (spontaneously rupture) either at fullterm or at preterm.

The physiological and the biomechanical properties of the weak zones, that may cause fetal membrane to rupture, have been, and continue to be the focus of research directed at prognosing premature ruptures of the fetal membrane and preterm birth. If a cause for these cases can be found, then instrumentation could be developed, which could function to predict these instances. Previous studies have examined amniotic epithelium support the belief that membrane rupture begins at the amniotic epithelium (Oyen, Cook, and Calvin , 2004).

Accordingly, the thicknesses of the fetal membranes were measured to determine the characteristics of the amnion and the chorion. It was reported that the thickness of the amnion is approximately $\frac{1}{4}$ the thickness of the chorion (Halaburt, Uldbjerg, Helmig, and Ohlsson , 1989;Jabareen, Mallik, Bilic, Zisch, and Mazza , 2009;Oxlund, Helmig, Halaburt, and Uldbjerg , 1990;Oyen, Cook, and Calvin , 2004). One study which focused on the amniotic sack's ultra structure concluded that the thickness is decreasing near the rupture side (Bou-Resli, Al-Zaid, and Ibrahim , 1981). Disorganized and diminished collagen fibers in the spongy layer and the fibroblast layers on the rupture side of the membranes were also observed (Bou-Resli, Al-Zaid, and Ibrahim , 1981). Some researchers have succeeded in determining the collagen content of fetal membranes biochemically (Bou-Resli, Al-Zaid, and Ibrahim , 1981). In one of the studies, it was demonstrated that total collagen content is % 50 less in the chorion (Al-Zaid, Bou-Resli, and Ibrahim , 1980) than in the amnion. Likewise, two different studies observed elasticity loss in early rupture cases (Parry-Jones and Priya , 1976;Artal, Sokol, Neuman, Burstein, and Stojkov , 1976).

In addition to these studies, the weak zones of membranes have been analyzed with biomechanical measurements such as uniaxial tensile, biaxial inflation burst, and biaxial puncture tests (Moore, Mansour, Redline, Mercer, and Moore , 2006). Concerning the tensile tests, it was reported that strips of membrane taken from along the membrane tear line were weaker than those taken non-adjacent to the tear line (Lavery and Miller , 1979;Lavery, Miller, and Knight , 1982;Lavery and Miller , 1977). In the latter, they noted that the amnion and the chorion were tightly adherent and supported each other. According to Lavery and Miller, the amnion is stronger than the chorion (Lavery and Miller , 1979;Lavery and Miller , 1977).

As the mapping was also an important point in this study, the definition of subzones was very important. One study defined the fetal membranes obtained from elective caesarean and spontaneous vaginal birth as the “placental edge”, the zone across from that as the “rupture zone”, and the region between these two is as the “mid-zone” (Helmig, Oxlund, Petersen, and Uldbjerg , 1993). In this study, there was no difference in regional thickness in elective caesarean membranes, whereas a reduced thickness was observed at the rupture region for spontaneous vaginal births.

Although it was reported that woman who delivered preterm had greater fetal membrane thickness than did those who delivered at term (Severi, Bocchi, Voltolini, Borges, Florio, and Petraglia , 2008), the results of the current study presents opposite. This difference in results could be attributed to a difference in sampling and methodology, since the other study used ultrasound technology on the pregnant women to measure and analyze the FM (Severi, Bocchi, Voltolini, Borges, Florio, and Petraglia , 2008). The techniques of the current study depend on the newly designed DIMPAST device and all experiments were performed on mapped membranes in-vitro. Another important point is that the results of the current study show the average values of the complete fetal membrane (for each group). Measurements in the other study were taken about 3cm from the umbilical cord (Severi, Bocchi, Voltolini, Borges, Florio, and Petraglia , 2008). The difference in measurement location could contribute to the difference in results between the two studies.

Optical Coherence Tomography (OCT) is a vital tool in the field of medical imaging (Huang, Swanson, Lin, Schuman, Stinson, Chang, Hee, Flotte, Gregory, Puliafito, and . 1991;Sepehr, Armstrong, Guo, Su, Perez, Chen, and Wong , 2008). OCT has been used

in many cancer studies to detect the mucosal patterns of the soft tissues (Escobar, Rojas-Espaillet, Tisci, Enerson, Brainard, Smith, Tresser, Feldchtein, Rojas, and Belinson , 2006). Prior medical investigations have demonstrated that the OCT data is more informative for organs with epithelial tissues (Escobar, Rojas-Espaillet, Tisci, Enerson, Brainard, Smith, Tresser, Feldchtein, Rojas, and Belinson , 2006). Using OCT in combination with catheters or endoscopes may enable the imaging of internal organs such as the cervix, uterus tissues, and the ovaries (Ascencio, Collinet, Cosson, and Mordon , 2007). While OCT imaging has proven useful for diagnosing other medical problems, this study focused on demonstrating the feasibility of performing in-vitro OCT scans on human fetal membranes.

For the first part of the study, the collected fetal membranes were analysed not only with OCT, but in parallel with histological analysis. This was necessary since this study marked the very first time that OCT imaging was used on fetal membranes in-vitro. The results showed that the histological analysis was more accurate than OCT, since OCT data did have larger **Standard Deviations (SD)** than histological results. However, there is still the possibility to increase the resolution of the OCT images and apply improved software to decrease the SD. Another possibility is to increase the number of fetal membranes samples, which would increase the amount of data recovered for all birth types and membrane zones. This additional information should smoothen the data spread and minimize the impact of data ambiguities on the SD.

Histological analysis of the Amnion is capable of showing all details of this part, including the **Amniotic cuboidal Epithelium (AE)**, **amniotic Basal Membrane (BM)**, **Compact layer (C)**, **Fibroblast layer (F)**, **Spongy layer (S)**, **Reticular layer (R)**, **Pseudoasal Basal Membrane (PBM)**, and **Trophoblast layer (T)**. OCT images are enough to determine the full thickness of fetal membrane and even chorion and amnion separately but, in order to define the parts of the amnion, the medical-imaging application (OCT) has to be improved. The different layers of the amnion could be a very good marker in diagnosing premature birth. The data obtained in this study so far is giving hope for future clinical applications. Epidemiological studies conducted with OCT could provide normal thickness ranges for fetal membranes, and might also be used for evaluating irregular cases.

Analyses conducted with both OCT and histological techniques illustrated that NB fetal membrane thicknesses were the greatest when compared to PROMB and PRB. This difference in membrane thickness may be attributed to the relationship between gestational length and water accumulation. Literature states that the approach of birth causes water accumulation, which is believed to be one of the onset markers for an approached birth (Sutherland , 1998). **Hyaluronic Acid (HA)** accumulates between the two main layers of the fetal membrane as the gestation period nears fulfillment (Sutherland , 1998). Since HA binds a large amount of water (up to six liters may be bound per gram of HA) (Sutherland , 1998), this might explain the difference in thickness between PRB and NB. As previously mentioned, while PROMB and NB do have the same gestation duration (40 ± 3 weeks), PROMB are characterized by membrane failure, prior to contractions and the onset of labour (Sutherland , 1998). This study assessed not only the full thickness of the fetal membranes, but also compared the areas on the fetal membrane as rupture side, mid zone and placental edges. The data showed the rupture side of the membrane was thinner than the rest. The thickest location was the placental edge of the membrane.

Bursting pressure method was used by Lavery and Miller (Lavery and Miller , 1979;Lavery, Miller, and Knight , 1982;Lavery and Miller , 1977). According to them, it was concluded that the amnion was stronger than the chorion. This observation is supported by the current study, which found that the chorion ruptured before the amnion during the bursting pressure test. Al-Zaid and Bou-Resli reported that membranes which rupture spontaneously at preterm are stronger than membranes which rupture spontaneously at term, according to bursting pressure comparison (Al-Zaid, Bou-Resli, and Goldspink , 1980). This comment directly supports the current study.

Furthermore, this study assessed the Stress-Strain ratio of the different membranes. Although the term “Young’s Modulus” is not valid for the tissues (Holzapfel, Sommer, and Regitnig , 2004;Staat, Sponagel, and Nhu Huynh Nguyen , 2009). Many researchers use that term instead of the Stress-Strain ratio. It was reported that when comparing preterm and fullterm amniotic membranes, the Young’s modulus of preterm amniotic membranes was found to be significantly higher than that of fullterm membranes (son-Martin, Zammaretti, Bilic, Schweizer, Portmann-Lanz, Burkhardt, Zimmermann, and Ochsenbein-Kolble , 2006). Thus, preterm amniotic membranes are stiffer than full term

membranes. They also reported that membranes which ruptured spontaneously are stiffer than prematurely ruptured membranes at fullterm (son-Martin, Zammaretti, Bilic, Schweizer, Portmann-Lanz, Burkhardt, Zimmermann, and Ochsenbein-Kolble , 2006). Interestingly, another research group reported that the Young's modulus of membranes which ruptured spontaneously during labour at fullterm is significantly higher than that of membranes which ruptured prematurely, in other words i.e., prior to the onset of labour, at fullterm (Artal, Sokol, Neuman, Burstein, and Stojkov , 1976). There are also another researchers who found that the concentration of collagen in the amnion of woman having either fullterm or preterm birth is lower with PROM than without PROM (Kanayama, Terao, Kawashima, Horiuchi, and Fujimoto , 1985), which indicates that the FM without PROM is more strength that the FM with PROM.

The studies stated above is encouraging the second part of the current. According to the bursting pressure and Stress-strain evaluations, spontaneously ruptured (rupture after onset of labour) membranes seemed to be stronger than the prematurely ruptured membranes. On the other hand, preterm membranes were stronger than fullterm membranes, which means that the PRB's membranes are stiffer than the other 3 types. The weakest type was the PROMB, and this difference was statistically significant.

According to the results, it can be concluded that if the thickness of the fetal membrane is more than 0.28 mm, then the type of birth can be either NB or PROMB. Additionally, if the average stress-strain ratio of the fetal membrane is also greater than 70 kPa, then the resulting birth should be normal (NB – fullterm with a spontaneous rupture).

This study is the first important step towards understanding of the complex relationship between the biomechanical structure of the fetal membranes and the premature rupture of the fetal membranes. The weakest zone of the FM was found to be close to the cervix, and can be observed on mapped membranes (Linder , 2006). This information is especially important in respect to in vivo measurements later on. The cervical area is the only area of the amniotic sac that is accessible from the outside.

Simultaneously, examinations which measure the collagen content in the tissue using autofluorescence can be performed. The UV-A induced autofluorescence of the collagen might be correlated to the average FM collagen content, previously determined

by molecular biologic methods. The knowledge about the exact amount and/or distribution of collagen is meant to support the prognostic in vivo studies.

Based on the results of this study, a first version of an in vivo probe was developed. This probe will be developed and then will be inserted through the cervix of the pregnant woman to conduct these measurements in-vivo.

6 First Version of the OCT Probe

This new OCT probe was designed and produced using the all of the results previously described in the study. The new OCT probe tried on in-vitro measurements, and can be interpreted as a first version of the in-vivo diagnostic probe. The OCT probe has four fiber optic cables inside which allow it to have four separate channels, all capable of performing individual A-Scans. These 4 fibers are controlled with fiber switches which is seen in figure 50B. This switch sequences each channels respectively. Each fiber's length has to be the same to measure the surface of the sample at the same depth. One of these 4 fibers which was named as channel 3 was fixed in length which is exactly the same length as the reference arm length (Figure 50D), so the other 3 fibers's length should be adjusted by using the length tuner (Figure 50A). There are also fiber polarizers (Figure 50C) on the control unit of the new OCT probe.

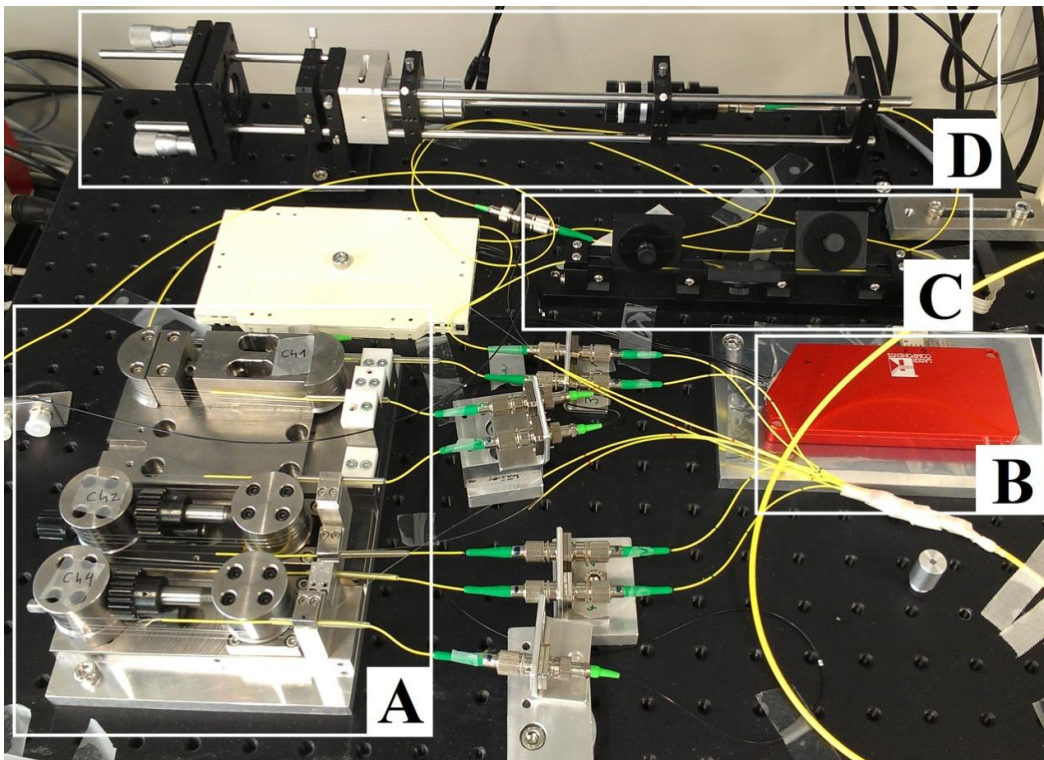


Figure 50: *The control unit of the new OCT probe.*

The new OCT probe is very small. Its diameter is 1,4mm which can be compared with M4 threads in figure 51.

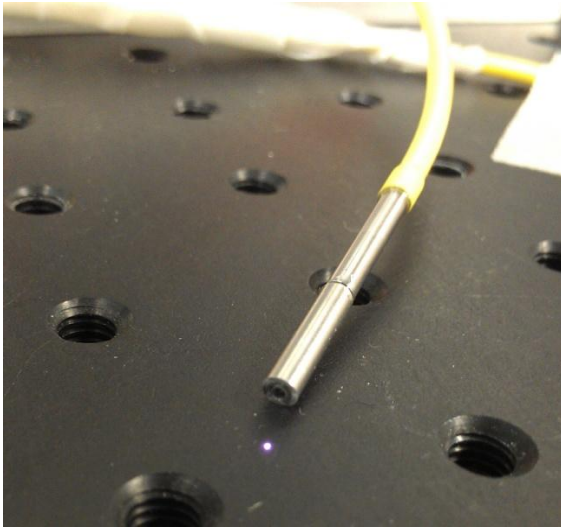


Figure 51: *The new OCT probe. It has 4 channels and each channel is controlled with a fiber optic switch. This photo was captured by a mobile phone, and infrared light from one of the channel can be seen in front of the OCT probe.*

The new OCT probe is controlled with a software which was written in Labview. A front panel of the software can be seen in figure 52. The OCT probe should be calibrated before performing measurements because it has four individual channels and if one of the fiber's length is changed then the position of the membrane surface will be different on that channel. Figure 52 A and C shows the front panel of the service software, figure 52 B and D shows the operating software. If the calibration of the probe is wrong, then the depth of the sample surface will be different for each channel as shown in Figure 52A and B. The length of each fiber should be set to the length of the fiber on channel 3, because the length of fiber on channel 3 was set to the reference arm's length before. When the length of all fibers on each channels are equal, the depth of sample surface will be at the same position (Figure 52 C and D), so the surface of the sample can be detected as a straight layer as shown in Figure 52D.

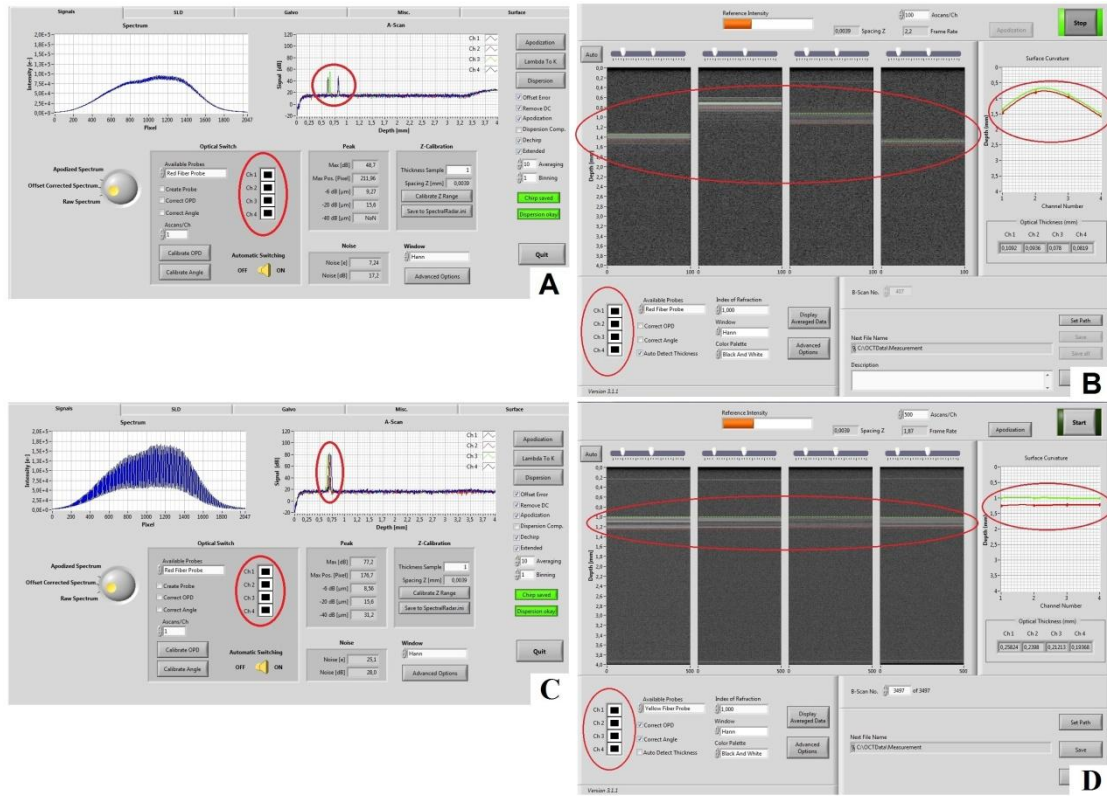


Figure 52: Front panel view of the service (A,C) and the operating (B,D) software of the new OCT probe before calibration (A,B) and after calibration (C,D).

Before trying the new OCT probe, the DIMPAST had to be improved, because the new OCT probe's parameters were different than the old commercial OCT device which was used to get the mechanical properties of the fetal membrane. The new DIMPAST has the same working principle, however the laser sensor (LLT 2700-50(500), Micro Epsilon, Ortenburg, Germany) and the pressure sensor (PA3026, ifm electronic gmbh, Essen, Germany) were different. The previous laser sensor was able to measure a change in distance of +/- 5mm. Therefore, its maximum range was 10mm which was not enough to measure the deflection after inflation of the membrane surface. The new laser sensor can measure a change in distance of +/- 50mm, so its maximum range is 100 mm which is really more than enough for in-vitro measurements. Additionally, the new laser sensor can measure in two dimensions, so the length of a curvature of the inflated membrane can also be recorded. The second difference is the new pressure sensor. It can work either with a fluid or with an air, so it was possible to inflate the membrane with a buffer solution which is more convenient to physiologic conditions.

General view of the new DIMPAST can be seen in figure 53. The new laser sensor and the new pressure sensor can be seen in figure 54.

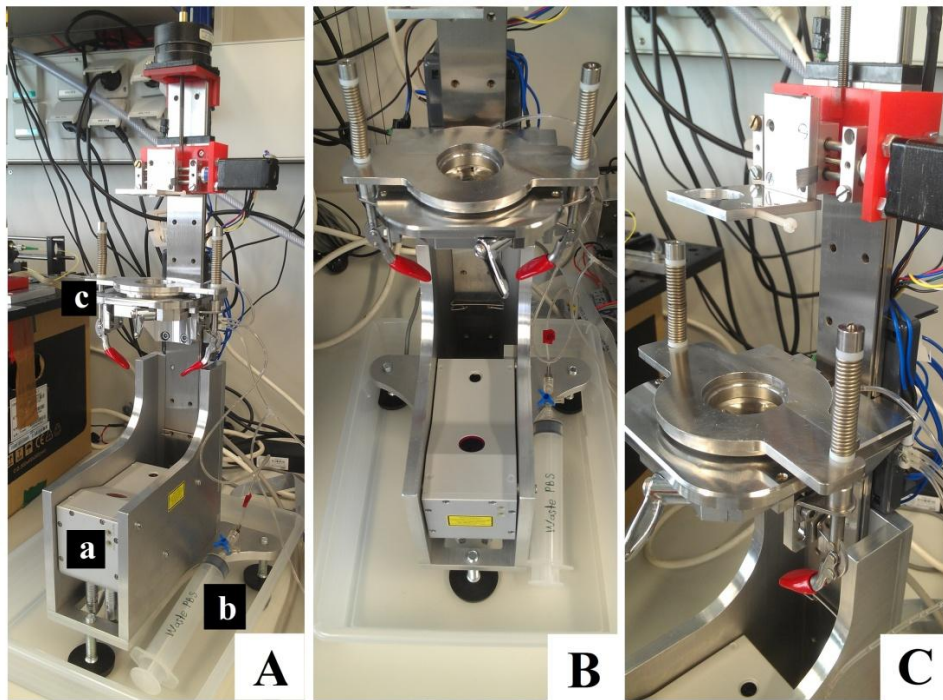


Figure 53: A view of the new DIMPAST. It has new laser sensor (a) which can measure in 2 dimensions. The new DIMPAST is working with a liquid to inflate the membrane, so there is a waste liquid collector (b) and it has a new membrane chamber (c) which has quick fastener system. (A) A general view, (B) a top view and (C) a side view of the DIMPAST shows details of the new system to observe the differences.



Figure 54: (A) A new laser sensor (LLT 2700-50(500), Micro Epsilon, Ortenburg, Germany) and (B) a new pressure sensor (PA3026, ifm electronic gmbh, Essen, Germany) of the new DIMPAST.

Preliminary measurements of the first version of OCT diagnostic probe were conducted with the new OCT probe in conjunction with the new DIMPAST. Figure 55 shows all steps before using the new OCT probe. The first step included stretching a tissue sample over the tissue chamber of the new DIMPAST (Figure 55 A), then using the new tissue fixer to fix the membrane in the targeted position (Figure 55 B). The new tissue fixer has two fast fastener clamps which proved to be simple to use and functioned to properly seal the tissue chamber. Once the tissue chamber was sealed, the membrane was inflated until the inner pressure of the chamber reached a constant pressure. A PBS buffer solution was used to inflate the membrane, while the laser sensor was recording the position of the membrane surface (Figure 55 C). The laser sensor simultaneously assessed the length and the curvature of the membrane surface simultaneously. After this step was completed, the new OCT probe was positioned over the membrane surface with the use of a computer controlled stepper motor. An air channel was mounted to the left hand side of the OCT probe to apply a constant 20 Psi air flow to the membrane surface from a distance of 5mm, and was positioned 2,40 mm away from the first channel of the OCT probe (Figure 55 D).

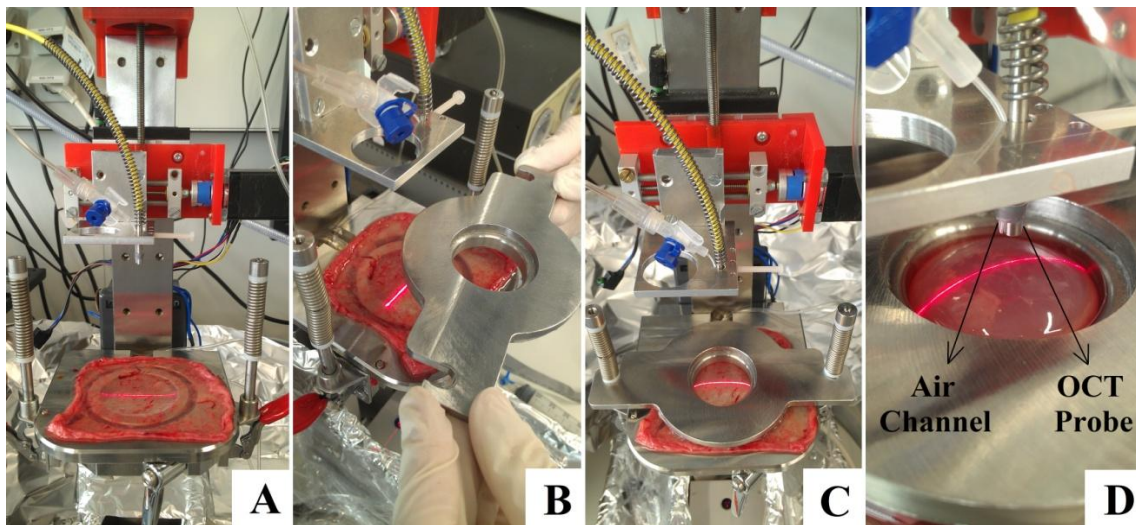


Figure 55: *New setup before using the OCT probe with an air flow.*

After these steps, the membrane was ready for deflection testing (Figure 56). The aim was to prove the feasibility of the OCT probe by conducting a deflection test. The membrane was first inflated to a pre-set pressure level. Next, the air flow, which was supplied and controlled by an air generator, was applied to the membrane surface. The

deflection of the membrane surfaces were measured and compared to one another, since the deflections were different according to the mechanical properties of the membranes.

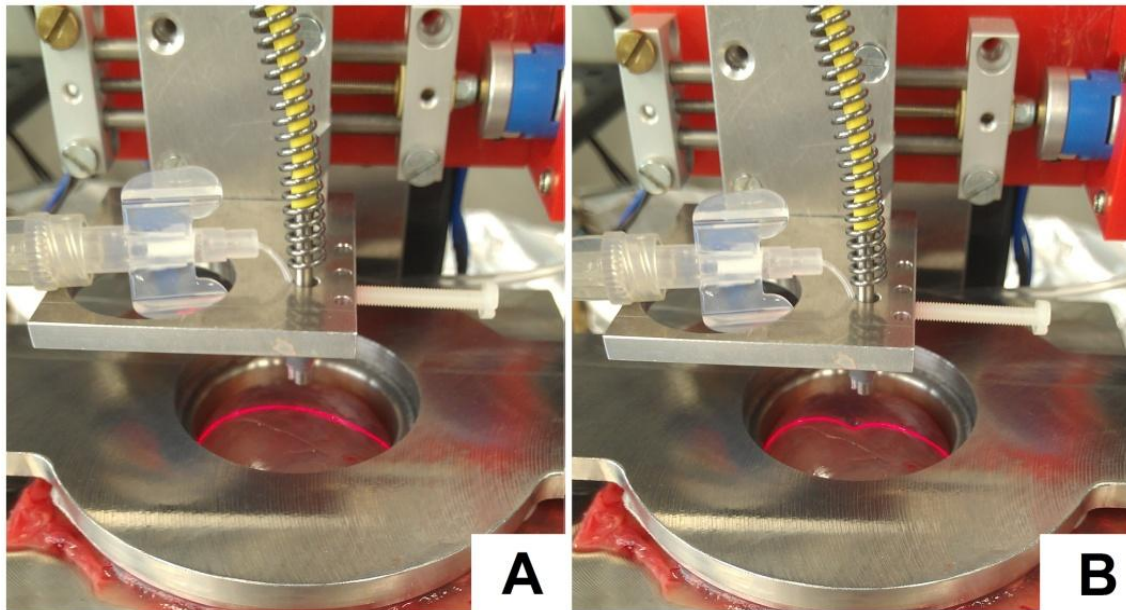


Figure 56: (A) Inflated membrane and (B) its deflection with an air flow.

After the membranes were inflated, the DIMPAST measured the deflection using a two-dimensional laser sensor, which was controlled by labview software. Three graphs were recorded for each measurement. First, the curvature of the inflated fetal membrane surface was captured. The length of curvature, and the radius of the circle, which was derived using curve fitting principles with respect to the curvature length, were recorded. Then the air flow was applied onto the inflated membrane surface to cause deflection. The measurements were performed again using the same parameters and the graph was recorded. Finally, the difference between these two graphs (with and without deflection) was drawn using labview software. All these steps can be seen in figure 57. The deflection was related to the air flow intensity and the inner pressure of the inflated fetal membrane. These two variables should be fixed to compare the deflection between the different kinds of birth.

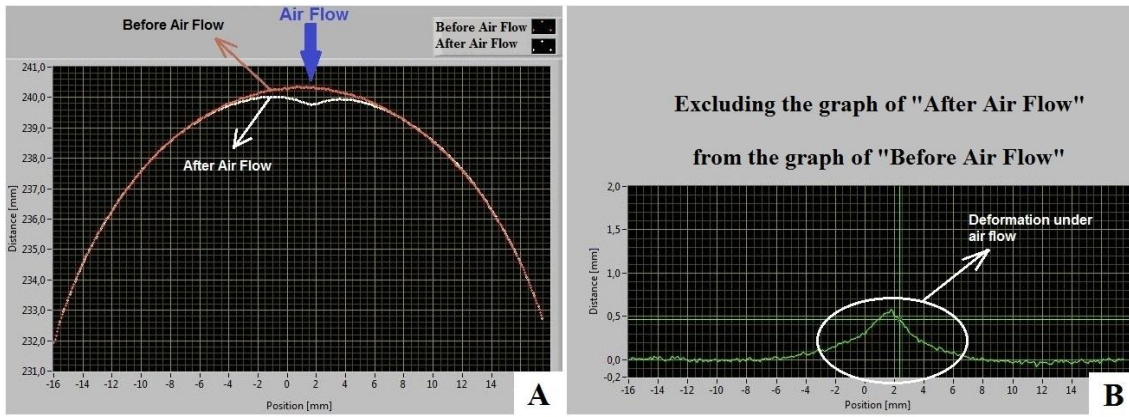


Figure 57: Curvature of the inflated membrane can be seen in this figure. (A) The red graph belongs to membrane without air flow, and the white graph belongs to the membrane at time air flow application. (B) The difference between these two graphs shows the deformation under air flow which is shown by the green graph.

These same measurements were repeated using the new OCT probe. It has four channels and measures the thickness provided by each channel separately. Each channel observed the depth of the upper layer at different positions due to the spherical shape of the inflated membrane. Figure 58 shows the new OCT probe's result. The thickness of the layer can be seen for each channel, so the profile of the upper – bottom layers and the thickness of the membrane can be drawn using these results.

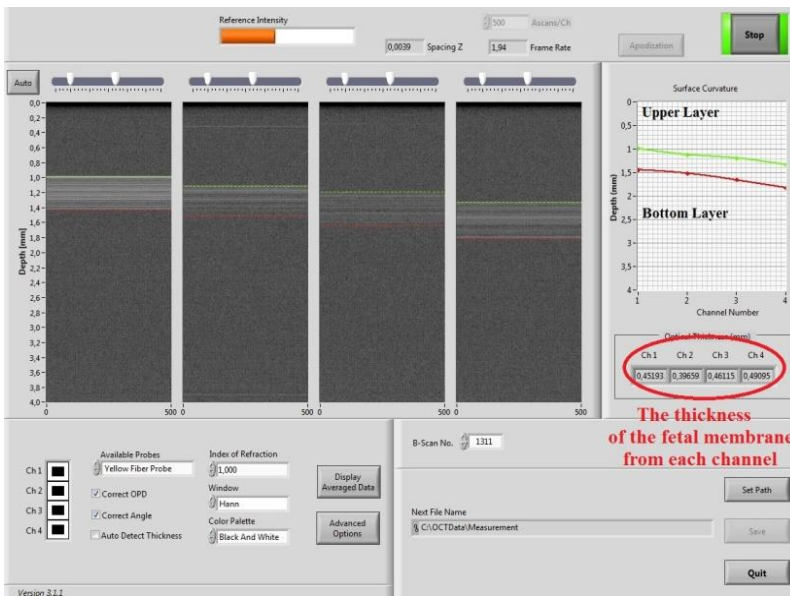


Figure 58: OCT view of the inflated fetal membrane using the new OCT probe, outfitted with four channels. The observed depth of the membrane surface was different for each channel because of the curvature. A green line shows the upper layer of the membrane and a red line shows the lower bottom layer of the membrane. The difference between these two layers shows the thickness of the membrane.

The deflection of the fetal membrane was detected using the new OCT probe after air flow applied. Figure 59 shows the deflection of the membrane's upper layer at the time of air flow application. A green line shows the upper layer of the membrane before application, and a red line shows the upper layer of the membrane after application. The displacement between the green and the red line is the deflection of the fetal membrane under air flow application.

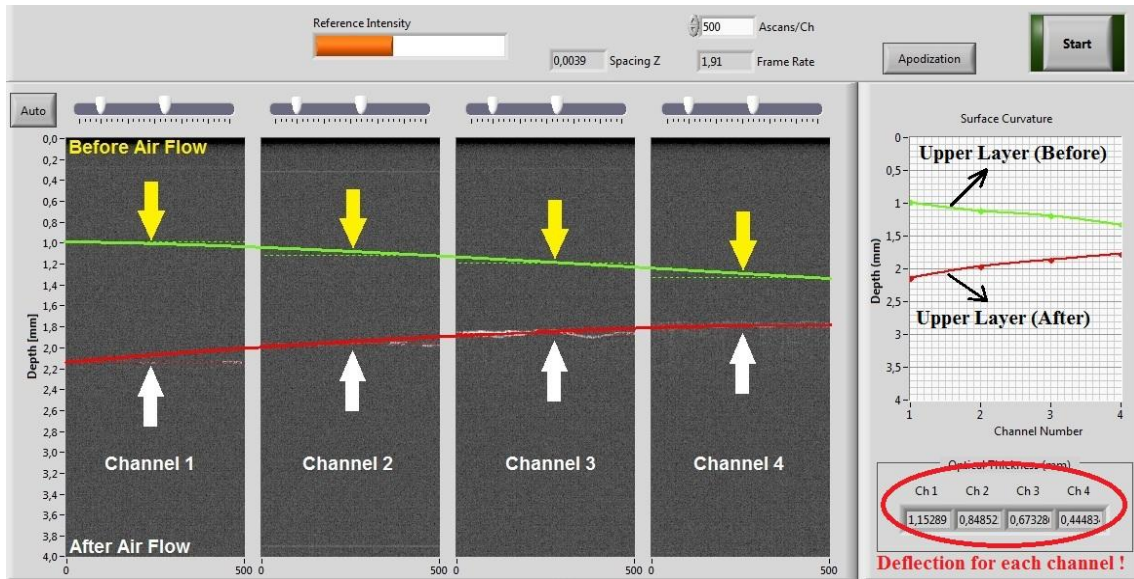


Figure 59: Calculation of the deflection with the OCT probe. Each channel measures separately.

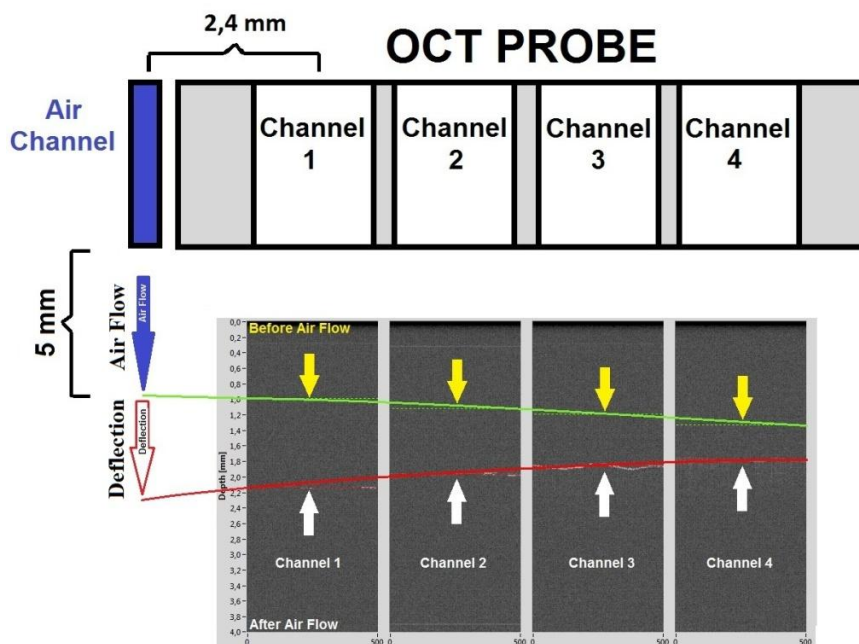
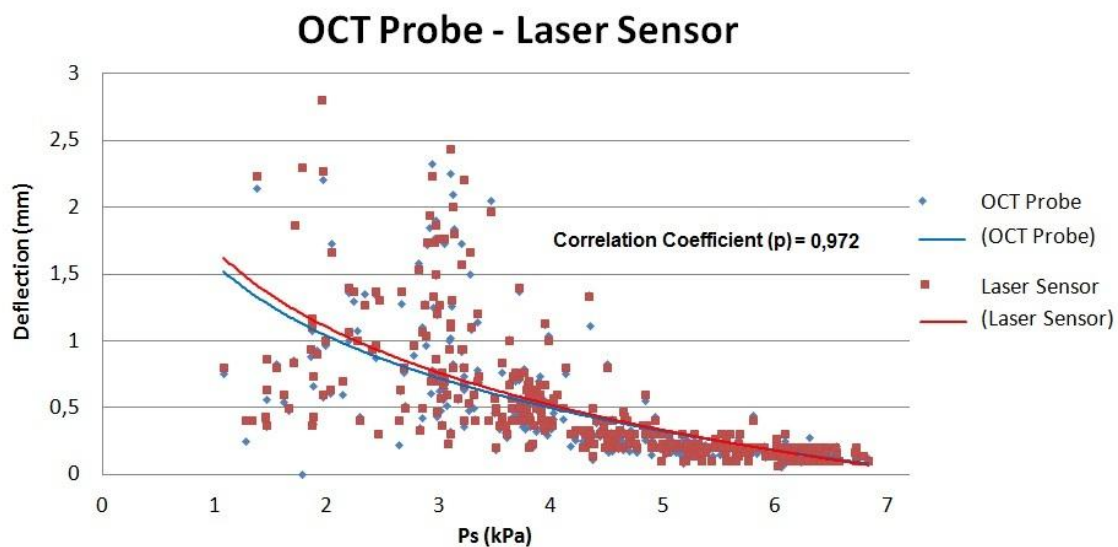


Figure 60: Design of the new OCT probe.

6.1. Preliminary Data With The New OCT Probe

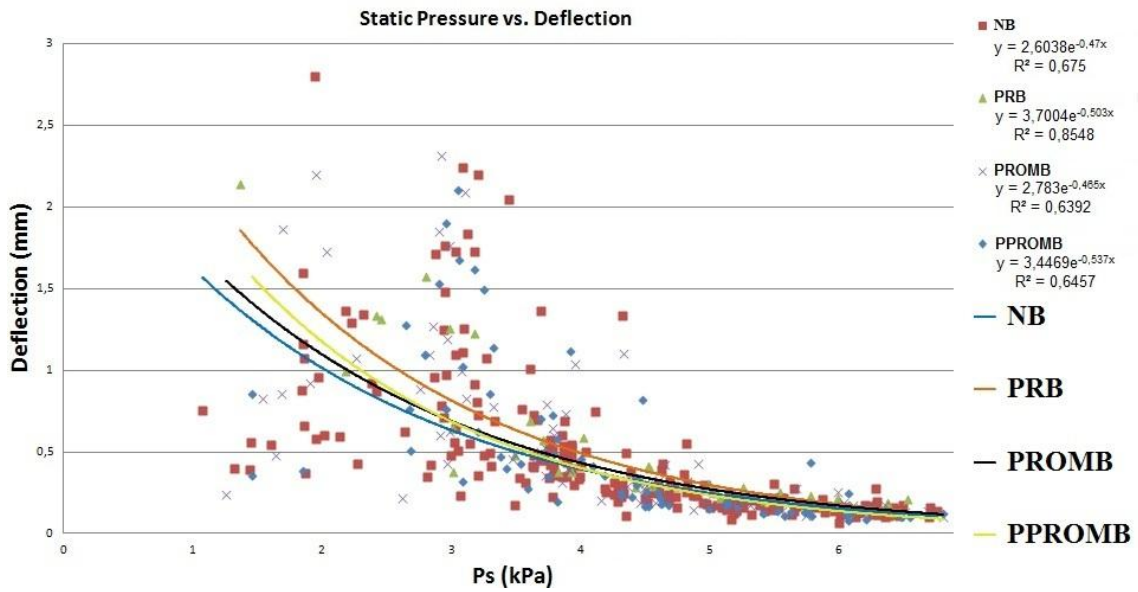
Results from this part of the study are promising. The new OCT probe was tested using a fetal membrane. Before testing the device, the fetal membrane was mapped as usual, and each piece of fetal membranes was observed using the new OCT probe and the new DIMPAST. Then the pieces of fetal membrane were placed onto the tissue chamber of the new DIMPAST independently, and inflated to a predetermined inner pressure level. Later, an air flow was applied on the middle of the FM sample. The air flow intensity was controlled using an air generator, which supplied a pressure of 20 Psi. The force caused by the 20 Psi air flow was 0,02 N on the surface of the piece of tissue. Finally, the deflection amounts were recorded using two methods. Measurements were performed at different inner pressure levels, which ranged between 2,34kPa and 7,7kPa. Graph 5 shows the relation between inner pressure (Ps) and deflection. While the inner pressure of the FM was increasing, the deflection amount was decreasing respectively.



Graph 5: *The amount of deflection with respect to the inner pressure. Deflection was measured with the new OCT probe and is compared with the laser sensor. OCT probe was in correlation with the laser sensor ($p=0,972$).*

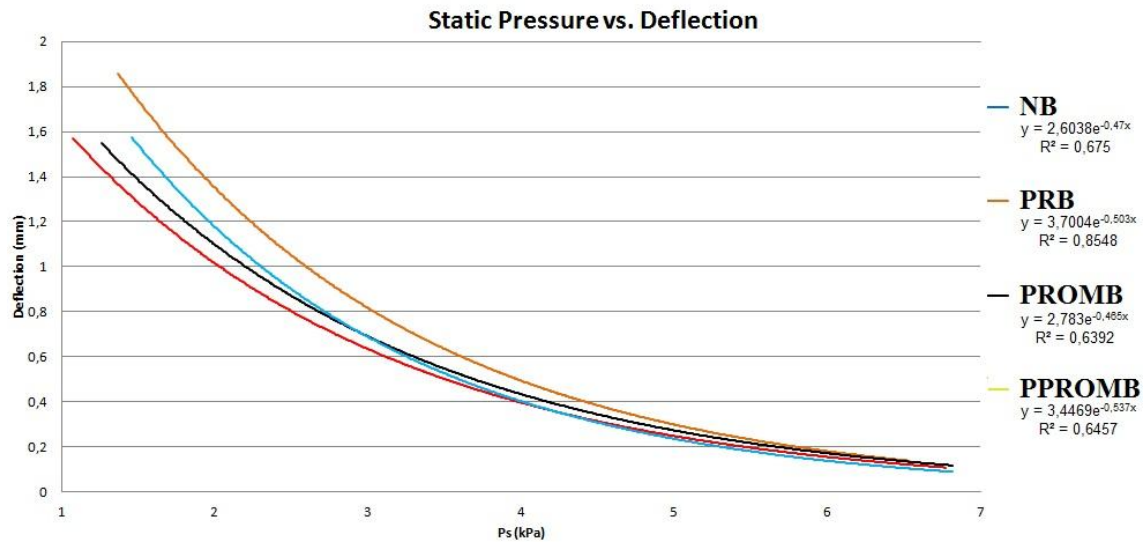
Graph 5 represents 382 measurements for each technique; the OCT probe and the laser sensor. The correlation between the new OCT probe and the laser sensor was strong according to spearman rank sum test ($p= 0,972$). After the strong correlation, distinction

of birth types according to inner-static pressure versus deflection data was tried to be observed. Graph 6 shows the all results with the new OCT probe respect to birth types.



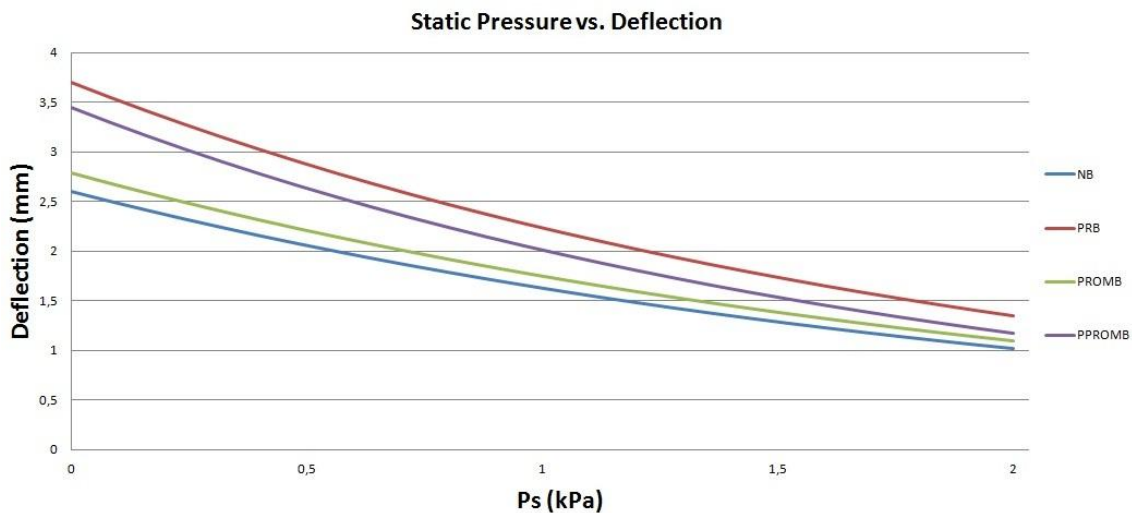
Graph 6: Pressure vs. Deflection Curve for all kinds of birth with the OCT probe. Each measurement is represented with a dot.

There was a negative correlation between pressure and deflection results for all FMs collected from different types of births. Each birth type’s pressure vs. deflection data was plotted by Microsoft Office Excel as it can be seen in graphs 6 and 7.



Graph 7: Pressure vs. Deflection Curve for all kinds of birth with the OCT probe. Charts were derived by the function of each birth types’ graph.

Measurements were done at between 1 kPa and 7 kPa, however a resting amniotic pressure can vary between 1,1mm Hg (0,15kPa) to 13,1 mm Hg (1,75kPa) (Fisk, Ronderos-Dumit, Tannirandorn, Nicolini, Talbert, and Rodeck , 1992) and **Intra-amniotic Pressure (IAP)** can increase maximum up to 2,66-3,99 kPa when Braxton-Hicks contractions occur in uterus (Fisk, Ronderos-Dumit, Tannirandorn, Nicolini, Talbert, and Rodeck , 1992;Moore, Mansour, Redline, Mercer, and Moore , 2006), so important inner pressure interval is up to 2 kPa in normal conditions. If birth types can be distinguished at between this physiologic normal IAP conditions, preterm births and prelabour ruptures can be predicted. For this reason, part of the chart, which is until 2kPa, is important. If the sampling rate of the new OCT probe is increased, then lower IAP levels can be observed better. Because, when IAP is less, vibration is more on the surface of the tissue at the time of air flow application, so OCT probe's speed should be high to catch the surface of the tissue. According to the function of the each birth types' graph, a new chart was plotted (graph 8) by a software (Sigma Plot for Windows Version 11,0), although the OCT probe could not measured the deflection at a IAP level that was lower than 1 kPa.



Graph 8: *Pressure vs. Deflection Curve for all kinds of birth with the OCT probe. Inner pressure value is up to 2 kPa which is the physiological limits of resting intra amniotic pressure.*

All types of birth can be distinguished when P_s is at between 0 kPa and 2 kPa which is a resting IAP interval (Fisk, Ronderos-Dumit, Tannirandorn, Nicolini, Talbert, and Rodeck, 1992).

As it can be seen in last four graphs (Graph 5, 6, 7 and 8), results with the new OCT probe are promising. All types of birth can be distinguished according to the deflection characteristics with the new OCT probe and also the physical dimensions of the new OCT probe are convenient for performing in-vivo measurements, which allows it to be used in in-vivo deflection measurement of the FM at IAP range. As a result, the mechanical parameters of the FM could be gathered in-vivo and used to further develop an in-vivo probe that is capable of diagnosing prelabour ruptures and preterm births.

7 Conclusion

Despite previously reported conflicting data, the thicknesses of PRB's membranes were found to be thinner than NB membranes in all locations. It was thought that the thickness of the fetal membrane can be a diagnostic marker to predict if the birth is coming and/or could indicate which pregnancies might be at risk of PRB. OCT resolution should be improved by upgrading the imaging software, even extending imaging capabilities to check the amnion layers separately one day. The number of measurements should also be increased to provide more data for statistical evaluations, which would also enhance the data concerning thickness properties of the fetal membrane. Furthermore, a follow-up study on water content between amnion and chorion would be desirable to enhance previous data and understand of its role in preterm births.

In conclusion, all these actions, along with improvements made to OCT technology could help predict the probability of preterm births and the prelabour rupture of membranes.

7.1 Outlooks

The results of the current study identified mechanical parameters of the FM that might be examined in-vivo with a properly designed probe. The extra experiments conducted and their results show that the structure of the FM can be also examined using optical methods. The probe should be hand held for practical usage, and should have a disposable penetration tip. There should also be a lavage channel to wash the FM surface to get rid of blood since hemoglobin and bilirubin are blood substances which interfere with collagen wavelength emissions.

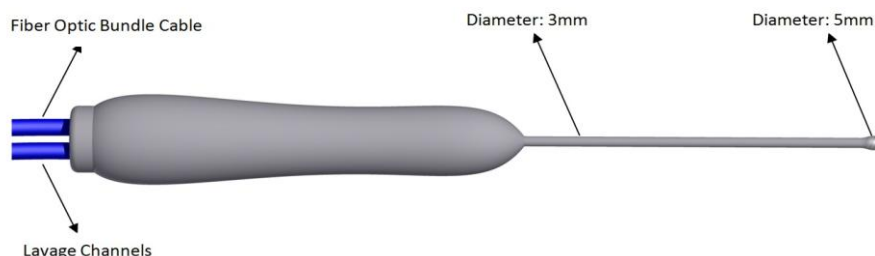


Figure 61: *Proposal for handheld in vivo diagnostic probe.*

The diameter of the probe tip is restricted by the inner diameter of a cervical channel. Lavage channels may have two pipes, one for pumping water and the other for sucking water. Due to the restricted diameter, data should be carried via fiber optic cables.

The deflection of the membrane under constant air flow can be calculated using four different measurement sensors in-vivo, rather than of scanning the total inspected area. If the air flow axis is accepted as a symmetric axis, then the four static OCT sensors which are all located on one side of the air focal point, can be used to measure the deflection of the membrane in vivo.

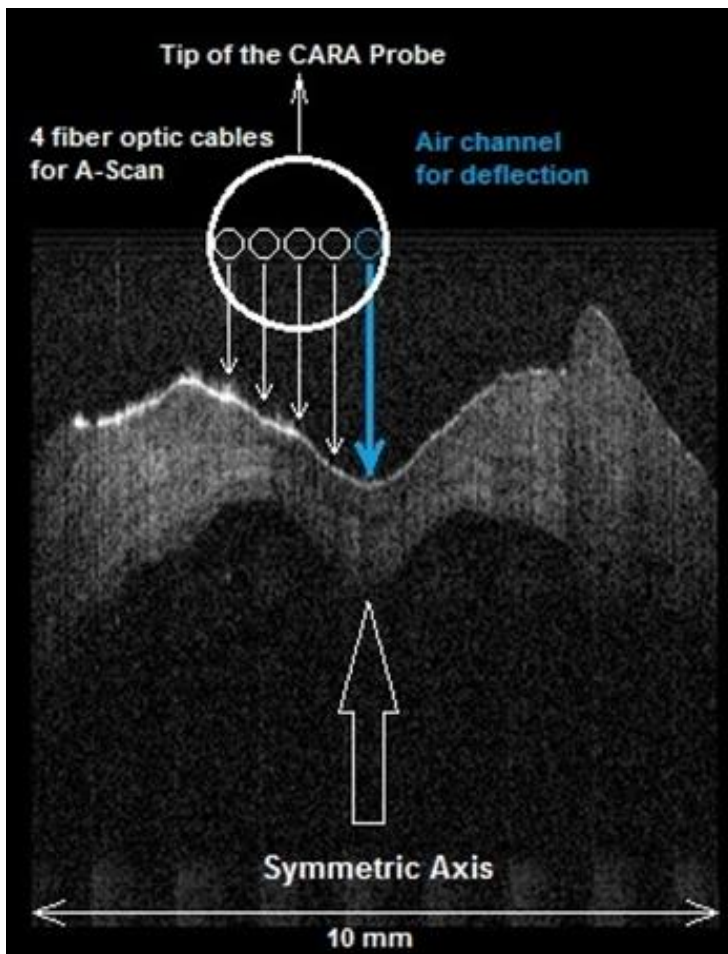


Figure 62: Deflection measurement with four fiber optic cables. A blue arrow shows the air flow direction, and the other four white arrows show the static OCT measurements.

The right and a left side of the deflection curve are symmetrical, so three dimensional deflections can be depicted using software and these 4 static measurements.

As a result, the thickness, the deflection, the spectrum of FM and the fluorescence of the FM can be measured in-vivo.

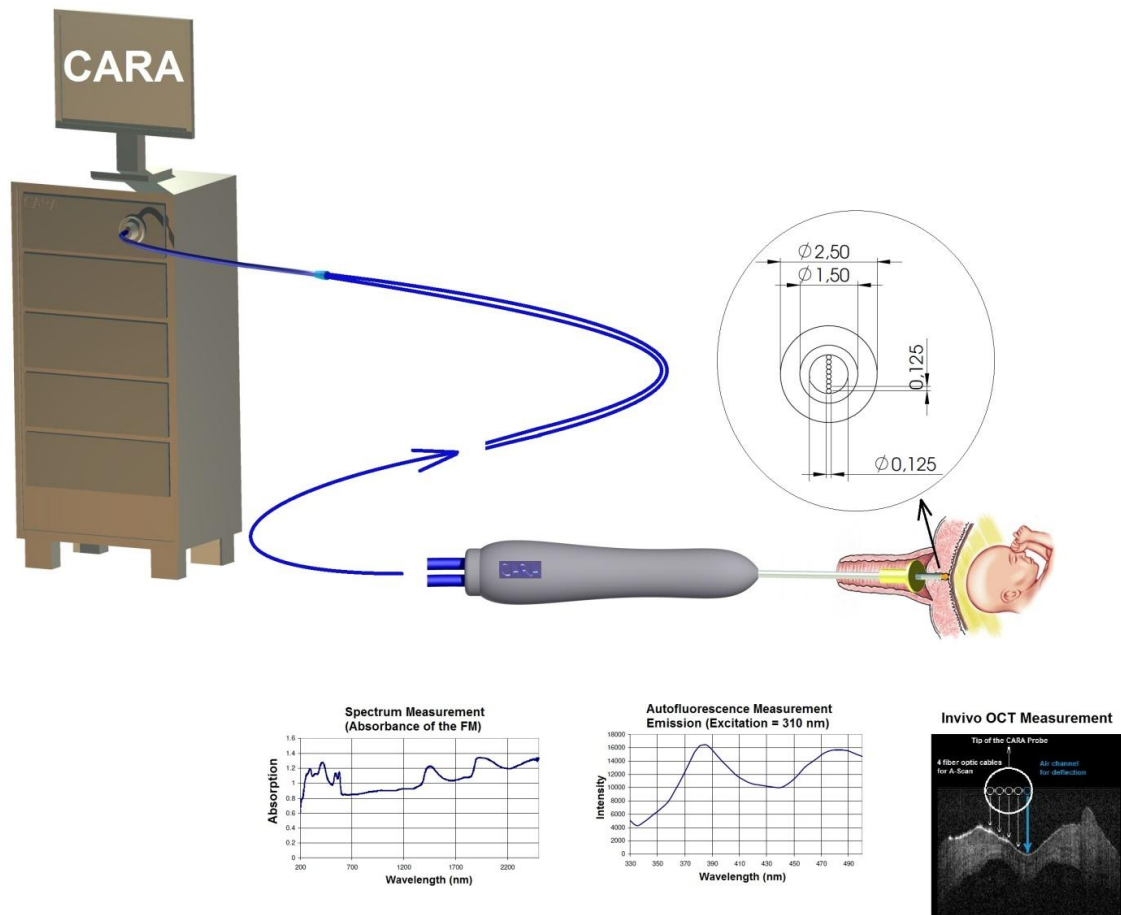


Figure 63: Setup of the diagnostic probe.

8 Summary

Newborns are defined as a “preterm” if the gestational age is younger than 37 weeks, and “fullterm” stands for births taking place between 37-42 weeks of gestation. Prelabour rupture of membrane (PROM) can occur in both at fullterm and preterm births. When birth occurs at fullterm without any PROM is called normal birth (NB). Similarly, if the birth occurs at preterm without any PROM is called preterm birth (PRB). However, if PROM occurs at fullterm, it is called prelabour rupture of membrane birth (PROMB), and if the PROM occurs at preterm then it is called preterm prelabour rupture of membrane birth (PPROMB).

PRBs are one of the most frequent causes of mortality during or after birth. The etiology of PRB is inadequately understood and many biochemical investigations have been undertaken in an attempt to find the cause, or causes. In most pregnancies, labor begins at full term with intact fetal membranes. However, PROM occurs in 10% of pregnancies at full term and exceed 40% of pregnancies at preterm.

The fetal membranes, chorion and amnion, form together a ~0.5 mm thin bi-layer that serves as a barrier and a container throughout gestation. The mechanical integrity of the fetal tissue is crucial for maintaining a healthy gestation. Altered tissue biomechanics can cause drastic changes in the labor type by contributing to premature cervical dilation and delivery.

Mechanical rupture of membranes is a part of the natural sequence for full term delivery. However, serious complications can arise if the membrane is ruptured prior to proper term length. In surviving infants, morbidity is often severe and includes chronic lung disease, neurologic sequela such as blindness, white matter damage and periventricular leukomalacia. Understanding the mechanical behavior of fetal membranes is a necessary issue for attempting to prognoses or even prevent prelabour ruptures in both full-term and pre-term. Significant information exists on the mechanical structure of amnion and chorion and their general relation to membrane strength.

Reduction of the collagen in tissue, affects the tensile strength of the membrane. Changes in the viscoelastic properties are affecting the tissue’s ability to adjust to

stretch forces caused by mechanical tissue damage (perhaps by realignment or disruption of interconnections of collagen fibers). Viscoelasticity is also an important factor in predicting the rupture of membranes. A lower Stress-Strain ratio as well as membrane stretching may cause the membrane to rupture.

The identification of mechanical characteristics of fetal membrane may help in understanding the mechanisms involved in rupture before the onset of labor. This knowledge is also essential in order to understand the role of fetal membrane changes associated with prelabour rupture. The purpose of this study was to examine the mechanical properties of the fetal membrane in order to interpret the causality of prelabour ruptures and preterm births. Furthermore, the results of this study were used to design a risk assessment profile and diagnostic tool, capable of prognosticating prelabour ruptures and preterm delivery.

A device (DIMPAST) capable of making in-vitro measurements was designed in three steps, and has become the basis for further potential projects. The DIMPAST uses different measurement techniques such as laser triangulation, air pressure measurement, and optical coherence tomography. A total of 87 fetal membranes were collected and analyzed before designing a new probe in this study. Samples from the 45 FMs used for comparing the thickness between histologic and OCT methods to prove the OCT's reliability, were fixed with a formaldehyde solution (3.7 %) and stored at 4 °C until they were tested later that day. Then the other 42 FM samples used for the evaluation of mechanical properties were prepared and stored at 4 °C before being tested.

The significance of the differences between the groups was calculated using Mann-Whitney rank sum test. The results of the study showed three important characteristics and are outlined as: Membranes do get thicker as the gestational time increases however, it should not be interpreted that thicker membranes are stronger. Stronger membranes do not rupture before labor begins. The average stress-strain ratio and the bursting pressure of PRB's fetal membranes are significantly higher than those for other types of membranes. Results from the three different measurement methods for each type of birth were summarized to draw conclusions. The three primary interests of this part of the study were the total thickness, the bursting pressure, and the average Stress-strain ratio for each type of fetal membrane.

According to these hopeful results, a new OCT probe was designed and manufactured. Preliminary data that was observed with a new OCT probe is willing hope for the future and its results are in correlation with the results which were taken with the DIMPAST, so the new probe can be used in clinical researches after improving its reliability.

In conclusion, this study provides an understanding of the complex relationship between the biomechanical structure of the fetal membrane and the prelabour rupture of the fetal membrane, which is the first step when predicting the likelihood of a preterm birth. The study also offers a new diagnostic probe for clinical praxis.

9 Zusammenfassung

Bei Neugeborenen spricht man von „Termingeborenen“, wenn die Dauer der Schwangerschaft 37-42 Wochen beträgt. Von einer zu frühen Geburt hingegen spricht man, wenn das Gestationsalter weniger als 37 Wochen beträgt. Ein vorzeitiger Blasensprung (engl.: PROM = Prelabour rupture of membrane) kann sowohl bei zu früh Geborenen als auch bei Termingeborenen auftreten. Wenn eine zeitlich regelgerechte Geburt ohne PROM erfolgt, spricht man von einer Normalgeburt (engl.: normal birth = NB). Wenn es sich hingegen um eine zu frühe Geburt ohne PROM handelt, nennt man dies Frühgeburt (engl.: preterm birth = PRB). Wenn bei einer zeitlich regelgerechten Geburt ein vorzeitiger Blasensprung auftritt, nennt man dies PROMB (engl. prelabour rupture of membrane birth, Geburt bei vorzeitigem Blasensprung) und wenn der vorzeitige Blasensprung bei einer Frühgeburt auftritt, spricht man von PPROMB (engl. preterm prelabour rupture of membrane birth, Geburt bei frühem vorzeitigem Blasensprung).

Frühgeburten sind eine der häufigsten Ursachen für die Mortalität während oder nach der Geburt. Die Ätiologie der Frühgeburt ist bisher nur unzureichend verstanden und viele biochemische Untersuchungen wurden mit dem Bestreben durchgeführt, die Ursache bzw. die Ursachen für eine solche Frühgeburt zu finden. In den meisten Schwangerschaften beginnen die Wehen zeitlich regelgerecht bei intakter Fruchtblase. Allerdings kommt es in 10% der Schwangerschaften, die zeitlich regelgerecht sind und sogar in 40% der Frühgeburten zu einem vorzeitigem Blasensprung.

Die fetalen Eihäute, bestehend aus Amnion und Chorion, bilden zusammen eine 0,5 mm dünne Doppelschicht, die als Barriere und Schutzhülle während der Schwangerschaft dient. Die mechanische Integrität der fetalen Eihäute ist für Aufrechterhaltung eines gesunden Schwangerschaftsverlaufs entscheidend. Eine Veränderte Biomechanik der Eihäute kann dabei eine drastische Änderung des Geburtstyps bewirken, die dann zu vorzeitigem Wehen und zur Frühgeburt beiträgt.

Das mechanische Reißen der Fruchtblase ist Teil der natürlichen Abfolge einer normalen Geburt. Ernsthafte Komplikationen können auftreten, wenn die Fruchtblase vor einer ausreichenden Schwangerschaftsdauer reißt. Überlebende Frühgeborene haben oft schwere Krankheiten wie z.B. eine Lungenerkrankung, neurologische Spätfolgen

wie Blindheit, Beschädigung der weißen Substanz und periventriculäre Leukomalazie. Es ist wichtig das mechanische Verhalten der Eihäute zu verstehen, damit eine Vorhersage oder sogar die Verhinderung eines vorzeitigen Blasensprungs in zeitlich regelgerechten Geburten sowie Frühgeburterfolgen kann. Es existieren bedeutende Erkenntnisse bezüglich der mechanischen Struktur von Amnion und Chorion und deren Bezug zur Membranfestigkeit.

Ein reduzierter Gehalt an Kollagen im Gewebe beeinflusst die Reißfestigkeit der Eihäute. Veränderungen der viskoelastischen Eigenschaften beeinflussen die Fähigkeit des Gewebes Dehnungskräfte erzeugt durch mechanische Gewebeschädigung (eventuell durch Neuordnung oder durch Unterbrechung der Kollagenfasern) zu regeln. Die Viskoelastizität spielt ebenfalls eine wichtige Rolle, wenn es darum geht einen Blasensprung vorherzusagen. Sowohl ein geringeres Spannungs-/Dehnungsverhältnis als auch eine Membranausdehnung können in ein Reißen der Fruchtblase verursachen.

Die Identifizierung der mechanischen Charakteristika der fetalen Eihäuten können dazu beitragen, die Mechanismen, die in das vorzeitige Reißen der Fruchtblasen involviert sind, zu verstehen. Diese Kenntnis ist außerdem notwendig, um die Rolle der Änderungen der fetalen Eihäute zu verstehen, die mit einem zu frühen Reißen der Fruchtblase einhergehen. Der Zweck dieser Studie war die Untersuchung der mechanischen Eigenschaften um die Kausalität der vorzeitigen Blasensprungs und der Frühgeburt zu interpretieren. Außerdem wurde die Ergebnisse dieser Studie verwendet, um ein Profil für eine Risikobewertung zu erstellen und ein diagnostisches Hilfsmittel zu entwerfen, das imstande ist einen vorzeitigen Blasensprung und eine Frühgeburt vorherzusagen.

In drei Schritten wurde ein Gerät (DIMPAST) entworfen, das imstande ist in-vitro Messungen durchzuführen. Dieses Gerät wurde die Basis für weitere mögliche Projekte. DIMPAST verwendet verschiedene Messmethoden wie beispielsweise dem Laser-Triangulationsverfahren, Luftdruck-Messungen und optische Kohärenztomographie. Insgesamt wurden 87 fetale Eihäute gesammelt und analysiert bevor eine neue Sonde in dieser Studie entworfen wurde. 45 der fetalen Eihaut-Proben wurden in einer Formaldehyd-Lösung (3,7%) fixiert und bis zur Messung später am Tag bei 4°C gelagert. Diese Eihäute dienten zum Vergleich der Dickenmessung zwischen der histologischen Messung und der OCT-Messung, um die Zuverlässigkeit des OCT zu

beweisen. Die übrigen 42 Eihauptproben, die für die Evaluation der mechanischen Eigenschaften verwendet wurden, wurden bei 4°C zur Messung vorbereitet und gelagert.

Die Signifikanz der Unterschiede zwischen den Gruppen wurde mittels Mann-Whitney U-Test ermittelt. Die Ergebnisse dieser Studie zeigt drei wichtige Besonderheiten: Membranen werden dicker je höher das Gestationsalter wird. Stabilere Membranen reißen nicht vor Wehenbeginn. Das durchschnittliche Spannungs-/Dehnungsverhältnis und der Reißdruck von Frühgeburt-Eihäuten sind signifikant höher als die Eihäute der anderen Geburtsarten. Die Ergebnisse der drei verschiedenen Messmethoden für jeden Geburtstyp wurden zusammengefasst um Schlussfolgerungen ziehen zu können. Die drei Hauptinteressen dieses Teils der Studie war die Gesamtdicke, der Reißdruck und das durchschnittliche Spannungs-/Dehnungsverhältnis für jeden Eihaut-Typ.

Durch den Gewinn dieser hoffnungsvollen Ergebnisse wurde eine Sonde entworfen und hergestellt. Vorläufige Daten die mit einer neuen Sonde gesammelt wurden, geben Hoffnung für die Zukunft. Die Ergebnisse der Messungen mit der Sonde korrelierten mit den DIMPAST-Messungen, sodass die neue Sonde in klinischen Studien eingesetzt werden kann um ihre Zuverlässigkeit zu beweisen.

Schlussendlich erlaubt diese Studie die komplexen Zusammenhänge zwischen biomechanischer Struktur und dem vorzeitigem Blasensprung der fetalen Eihäute zu verstehen. Dies stellt einen ersten wichtigen Schritt dar, wenn es darum geht, die Wahrscheinlichkeit einer Frühgeburt vorhersagen zu wollen.

Diese Studie zeigt außerdem eine neue diagnostische Sonde für die klinische Praxis.

10 Reference List

1. Aijaz Farooqi (2008). *School-age Outcomes of Children Born at the Limit of Viability: Functional Limitations, Growth, Mental Health, Social Competencies, Executive Functions, and Special Health Care Needs at 10 to 12 Years* .
2. Al-Zaid NS, Bou-Resli MN, Goldspink G (1980). Bursting pressure and collagen content of fetal membranes and their relation to premature rupture of the membranes. *Br J Obstet Gynaecol* 87: 227-229.
3. Al-Zaid NS, Bou-Resli MN, Ibrahim ME (1980). Study of the connective tissue of human fetal membranes. *J Reprod Fertil* 59: 383-386.
4. Alger LS, Pupkin MJ (1986). Etiology of preterm premature rupture of the membranes. *Clin Obstet Gynecol* 29: 758-770.
5. Artal R, Sokol RJ, Neuman M, Burstein AH, Stojkov J (1976). The mechanical properties of prematurely and non--prematurely ruptured membranes. Methods and preliminary results. *Am J Obstet Gynecol* 125: 655-659.
6. Ascencio M, Collinet P, Cosson M, Mordon S (2007). The role and value of optical coherence tomography in gynecology. *J Gynecol Obstet Biol Reprod (Paris)* 36: 749-755.
7. Botsis D, Makrakis E, Papagianni V, Kouskouni E, Grigoriou O, Dendrinou S et al (2006). The value of cervical length and plasma proMMP-9 levels for the prediction of preterm delivery in pregnant women presenting with threatened preterm labor. *Eur J Obstet Gynecol Reprod Biol* 128: 108-112.
8. Bou-Resli MN, Al-Zaid NS, Ibrahim ME (1981). Full-term and prematurely ruptured fetal membranes. An ultrastructural study. *Cell Tissue Res* 220: 263-278.
9. Boume GL (2011). The microscopic anatomy of the human amnion and chorion. *American Journal of Obstetrics and Gynecology* 79: 1070-1086.

10. Brezinski ME, Tearney GJ, Bouma BE, Izatt JA, Hee MR, Swanson EA et al (1996). Optical coherence tomography for optical biopsy. Properties and demonstration of vascular pathology. *Circulation* 93: 1206-1213.
11. Bruce Alberts, Alexander Johnson, Julian Lewis, Martin Raff, Keith Roberts, Peter Walter (2007). *Molecular Biology of the Cell* . 5 ed: Garland Science.
12. Carrascosa A, Yeste D, Copil A, Almar J, Salcedo S, Gussinye M (2004). Anthropometric growth patterns of preterm and full-term newborns (24-42 weeks' gestational age) at the Hospital Materno-Infantil Vall d'Hebron (Barcelona) 1997-2002). *An Pediatr (Barc)* 60: 406-416.
13. Cho CK, Shan SJ, Winsor EJ, Diamandis EP (2007). Proteomics analysis of human amniotic fluid. *Mol Cell Proteomics* 6: 1406-1415.
14. Chuileannain FN, Brennecke S (1998). Prediction of preterm labour in multiple pregnancies. *Baillieres Clin Obstet Gynaecol* 12: 53-66.
15. Chuileannain FN, Brennecke SP (1999). Recent advances in the prediction of preterm labour. *Current Obstetrics & Gynaecology* 9: 153-157.
16. Coleman AC (1998). Fetal fibronectin detection in preterm labor : Evaluation of prototype beside dipstick technique and cervical assessment. *Am J Obstet Gynecol* 179: 1553-1558.
17. Dara Brodsky, Mary Ann Ouellette (2007). *Primary Care of The Premature Infant* : Saunders.
18. Di Lullo GA, Sweeney SM, Korkko J, la-Kokko L, San Antonio JD (2002). Mapping the ligand-binding sites and disease-associated mutations on the most abundant protein in the human, type I collagen. *J Biol Chem* 277: 4223-4231.
19. Dictionary.com, (2010). Birth.
20. Donald L.Pavia, Gary M.Lampman, George S.Kriz, James R.Vyvyan (2000). *Introduction to Spectroscopy* . 3 ed. Belmont: Brooks Cole.

21. Drexler W, Fujimoto JG (2008). Introduction to Optical Coherence Tomography *Optical Coherence Tomography*: Springer, p. 1-40.
22. E.Harris Ruddochk, T.Miller Neatby (2005). *Diseases of Infants and Children and Their Homeopathic and General Treatment* . 8 ed. New Delhi: B. Jain Publishers.
23. Escobar PF, Rojas-Espailat L, Tisci S, Enerson C, Brainard J, Smith J et al (2006). Optical coherence tomography as a diagnostic aid to visual inspection and colposcopy for preinvasive and invasive cancer of the uterine cervix. *Int J Gynecol Cancer* 16: 1815-1822.
24. Fischbach,F, Dunning,MB (2008). *A Manual of Laboratory and Diagnostic Tests* . 8 ed: Lippincott Williams & Wilkins.
25. Fisk NM, Ronderos-Dumit D, Tannirandorn Y, Nicolini U, Talbert D, Rodeck CH (1992). Normal amniotic pressure throughout gestation. *Br J Obstet Gynaecol* 99: 18-22.
26. Fortunato SJ, LaFleur B, Menon R (2003). Collagenase-3 (MMP-13) in fetal membranes and amniotic fluid during pregnancy. *Am J Reprod Immunol* 49: 120-125.
27. Fortunato SJ, Menon R, Lombardi SJ (1998). Presence of four tissue inhibitors of matrix metalloproteinases (TIMP-1, -2, -3 and -4) in human fetal membranes. *Am J Reprod Immunol* 40: 395-400.
28. Fujimoto JG, Brezinski ME, Tearney GJ, Boppart SA, Bouma B, Hee MR et al (1995). Optical biopsy and imaging using optical coherence tomography. *Nat Med* 1: 970-972.
29. Goldenberg RL, Iams JD, Miodovnik M, Van Dorsten JP, Thurnau G, Bottoms S et al (1996). The preterm prediction study: risk factors in twin gestations. National Institute of Child Health and Human Development Maternal-Fetal Medicine Units Network. *Am J Obstet Gynecol* 175: 1047-1053.

30. Gomez DE, Alonso DF, Yoshiji H, Thorgeirsson UP (1997). Tissue inhibitors of metalloproteinases: structure, regulation and biological functions. *Eur J Cell Biol* 74: 111-122.
31. Gonzalez JM, Dong Z, Romero R, Girardi G (2011). Cervical remodeling/ripening at term and preterm delivery: the same mechanism initiated by different mediators and different effector cells. *PLoS One* 6: e26877.
32. Gonzalez JM, Franzke CW, Yang F, Romero R, Girardi G (2011). Complement activation triggers metalloproteinases release inducing cervical remodeling and preterm birth in mice. *Am J Pathol* 179: 838-849.
33. Gratacos E, Sanin-Blair J, Lewi L, Toran N, Verbist G, Cabero L et al (2006). A histological study of fetoscopic membrane defects to document membrane healing. *Placenta* 27: 452-456.
34. Greig PC, Murtha AP, Jimmerson CJ, Herbert WN, Roitman-Johnson B, Allen J (1997). Maternal serum interleukin-6 during pregnancy and during term and preterm labor. *Obstet Gynecol* 90: 465-469.
35. H.Lodish, A.Berk, S.L.Zipursky, P.Matsudaira, D.Baltimore, J.E.Darnell (2001). *Molekulare Zellbiologie* : Gustav Fischer.
36. Halaburt JT, Uldbjerg N, Helmig R, Ohlsson K (1989). The concentration of collagen and the collagenolytic activity in the amnion and the chorion. *Eur J Obstet Gynecol Reprod Biol* 31: 75-82.
37. Halberstadt E (1984). Membrane rupture and tocolysis. *Gynakologe* 17: 230-235.
38. Hampson V, Liu D, Billett E, Kirk S (1997). Amniotic membrane collagen content and type distribution in women with preterm premature rupture of the membranes in pregnancy. *Br J Obstet Gynaecol* 104: 1087-1091.
39. Helmig R, Oxlund H, Petersen LK, Uldbjerg N (1993). Different biomechanical properties of human fetal membranes obtained before and after delivery. *Eur J Obstet Gynecol Reprod Biol* 48: 183-189.

40. Holanda MR, Melo AN (2006). Comparative clinical study of preterm and full-term newborn neonatal seizures. *Arq Neuropsiquiatr* 64: 45-50.
41. Holzapfel GA, Sommer G, Regitnig P (2004). Anisotropic mechanical properties of tissue components in human atherosclerotic plaques. *J Biomech Eng* 126: 657-665.
42. Huang D, Swanson EA, Lin CP, Schuman JS, Stinson WG, Chang W et al (1991). Optical coherence tomography. *Science* 254: 1178-1181.
43. Huang D, Wang J, Lin CP, Puliafito CA, Fujimoto JG (1991). Micron-resolution ranging of cornea anterior chamber by optical reflectometry. *Lasers Surg Med* 11: 419-425.
44. Iams JD (2003). The epidemiology of preterm birth. *Clin Perinatol* 30: 651-664.
45. Jabareen M, Mallik AS, Bilic G, Zisch AH, Mazza E (2009). Relation between mechanical properties and microstructure of human fetal membranes: an attempt towards a quantitative analysis. *Eur J Obstet Gynecol Reprod Biol* 144 Suppl 1: S134-S141.
46. Jackson GM, Ludmir J, Bader TJ (1992). The accuracy of digital examination and ultrasound in the evaluation of cervical length. *Obstet Gynecol* 79: 214-218.
47. Joerges J, Schulz T, Wegner J, Schumacher U, Prehm P (2012). Regulation of cell volume by glycosaminoglycans. *J Cell Biochem* 113: 340-348.
48. John T. Queenan, John C. Hobbins, Catherine T. Spong (2005). Obstetric Problems *Protocols for High-Risk Pregnancies*, 4 ed: Blackwell Publishing, p. 381-513.
49. Joseph R. Lakowicz (2010). *Principle of Fluorescence Spectroscopy*. 4 ed. New York: Springer.
50. Joyce EM, Moore JJ, Sacks MS (2009). Biomechanics of the fetal membrane prior to mechanical failure: review and implications. *Eur J Obstet Gynecol Reprod Biol* 144 Suppl 1: S121-S127.

51. Kakizoe E, Kobayashi Y, Shimoura K, Hattori K, Jidoi J (1992). Real-time measurement of microcirculation of skin by reflectance spectrophotometry. *J Pharmacol Toxicol Methods* 28: 175-180.
52. Kanayama N, Terao T, Kawashima Y, Horiuchi K, Fujimoto D (1985). Collagen types in normal and prematurely ruptured amniotic membranes. *Am J Obstet Gynecol* 153: 899-903.
53. Keelan JA, Coleman M, Mitchell MD (1997). The molecular mechanisms of term and preterm labor: recent progress and clinical implications. *Clin Obstet Gynecol* 40: 460-478.
54. Keirse MJ (1989). An evaluation of formal risk scoring for preterm birth. *Am J Perinatol* 6: 226-233.
55. Kimura T, Tsushima N, Yoshizaki S, Nakayama R (1988). Study on reaction of subpapillary venous plexus in patients with arterial occlusive diseases of lower extremity by reflective spectrophotometry. *Angiology* 39: 858-864.
56. Laura Riley (2006). *Pregnancy: Your Ultimate Week-by-Week Pregnancy Guide* . 1 ed: Wiley.
57. Lavery JP, Miller CE (1977). The viscoelastic nature of chorioamniotic membranes. *Obstet Gynecol* 50: 467-472.
58. Lavery JP, Miller CE (1979). Deformation and creep in the human chorioamniotic sac. *Am J Obstet Gynecol* 134: 366-375.
59. Lavery JP, Miller CE, Knight RD (1982). The effect of labor on the rheologic response of chorioamniotic membranes. *Obstet Gynecol* 60: 87-92.
60. Lim K, Butt K, Crane JM (2011). SOGC Clinical Practice Guideline. Ultrasonographic cervical length assessment in predicting preterm birth in singleton pregnancies. *J Obstet Gynaecol Can* 33: 486-499.
61. Linder,P. Examination of Mechanical Properties of Human Amniotic Sac Membranes. 39-40. 2006. Juelich, Biomedical Engineering, FH-Aachen.
Ref Type: Thesis/Dissertation

62. Linder P, Trzewik J, Ruffer M, Artmann GM, Digel I, Kurz R et al (2010). Contractile tension and beating rates of self-exciting monolayers and 3D-tissue constructs of neonatal rat cardiomyocytes. *Med Biol Eng Comput* 48: 59-65.
63. Lockwood CJ, Senyei AE, Dische MR, Casal D, Shah KD, Thung SN et al (1991). Fetal fibronectin in cervical and vaginal secretions as a predictor of preterm delivery. *N Engl J Med* 325: 669-674.
64. Lubchenco LO, Searls DT, Brazie JV (1972). Neonatal mortality rate: relationship to birth weight and gestational age. *J Pediatr* 81: 814-822.
65. M.E.Nimni (2005). *Collagen : Biochemistry, Biomechanics, Biotechnology* . FL: Crc Press Inc.
66. MacDorman MF, Kirmeyer S (2009). Fetal and perinatal mortality, United States, 2005. *Natl Vital Stat Rep* 57: 1-19.
67. Mark Brezinski (2006). Optical Coherence Tomography Theory *Optical Coherence Tomography, Principles and Applications*: Academic Press.
68. Mead PB (1980). Management of the patient with premature rupture of the membranes. *Clin Perinatol* 7: 243-255.
69. Medina TM, Hill DA (2006). Preterm premature rupture of membranes: diagnosis and management. *Am Fam Physician* 73: 659-664.
70. Meinert M, Malmstrom A, Tufvesson E, Westergren-Thorsson G, Petersen AC, Laurent C et al (2007). Labour induces increased concentrations of biglycan and hyaluronan in human fetal membranes. *Placenta* 28: 482-486.
71. Modena AB, Fieni S (2004). Amniotic fluid dynamics. *Acta Biomed* 75 Suppl 1: 11-13.
72. Moore RM, Mansour JM, Redline RW, Mercer BM, Moore JJ (2006). The physiology of fetal membrane rupture: insight gained from the determination of physical properties. *Placenta* 27: 1037-1051.

-
73. Nagase H (1996). Zinc Metalloproteases. In: Hooper N.M., editor. *Health and Disease*. London: Taylor & Francis, p. 153-204.
74. Oxlund H, Helmig R, Halaburt JT, Uldbjerg N (1990). Biomechanical analysis of human chorioamniotic membranes. *Eur J Obstet Gynecol Reprod Biol* 34: 247-255.
75. Oyen ML, Cook RF, Calvin SE (2004). Mechanical failure of human fetal membrane tissues. *J Mater Sci Mater Med* 15: 651-658.
76. Parry S, Strauss JF, III (1998). Premature rupture of the fetal membranes. *N Engl J Med* 338: 663-670.
77. Parry-Jones E, Priya S (1976). A study of the elasticity and tension of fetal membranes and of the relation of the area of the gestational sac to the area of the uterine cavity. *Br J Obstet Gynaecol* 83: 205-212.
78. Peter von Theobald, Carl W.Zimmerman, G.Willy Davila (2011). *New Techniques in Genital Prolapse Surgery* . 1 ed: Springer.
79. Pircon RA, Strassner HT, Kirz DS, Towers CV (1989). Controlled trial of hydration and bed rest versus bed rest alone in the evaluation of preterm uterine contractions. *Am J Obstet Gynecol* 161: 775-779.
80. Reynolds LP, Redmer DA (1995). Utero-placental vascular development and placental function. *J Anim Sci* 73: 1839-1851.
81. Roland Devlieger. Fetal Membrane Healing: Experimental Models & Preventive Strategies. 2003. Leuven, Leuven University.
Ref Type: Thesis/Dissertation
82. Romero R, Ceska M, Avila C, Mazor M, Behnke E, Lindley I (1991). Neutrophil attractant/activating peptide-1/interleukin-8 in term and preterm parturition. *Am J Obstet Gynecol* 165: 813-820.
83. S.Ayad, R.P.Boot-Hanford, M.J.Humphries, K.E.Kadler, C.A.Shuttleworth (1994). Collagen Type 1 *The extracellular matrix (facts book)*: Academic Press, p. 43-48.

-
84. Sepehr A, Armstrong WB, Guo S, Su J, Perez J, Chen Z et al (2008). Optical coherence tomography of the larynx in the awake patient. *Otolaryngol Head Neck Surg* 138: 425-429.
85. Serap Cilaker Micili. Deneysel Olarak Hipertansiyon ve Diyabet Oluşturulmuş Ratlarda Glomerüler Değişikliklerin Elektronmikroskopik ve İmmünohistokimyasal Olarak İncelenmesi. 2011. University of Dokuz Eylül, Department of Histology and Embryology, Izmir, Medical Faculty.
Ref Type: Thesis/Dissertation
86. Severi FM, Bocchi C, Voltolini C, Borges LE, Florio P, Petraglia F (2008). Thickness of fetal membranes: a possible ultrasound marker for preterm delivery. *Ultrasound Obstet Gynecol* 32: 205-209.
87. Skinner SJ, Campos GA, Liggins GC (1981). Collagen content of human amniotic membranes: effect of gestation length and premature rupture. *Obstet Gynecol* 57: 487-489.
88. Skinner SJ, Liggins GC (1981). Glycosaminoglycans and collagen in human amnion from pregnancies with and without premature rupture of the membranes. *J Dev Physiol* 3: 111-121.
89. son-Martin J, Zammaretti P, Bilic G, Schweizer T, Portmann-Lanz B, Burkhardt T et al (2006). The Young's modulus of fetal preterm and term amniotic membranes. *Eur J Obstet Gynecol Reprod Biol* 128: 103-107.
90. Staat,M, Sponagel,S, and Nhu Huynh Nguyen. Experiment and material model for soft tissue materials. 6th European Conference on Constitutive Models for Rubber (ECCMR09). 2009.
Ref Type: Conference Proceeding
91. Sutherland IW (1998). Novel and established applications of microbial polysaccharides. *Trends Biotechnol* 16: 41-46.
92. Takada K, Yokohama I, Chida K, Noda J (1987). New measurement system for fault location in optical waveguide devices based on an interferometric technique. *Appl Opt* 26: 1603-1606.

-
93. Tang J, Zeng F, Savage H, Ho PP, Alfano RR (2000). Laser irradiative tissue probed in situ by collagen 380-nm fluorescence imaging. *Lasers Surg Med* 27: 158-164.
 94. Taylor J, Garite TJ (1984). Premature rupture of membranes before fetal viability. *Obstet Gynecol* 64: 615-620.
 95. Tsoi E, Akmal S, Rane S, Otigbah C, Nicolaides KH (2003). Ultrasound assessment of cervical length in threatened preterm labor. *Ultrasound Obstet Gynecol* 21: 552-555.
 96. van Herendael BJ, Oberti C, Brosens I (1978). Microanatomy of the human amniotic membranes. A light microscopic, transmission, and scanning electron microscopic study. *Am J Obstet Gynecol* 131: 872-880.
 97. Ventura SJ, Abma JC, Mosher WD, Henshaw SK (2008). Estimated pregnancy rates by outcome for the United States, 1990-2004. *Natl Vital Stat Rep* 56: 1-25, 28.
 98. Vladimir N.Uversky, Eugene A.Permyakov (2007). *Methods in Protein Structure and Stability Analysis: Vibrational spectroscopy* . Newyork: Nova Science.
 99. Werkmeister JA, Ramshaw JA (2012). Recombinant protein scaffolds for tissue engineering. *Biomed Mater* 7: 012002.
 100. Wiemer,E. Human Fetal Membranes' Collagen Content and their structural Properties by Optical Techniques. 17-18. 2009. FH-Aachen, Juelich, Medizintechnik und Technomathematik.
Ref Type: Thesis/Dissertation
 101. Woessner JF, Jr. (1991). Matrix metalloproteinases and their inhibitors in connective tissue remodeling. *FASEB J* 5: 2145-2154.
 102. Wojtkowski M, Leitgeb R, Kowalczyk A, Bajraszewski T, Fercher AF (2002). In vivo human retinal imaging by Fourier domain optical coherence tomography. *J Biomed Opt* 7: 457-463.

103. Youngquist RC, Carr S, Davies DE (1987). Optical coherence-domain reflectometry: a new optical evaluation technique. *Opt Lett* 12: 158-160.

11 Figure Legends:

Figure 1: *Stage of life: 8 days. Shown here is an 8-day-old embryo (that’s the round object near the bottom) implanted in a uterus (Laura Riley , 2006).*..... 6

Figure 2: *Figure on the left hand side: Stage of life - 46 days. This embryo, which is less than 2,54cm long, gets all the nutritional supply it needs from the blood that flows to and from it through vessels in the umbilical cord (Laura Riley , 2006). Figure on the right hand side: Stage of life - 13 weeks. This baby has just been through an ultrasound exam and is having a rest in this photograph. The round object above the baby’s head is the yolk sac (Laura Riley , 2006).*..... 6

Figure 3: *Figure on the left hand side: Stage of life - 17 weeks. It is easy to count 10 toes and 10 fingers on this fetus, and facial features are also becoming more defined. The amniotic fluid that surrounds the fetus gradually increases throughout pregnancy to allow the baby to move about (Laura Riley , 2006). Figure on the right hand side -Stage of life: 24 weeks. By now the baby is almost 30,48cm (12 inches) long and weighs a little over 450 grams (1 pound). There’s still a lot of growing to do, however, in the next 16 weeks! A fullterm “average” baby usually weighs between 2700 – 3600 grams (6 – 8 pounds) at birth (Laura Riley , 2006).*..... 7

Figure 4: *Figure on the left hand side: Stage of life - 27 weeks. The cheeks aren’t quite as chubby as they will be at birth (this baby will still gain about 1800 grams (four pounds) before it enters the world), but the face is completely developed. The eyes even open and shut (Laura Riley , 2006). Figure on the right hand side: Stage of life - 36 weeks. It won’t be long now until this baby is born. During the next few weeks, the baby’s lung will finish developing; they are the last organ that needs to mature. By now the baby has learned to suck in preparation for feeding and may have even started sucking his or her thumb (Laura Riley , 2006).*..... 7

Figure 5: *Histologic cross-sectional view of the Fetal Membrane (FM) under microscope (Halberstadt , 1984). Magnification: 200 times.* 9

Figure 6: *Composition of a collagen fiber bundle (S.Ayad, R.P.Boot-Hanford, M.J.Humphries, K.E.Kadler, and C.A.Shuttleworth , 1994).*..... 15

Figure 7: *Group of collagen fibers. Stretch (λ): A measure of deformation defined as $\lambda = L/L_0$, where L is the current length of the fiber and L_0 is the original length. Gradual recruitment of collagen fibers results in a non-linear stress strain relationship (Regions I, II, III). Once all collagen fibers straighten, the stress–stretch curve transitions into a linear region (Region IV) (Joyce, Moore, and Sacks , 2009).*..... 16

Figure 8: *Fetal mortality versus period of gestation graph: United States, 1990 – 2005. Data is presented according to maternal age, marital status, race, Hispanic origin, and state of residence; and by fetal gestational age at delivery, birth weight, plurality, and sex (MacDorman and Kirmeyer , 2009)* 19

Figure 9: *Conditions and mechanisms that can lead to a preterm birth.* 20

Figure 10: *Jablonski scheme of fluorescent and phosphorescent energy levels in multiatomic molecules, with transitions shown (Tang, Zeng, Savage, Ho, and Alfano , 2000).*..... 29

Figure 11: *Fluorescent emission of pure collagen type I at different excitation levels, using a high-pressure xenon lamp (Wiemer , 2009).*..... 30

Figure 12: *“OCT generates cross-sectional or three-dimensional images by measuring the magnitude and echo time delay of light. Axial scans (A-scans) measure the backreflection or backscattering versus depth. Cross-sectional images are generated by performing a series of axial scans at different transverse positions to generate a two-dimensional data set (B-scan), which is displayed as a grey scale or false color image. Three-dimensional data sets (3D-OCT) can be generated by raster scanning a series of two-dimensional data sets (B-scans).” (Drexler and Fujimoto , 2008).* 32

Figure 13: *A simplified schematic of an interferometer. The source light is divided into two parts by a beam splitter. Half of the light is directed onto a sample via the sample arm, while the other half of the light is directed into a mirror attached to the reference arm. Light is reflected back from both arms by mirrors (from the sample and reference arms) and are recombined at the beam splitter. Part of the light is then directed into a detector (Mark Brezinski , 2006).* 34

Figure 14: *Sketch of the Cell Drum-like measurement principle.* 36

Figure 15: <i>A: laser-triangulation-sensor (Keyence, LK-G 3001P, Osaka, Japan) and B: measuring head (Keyence, LK-G, Osaka, Japan).</i>	37
Figure 16: <i>Syringe Pump System.</i>	38
Figure 17: <i>Pressure sensor (Keyence, AP-C40W, Osaka, Japan).</i>	38
Figure 18: <i>Tissue Chamber (A) with fixing ring (B) fixed by clamps (C).</i>	39
Figure 19: <i>NI-USB 6251 Data-Acquisition Unit (National Instruments, NI-USB 6251 DAQ, Austin, USA).</i>	40
Figure 20: <i>Aluminum Construct containing laser sensor and OCT.</i>	41
Figure 21: <i>OCT control part of the operating software.</i>	42
Figure 22: <i>Data acquisition view. (A) General view of the main control window and (B) control menu of the software.</i>	43
Figure 23: <i>A part of the block diagram.</i>	43
Figure 24: <i>View of the amniotic sac tissue. The fetal membrane (A) and the placenta (B) are connected to each other. The Umbilical cord (C) connects the fetus to the placenta.</i>	44
Figure 25: <i>Mapping the fetal membrane. Fetal membrane with placenta (A), separation of the placenta from the fetal membrane (B), the placenta and fetal membrane respectively from left to right hand side (C), cutting the edges of the fetal membrane to flatten it (D), flattened view of the fetal membrane (E), sample preparation of the fetal membrane (F), mapped view shows samples` location on the fetal membrane (G).</i>	45
Figure 26: <i>Histological evaluation method (Serap Cilaker Micili , 2011).</i>	47
Figure 27: <i>Figure on the left hand side; Measurement zones on the same sample. Figure on the right hand side; A view of Image Tool Software (Uthsca-version 3.00 for Windows) and scale is seen for both figures.</i>	49
Figure 28: <i>Light micrograph of the fetal membrane (haematoxylin and eosin stained). It shows the different layers of the amnion-chorion and decidua. (AE) A single layer</i>	

Amniotic cuboidal Epithelium, (BM) amniotic Basal Membrane, (C) Compact layer, (F) Fibroblast layer, (S) Spongy layer, (R) Reticular layer, (PBM) Pseudoasal Basal Membrane, (T) Trophoblast layer. Magnification is X400. 49

Figure 29: *OCT setup and steps for making OCT measurements. An additional device needed to conduct the OCT measurements was designed and manufactured in the period of this study (A), sample is positioned on the OCT working surface(B), the round platform stretches tissue into the target position (C), 3 clamps are applied to compress the round platform with constant force (D), OCT position controlled with a stepper motor via Labview software (E). 50*

Figure 30: *Measurement technique and the DIMPAST (Device for the Investigation of the Mechanical Properties of Amniotic Sac Tissue). 52*

Figure 31: *Measurement setup. (q) OCT control unit, (r) DAQ-Pad, (s) DIMPAST control unit, (t) air pump system, (u) air generator, (v) computer, (w) OCT view (cross-sectional view of the membrane), (x) labview view (part of the software to control the DIMPAST and read the values on sensors). 53*

Figure 32: *OCT chamber of the DIMPAST holds the hand-held part of the OCT (D), over the sample. OCT works near infra-red zone and the light is transmitted by a fiber optic cable (A). The height position of the OCT is controlled by a stepper motor and it stops at a lower switch level (B). The 3 clamps (C) stretch the sample under the fixing ring. 54*

Figure 33: *Cross-sectional view of the fetal membrane. This view was captured with the Optical CohorenceTomograpy (OCT). The amnion and chorion layers are easily identified, and the spongy layer is obvious. 55*

Figure 34: *Visible gap between the amnion (upper layer) and chorion (lower layer). . 55*

Figure 35: *Positioning of the sample on the tissue chamber. 56*

Figure 36: *Air pump system. 56*

Figure 37: *Bursting of the fetal membrane. First the chorion ruptured (A), then the amnion burst (C). The graph (B) shows the relation between inner pressure of the tissue chamber and the tissue's strength.* 57

Figure 38: *This figure clarifies the calculation of the average Stress-Strain Ratio of the fetal membrane. (A) The piece of fetal membrane was inflated until a constant deflection of $h_{max}=8mm$ was achieved, forming a spherical segment over the chamber. (B, C) The height of this spherical segment was equal to the deflection value (h) which increased up to 8mm. The bottom diameter was equal to the chamber diameter ($L_0=34mm$). (D) The elongation (ϵ) values were calculated for every point of the Pressure – Deflection curves to derive the Pressure (kPa) – Elongation (ϵ) curve.* 58

Figure 39: *OCT tip for the deflection measurement (A), and a sketch of the process (B).* 60

Figure 40: *Fluorescence response of the dried collagen fibers (A) and the fetal membrane (B) (Keyence, BZ 8100, Osaka, Japan).* 62

Figure 41: *OCT view of the fetal membrane. The CCD camera view can be seen in the lower left-hand corner, and is used for positioning the OCT head over the inspection area. Total thickness, as well as the amnion and chorion can be easily detected. (AE) Amniotic cuboidal Epithelium, (S) Spongy layer, (R) Reticular layer.* 64

Figure 42: *Light micrograph of the fetal membrane (haematoxylin and eosin stained). It shows the different layers of the amnion-chorion and decidua. (AE) a single layer Amniotic Cuboidal epithelium, (BM) amniotic Basal Membrane, (C) Compact layer, (F) Fibroblast layer, (S) Spongy layer, (R) Reticular layer, (PBM) Pseudoasal Basal Membrane, (T) Trophoblast layer. Magnification X400.* 64

Figure 43: *A special OCT tip for the deflection measurements in-vitro. Air channels are positioned at an approximate angle of 70^0 from the horizontal axis and focus the air stream at the surface examined by OCT. OCT scans the surface to detect the structures of the cross-sectional plane.* 72

Figure 44: *Application parameters of the new OCT tip. When air flow is applied from a distance of 2mm, an affected area's diameter is 1,2mm.* 72

Figure 45: A view of the FM before and after the air application. Structures and the thickness of the FM can be easily examined. The deflection is 2,83 mm when the inner pressure of the membrane chamber is 0,8 kPa. 73

Figure 46: A view of the FM before and after the air application. Structures and the thickness of FM can be easily examined. The deflection is 1,78mm when the inner pressure of the membrane chamber is 1,3kPa. 73

Figure 47: Absorption of the FM. Three strong absorption zones exist. 74

Figure 48: Transmission of the FM. Spectrum of light at between 400nm – 750nm. 75

Figure 49: Autofluorescence measurement. Excitation and emission values are at the same graph. 76

Figure 50: The control unit of the new OCT probe. 83

Figure 51: The new OCT probe. It has 4 channels and each channel is controlled with a fiber optic switch. This photo was captured by a mobile phone, and infrared light from one of the channel can be seen in front of the OCT probe. 84

Figure 52: Front panel view of the service (A,C) and the operating (B,D) software of the new OCT probe before calibration (A,B) and after calibration (C,D). 85

Figure 53: A view of the new DIMPAST. It has new laser sensor (a) which can measure in 2 dimensions. The new DIMPAST is working with a liquid to inflate the membrane, so there is a waste liquid collector (b) and it has a new membrane chamber (c) which has quick fastener system. (A) A general view, (B) a top view and (C) a side view of the DIMPAST shows details of the new system to observe the differences. 86

Figure 54: (A) A new laser sensor (LLT 2700-50(500), Micro Epsilon, Ortenburg, Germany) and (B) a new pressure sensor (PA3026, ifm electronic gmbh, Essen, Germany) of the new DIMPAST. 86

Figure 55: New setup before using the OCT probe with an air flow. 87

Figure 56: (A) Inflated membrane and (B) its deflection with an air flow. 88

Figure 57: *Curvature of the inflated membrane can be seen in this figure. (A) The red graph belongs to membrane without air flow, and the white graph belongs to the membrane at time air flow application. (B) The difference between these two graphs shows the deformation under air flow which is shown by the green graph. 89*

Figure 58: *OCT view of the inflated fetal membrane using the new OCT probe, outfitted with four channels. The observed depth of the membrane surface was different for each channel because of the curvature. A green line shows the upper layer of the membrane and a red line shows the lower bottom layer of the membrane. The difference between these two layers shows the thickness of the membrane. 89*

Figure 59: *Calculation of the deflection with the OCT probe. Each channel measures saperately. 90*

Figure 60: *Design of the new OCT probe..... 90*

Figure 61: *Proposal for handheld invivo diagnostic probe..... 95*

Figure 62: *Deflection measurement with four fiber optic cables. A blue arrow shows the air flow direction, and the other four white arrows show the static OCT measurements. 96*

Figure 63: *Setup of the diagnostic probe..... 97*

Table 1: <i>Schedule of mammalian MMPs (Woessner, Jr. 1991)</i>	11
Table 2: <i>Terminology of birth types.</i>	18
Table 3: <i>Data groups. Normal Birth (NB); Preterm Birth (PRB); Premature Rupture of Membrane Birth (PROMB, number of membranes (n), number of samples (s))</i>	46
Table 4: <i>PAS staining method. Entellan (Merck 1.07961.0100, Darmstadt, Germany), Lamel (Isotherm 76X26 mm), Light microscope (Olympus DP70), Microtome (RM 2255, Leica), Digital camera (Olympus DP71), Computer Analysis system Image Tool software (Uthsca-version 3.00 for Windows).</i>	48
Table 5: <i>The number of experiments made for each group during the evaluation of mechanical properties, with and without consideration of birth type.</i>	51
Table 6: <i>Comparing the total thickness of the fetal membranes. OCT data vs. Histological data.</i>	65
Table 7: <i>Comparison of the total thickness of the fetal membranes in subgroups. OCT data vs. Histological data.</i>	66

Graph 1: *Fetal membrane thickness at different membrane locations: C, Controls of normal birth. indices: P, Placental edge, R, Rupture side, M, Mid-zone etc.; index numbers: 1, OCT data, 2, histological data.* 67

Graph 2: *Total thickness comparison;* 69

Graph 3: *Bursting pressure comparison;* 70

Graph 4: *Stress-Strain Ratio comparison;* 71

Graph 5: *The amount of deflection with respect to the inner pressure. Deflection was measured with the new OCT probe and is compared with the laser sensor. OCT probe was in correlation with the laser sensor ($p=0,972$).* 91

Graph 6: *Pressure vs. Deflection Curve for all kinds of birth with the OCT probe. Each measurement is represented with a dot.* 92

Graph 7: *Pressure vs. Deflection Curve for all kinds of birth with the OCT probe. Charts were derived by the function of each birth types' graph.* 92

Graph 8: *Pressure vs. Deflection Curve for all kinds of birth with the OCT probe. Inner pressure value is up to 2 kPa which is the physiological limits of resting intra amniotic pressure.* 93

12 Lebenslauf**Persönliche Daten**

Name	Hakan Oflaz
Geburtsdatum	09.11.1980
Geburtsort	Merzifon / Türkei

Seit 10/2009 Kooperative Promotion an der FH Aachen, Campus Jülich;
Labor für Medizinische & Molekulare Biologie mit der
Universität zu Köln

Seit 02/2012 wissenschaftliche Mitarbeiterin an der FH Aachen, Campus
Jülich;
Labor für Zellbiophysik und Medizinische & Molekulare
Biologie

10/2011 - 02/2012 wissenschaftliche Mitarbeiterin an der Universität zu Lübeck;
Institut für Biomedizinische Optik

05/2008 - 10/2011 wissenschaftliche Mitarbeiterin an der FH Aachen, Campus
Jülich;
Labor für Zellbiophysik und Medizinische & Molekulare
Biologie

09/2004 - 05/2008 Master Arbeit an der Universität zu Dokuz Eylul, Izmir –
Türkei;
Labor für Biomechanik

04/2006 – 10/2006 Auslandsaufenthalt in den Deutschland (als Erasmus
Exchange student);
an der FH Aachen, Campus Jülich, Labor für Biomechanik

09/1999 – 09/2003 Studium Elektrotechnik an der Universität zu Pamukkale,
Denizli - Türkei
Abschluss: Ingenieur für Elektrotechnik

09/1992 – 07/1999 Gymnasium (Ozel Izmir Fen Lisesi) an der Izmir, Türkei

Software

- gute Kenntnisse in MS Office Anwendungen (Word, Excel, PowerPoint)
- Basiskenntnisse in SPSS von SPSS Inc.

Sprachen

- gute Englischkenntnisse in Wort und Schrift

Freizeit

- Fussball, Reisen, Kino, lesen